



# AN ANALYSIS OF TENSION PILE FOUNDATIONS IN TUNNEL ENTRANCES

Master thesis

Author:  
S.J. van Brussel

Delft University of Technology  
Faculty of Civil Engineering & Geosciences – Section Geotechnical Engineering  
Rijkswaterstaat GPO  
Team Tunnels & Natte Kunstwerken



# **An analysis of tension pile foundations in immersed tunnel entrances**

**MSc thesis**

By  
S.J. van Brussel  
Student nr. 4928458

Master track: Geo-engineering

## *Graduation committee*

### **Chair/supervisor**

Dr. Ir. W. Broere

### **Supervisor**

Dr. Y. Yang

### **Company supervisor**

Ir. H.R.E. Dekker



Rijkswaterstaat  
Ministerie van Infrastructuur en Milieu



## Foreword

This document contains the master thesis written for the finalization of my Master of Science in Civil Engineering at the Delft University of Technology in the track Geotechnical engineering. This means the end of my time as a student at this university. It was a very memorable journey that I am very grateful for.

Halfway my Bachelor I started as a working student at Rijkswaterstaat GPO team TeNK. This time has proven invaluable to me because after the passing of this thesis, I will have graduated at Rijkswaterstaat for both my Bachelor and Master degree. From both the working studentship and the graduation projects I have learned more than I could ever imagine and I have been able to be assist and be responsible for a multitude of civil projects in the Netherlands. This job strengthened my passion for civil/geotechnical engineering greatly. I want to thank the colleagues of my team and especially H. Dekker and S. van der Horst for providing me with supervision for my graduation projects. I am grateful for your inputs and assistance where required.

Furthermore I want to thank W. Broere for supervising me during both my Bachelor and Master graduation projects. The sparring sessions really helped me go forward and the input has been very valuable in shaping this thesis.

When the going got tough during this time, as it was not always easy, I could always count on my family to support me. The walks with my mom, the sparring sessions with my dad or support from my sister, the philosophical sessions with my ducks, I could not have done it without it. I would like to express my endless gratitude to them.

*Stevin van Brussel  
Den Haag, April 2025*



# Abstract

This thesis investigates the behavior of tension pile foundations and their failure mechanisms. The objective was motivated by the incident that occurred in the entrance ramp of the Prinses Margriet tunnel, which was caused by the failure of the tension pile foundation. The cause of the failure is believed to be stress corrosion in the reinforcement of the tension pile. Given that there are several tunnel entrances with a similar tension pile foundation to the Prinses Margriet tunnel, motivated the initiation of a project by Rijkswaterstaat in which these tunnels are investigated on this particular failure mechanism. One of these tunnels is the First Heinenoordtunnel which is analyzed in this thesis as a case study.

The stress corrosion in the reinforcement caused premature brittle failure of the steel, which causes the tension pile to lose its connection with the tunnel floor, making the pile lose its tensile capacity completely. For stress corrosion to occur in tension pile reinforcement, three main conditions are defined. Firstly the utilization of a high quality steel, secondly an environment in the subsoil which enables corrosion and thirdly the amount & variation of tensile stress in the material. For the First Heinenoordtunnel, these conditions are all met and the pile failure due to stress corrosion should be taken into account as a failure mechanism.

The design methodology of this tunnel and the general design methodology of tension piles in the Netherlands is summarized. This information is used to validate models, to define and model the geometry of the critical element along with its tension pile foundation. The safety philosophies between the time of construction of the tunnel and now are compared as well. Here it is found that more complex tension pile calculation models allow for lower safety factors, which cause the calculated capacity of the tension piles with current models ended up having a higher capacity

The development of stress corrosion in the tension piles is difficult to detect due to the coverage of the tunnel floor and daily traffic. The development of a numerical model made it possible to monitor the stress corrosion based on the displacement of the tunnel floor/walls.

The geometry of the critical tunnel entrance elements along with the soil profile and tension pile foundation of the First Heinenoordtunnel are modelled numerically in the Plaxis3D software. There are two critical tunnel elements defined, namely in the northern entrance element 3N and southern entrance element 3Z.

In order to simulate the failure mechanism, a Python algorithm was used to set up a Monte-Carlo analysis in which the tension piles fail sequentially, in random sequences as the distribution and development of stress corrosion in the tension piles is unknown.

DFoundation software was used to validate the numerical models using the NEN 9997-1 norm. The outcome of this validation was satisfactory resulting in an overestimation of 1.7% and 17% of the safe capacity and 21% and 10% of the limit capacity for north and south respectively.

The algorithm was used to perform a total of 50 Monte-Carlo iterations for both elements 3N and 3Z. The result was the displacement profile of the tunnel floor and walls as piles fail sequentially in randomly determined pile sequences. When analyzing the results of the analysis it is found that the numerical models fail when roughly 60-70% piles have failed due to stress corrosion. The model failure occurred at displacement values up to 25 mm for north and 60 mm for south. The profile of displacement of the tunnel floor/walls as more piles fail sequentially can be used for monitoring the uplift failure mechanism due to stress corrosion.

Warning values for monitoring the critical moment of failure were defined based upon the tunnel floor displacement profiles. For element 3N a signal value of 4 mm was determined and an intervention value of 7 mm. For element 3Z a signal value of 5 mm was determined and an intervention value of 10 mm. It was found that for element 3Z displacements increase more rapidly as the failure mechanism progresses comparing to element 3N.

It is found that there is no imminent risk of the uplift failure due to stress corrosion for the tunnel entrances of the First Heinenoordtunnel using available INSAR-data trends. However, the monitoring should continue as it is very difficult to determine the current state of stress corrosion in the tension piles and therefore unknown how fast the mechanism actually progresses. The monitoring of displacement of tunnel floor/walls can be used for the monitoring of stress corrosion in the tension piles utilizing the models made for this research.

# Table of contents

1. Introduction.....	1
2. Pile foundations.....	4
2.1 Driven piles.....	4
2.2 Auger piles.....	5
2.3 Combined methods.....	5
3. Failure mechanism .....	6
3.1 Background.....	6
3.2 Corrosion in steel .....	7
3.2.1 Prevention & detection methods .....	10
4. Capacity determination tension piles .....	13
4.1 Dutch methods throughout the years.....	13
4.1.1 Before 1991 – Grondmechanica Delft.....	13
4.1.2 1991-2005: TGB 1990 + NEN 6740 series + CUR 98-9 .....	14
4.1.3 2005 – present – Eurocode 7 + Dutch Annex NEN 9997-1 .....	17
4.2 Other methods.....	19
4.3.1 Empirical methods .....	19
4.3.2 Semi-empirical methods.....	19
5. Numerical design .....	20
5.2 Tension piles with the Finite Element Method.....	21
6. Case: EHT .....	24
6.1 Background.....	24
6.2 Tension pile foundation.....	26
6.3 Geotechnical & hydrological situation.....	28
6.3.1 Geohydrological.....	28
6.3.2 Geotechnical.....	31
6.3.2.1 Geotechnical profile .....	31
6.4 Failure mechanism & Critical element.....	34
6.5 Model choice.....	35
6.6 Pile load tests .....	36
6.6.1 Pile load test GD (1968).....	36
6.6.2 Pile load test Heijmans (2018) .....	38
7. Geotechnical capacity of a tension pile.....	39
7.1 Pile load tests GeoDelft.....	40
7.2 Theoretical capacity calculation.....	41
7.3 Numerical simulation .....	43
7.3.1 Volume pile.....	43
7.3.2 Embedded beam .....	44

7.3.3 Comparison of numerical models.....	46
7.4 Comparison of limit carrying capacities .....	48
8. Capacity of the critical elements .....	49
8.1 Modelling northern element 3N .....	52
8.2 Modelling southern element 3Z .....	55
8.3 Comparison of results .....	58
9. Analysis of corrosion failure .....	59
9.1 Stress corrosion .....	59
9.2 Corrosion fatigue.....	60
9.3 Modelling failure mechanism.....	65
9.3.1 Sensitivity analysis.....	66
9.3.2 Tunnel element 3N .....	69
9.3.3 Tunnel element 3Z .....	73
9.4 Monitoring the warning levels .....	77
10. Conclusions .....	80
11. Recommendations .....	82
12. Bibliography.....	84
13. Appendix .....	86
A1: Finite element method.....	86
A2: Plaxis3D .....	87
A3: Dynamic loads on tension piles.....	92
A4: Plaxis3D model failure.....	96

## List of figures

Figure 1: Vibro installation method step-by-step.....	5
Figure 2: Fracture surface of steel reinforcement (Borsje & Schuring, 2023) .....	6
Figure 3: Corrosion detection using ultrasonic detection (Hernandez-Valle, Clough, & Edwards, 2014).....	11
Figure 4: Corrosion cracking detection using acoustic emission (Ramadan, Gaillet, Tessier, & Idrissi, 2008) ...	12
Figure 5: Silo shaped soil clod dimensions (van Noortwijk, Everts, & Janse, 1994).....	14
Figure 6: Geometry of a piled raft foundation as a PLAXIS 3D model (Ryltenius, 2011) .....	21
Figure 7: Overview of the location EHT (Google Maps, 2024).....	24
Figure 8: Longitudinal section of EHT (TEK HE757).....	25
Figure 9: Top view of the EHT (TEK HE757) .....	25
Figure 10: Tension pile foundation Northern entrance (TEK HE759, 1962).....	26
Figure 11: Tension pile foundation Southern entrance (TEK HE765, 1962).....	26
Figure 12: Tension pile schematic (RWS directie sluizen & stuwen, 1962).....	27
Figure 13: Tension pile connection to tunnel floor (TEK HE759, 1962).....	27
Figure 14: Locations of installed piezometers (Fugro, 2024) .....	28
Figure 15: Evolution of phreatic water levels through time (Fugro, 2024).....	29
Figure 16: Evolution of deep water levels through time (Fugro, 2024) .....	29
Figure 17: Geotechnical longitudinal section of the tunnel (Grondmechanica Delft, 1994).....	31
Figure 18: Locations boreholes & CPT's north (DINO-loket, 2024) .....	32
Figure 19: Locations boreholes and CPT's south (DINO-Loket, 2024).....	33
Figure 20: Different tension pile footing shapes (1994) .....	36
Figure 21: Load-displacement curves of various performed pile load tests (1968) .....	37
Figure 22: Pile load tests 2,7 & 8 performed by Grondmechanica Delft (1968).....	40
Figure 23: Displacement distribution for volume pile .....	43
Figure 24: Time-displacement and force-displacement diagram for volume pile.....	44
Figure 25: Displacement distribution for embedded beam .....	45
Figure 26: Time-displacement diagram for embedded beam .....	45
Figure 27: Comparison displacement volume & embedded pile Plaxis3D .....	46
Figure 28: Time-displacement diagrams of pull-out tests and PLAXIS 3D models .....	47
Figure 29: DFoundation output element 3N with safety factors .....	52
Figure 30: DFoundation output element 3N without safety factors .....	52
Figure 31: Displacement of floor plate element SLS 3N .....	53
Figure 32: Deformation of soil body element 3Z.....	53
Figure 33: Displacement of floor plate element ULS 3N.....	54
Figure 34: Deformation of soil body ULS 3N .....	54
Figure 35: DFoundation output element 3Z with safety factors.....	55
Figure 36: DFoundation output element 3Z without safety factors.....	55
Figure 37: Displacement of floor plate element SLS 3Z.....	56
Figure 38: Deformation of soil body SLS 3Z.....	56
Figure 39: Displacement of floor plate element ULS 3Z .....	57
Figure 40: Deformation of soil body SLS 3Z.....	57
Figure 41: INSAR data of tunnel element plotted with weekly temperature data (KNMI, 2025).....	61
Figure 42: Profile of various cyclic loads on tunnel element 1 week.....	62
Figure 43: Combined profile of cyclic loads on tunnel element 1 week .....	62
Figure 44: Various cyclic loads on tunnel element 1 year .....	63
Figure 45: Combined cyclic loads on tunnel element 1 year .....	63
Figure 46: Sensitivity analysis of tunnel floor stiffness .....	66
Figure 47: Sensitivity analysis of tension pile stiffness .....	67
Figure 48: Sensitivity analysis of soil parameters .....	68
Figure 49: Sensitivity analysis of wall friction number .....	68
Figure 50: 50 Monte Carlo iterations of piles failing sequentially in element 3N .....	69
Figure 51: Histogram of model failure occurring at % of piles failed 3N.....	70
Figure 52: Fitted left-skewed Gumbel distribution to histogram 3N .....	70

Figure 53: Warning zones of uplift failure due to stress corrosion element 3N .....	72
Figure 54: 50 Monte Carlo iterations of piles failing sequentially in element 3Z .....	73
Figure 55: Histogram of percentage failed piles at model failure .....	74
Figure 56: Fitted left-skewed Gumbel distribution to histogram 3Z.....	74
Figure 57: Warning zones uplift failure due to stress corrosion element 3Z.....	76
Figure 58: INSAR Data 3N & 3Z 2009-2024 (RWS CIV, 2024) .....	77
Figure 59: INSAR-data 3N with warning levels .....	78
Figure 60: INSAR-data 3Z with warning levels .....	79

## List of Tables

Table 1: Correlation factor based on M tension piles and N CPT's (NEN 6740, 1991) .....	14
Table 2: Alpha values for different pile installation types (CUR98-9, 2001) .....	15
Table 3: Alpha values for different types of installation piles and soils (NEN 9997-1, 2023) .....	17
Table 4: Correlation factors for N CPT's (NEN 9997-1, 2023).....	18
Table 5: Historical timeline of global and partial safety factors in Dutch Norms .....	18
Table 6: Amount of tension piles per tunnel element (TEK HE759 & HE765, 1962).....	26
Table 7: Phreatic and deep water levels for both North & South.....	30
Table 8: Governing geotechnical cross section north.....	32
Table 9: Governing geotechnical cross section south .....	33
Table 10: Utilized geotechnical cross section for models .....	39
Table 11: calculated capacities using different methods .....	42
Table 12: Limit carrying capacities for tension piles from different sources .....	48
Table 13: Structures model and construction phases of tunnel element as in PLAXIS 3D.....	49
Table 14: Repetition governing geotechnical cross section North .....	51
Table 15: Repetition governing geotechnical cross section South .....	51
Table 16: Comparison of element 3N & 3Z.....	58
Table 17: Information on fatigue resistance= steel .....	64
Table 18: Algorithm for simulating piles failing due to stress corrosion in numerical model .....	65



# 1. Introduction

On December 13<sup>th</sup> 2022, an incident occurred in the Prinses Margriettunnel, which is a tunnel providing the connection of the highway A7 between Sneek and Joure in the north of the Netherlands. It was observed that one of the access ramp element in the western entrance of the Prinses Margriettunnel had moved upwards. This happened as a result of the foundation of the element failing. After carrying out the required investigations, it was observed that the reinforcement of some of the installed tension piles had failed, which resulted in a loss of their tensile bearing capacity. The loss of bearing capacity resulted in a disruption of the vertical equilibrium, which eventually resulted in the upward movement of an element in the access ramp of the tunnel, as the tension pile foundation with a reduced number of active tension piles was not able to withstand the upward force exerted on the tunnel element by the groundwater. The tunnel had to be closed for an extended period after this incident, which caused large unplanned time delays and costs. As of 29<sup>th</sup> of March 2025, the tunnel is yet to be reopened completely and the restoration works for the foundation are still ongoing.

The Prinses Margriettunnel was constructed in 1976 as an immersed tunnel. This immersed tunnel has both an open and closed part. The open part consist of the entrances of the tunnel, and the closed part is submerged under the waterway. The maximum depth of the tunnel entrances is around NAP – 12 meters, which approximately 11 meters under the ground water level. Apart from the construction of the tunnel entrance itself, there is no surcharge weight present in the tunnel entrances. The tunnel has to withstand buoyant forces due to the water being retained from the tunnel entrances (Rijkswaterstaat, 2024). Since there is no surcharge weight present, a different method has to be applied to resist the upward water force. For this tunnel specifically, it was achieved through the application of a tension pile foundation connected with the floor of the tunnel entrance. The tension pile foundation was applied at the locations the upward force exerted by the groundwater was expected to exceed the self-weight of the tunnel, resulting in a vertical upward resultant force. The function of the tension pile foundation at these locations is to maintain vertical equilibrium. If these tension piles do not fulfill their function, the resultant vertical force on the tunnel element will cause an upward movement.

The specific type of tension piles used are so called ‘Vibropalen’ which are cast-in-place concrete tension piles with a thin rod of high quality steel as reinforcement with a diameter of around 32 mm. These steel rods are generally coated with grease or asphalt as a protective measurement for corrosion. These piles are put in place to withstand upward force and maintain vertical equilibrium during the lifetime of the tunnel (Borsje & Schuring, 2023).

The main cause of the tension piles breaking has been identified by TNO as stress corrosion of the reinforcement steel. Stress corrosion can occur in specific materials under specific circumstances. In this case specifically, the main constituents of stress corrosion are the combination high quality carbon steel withstanding high varying tensile stresses in a corrosive environment. Due to traffic loads, the stresses are varying in the tension piles. The corrosive environment is created through either presence of chlorides or an acidic or alkaline environment around the material (Bonfix, 2023).

Failure due to stress corrosion occurs through the formation and propagation of cracks in the material. In the case the tensile stress in the material is varying, the stress corrosion process is accelerated. Chlorides have possibly come in contact with the reinforcement steel due to salt intrusion in the tension piles. The acidic or alkaline environment is formed through the presence of low and high pH solutions in the subsoil around the tension piles. The stress corrosion cracking eventually led to a brittle failure of the reinforcements of the tension piles, ultimately causing the failure of the tension piles (Borsje & Schuring, 2023). The reinforcement rods in the tension piles are coated with grease as a measure for corrosion protection (Stevelling, 1969). This measure however has not proven to provide enough corrosion protection, as the stress corrosion still took place in the reinforcement steel. The exact cause for this corrosion still happening is yet to be determined and is still being researched.

The ongoing restoration works of the tension pile foundation consists of the installation of 1.150 new tension piles (Rijkswaterstaat, 2024). This is a very costly operation in terms of time and money. This incident has also been harmful for the reputation of Rijkswaterstaat. In order to maintain the level of mobility of the Dutch transport network, it is desired that certain links of this network not become unavailable due to infrastructural components such as the Prinses Margrietunnel failing. Especially when this unavailability is unplanned. This will cause heavy delays and costs for both the maintaining and exploiting stakeholders. Also, the tunnels failing pose a risk of safety for the road users.

In November, 2010 a similar incident had already happened with the Vlaketunnel, located in the Netherlands. The applied tension pile foundation of the Vlaketunnel was designed in a similar fashion to that of the Prinses Margrietunnel, specifically the use of the same type of tension piles used in the Prinses Margrietunnel. At the time the incident occurred, it was decided by Rijkswaterstaat that the incident had happened due to local environmental effects and that there was no further research necessary for objects with a similar foundation method. (Borsje & Schuring, 2023). The second calamity regarding the tension piles which happened in the Prinses Margrietunnel however, motivated Rijkswaterstaat to analyze the applied tension pile foundation methods of other tunnels in the Netherlands, in order to determine whether the same foundation method as the Vlaketunnel and Prinses Margriet tunnel was applied and thus the same risk for stress corrosion occurring was present.

After the tunnels where the similar foundation type is applied were identified, initiative was taken by Rijkswaterstaat to start research into preventive and corrective measures in order to prevent or mitigate a similar calamity from happening in the future to another tunnel.

Eventually, a total of four tunnels under the maintenance by Rijkswaterstaat have been identified to have a similar foundation to that of the Prinses Margriet tunnel and Vlaketunnel (Rijkswaterstaat, 2024). One of these tunnels is the First Heinenoordtunnel. This tunnel provides the connection of the highway A29 and is an important link between the western and southern part of the Netherlands (Wegenwiki, 2023). The First Heinenoordtunnel is abbreviated as 'EHT' in this report.

This thesis aims to analyze the potential failure mechanisms of the tension pile foundation applied for the EHT, as well as analyzing the reliability of the current tension pile foundation at the critical location of the tunnel entrance and investigate whether imminent failure can be detected and possibly prevented before full failure happens. To achieve this, known failure mechanisms for tension pile foundations are researched, also relevant analytical calculation methods of tension pile foundations throughout the years are reviewed. Also, a numerical model of the most critical section of the tension pile foundation of the EHT is constructed in order to perform simulations. The analytical and numerical models are then used to determine the interplay of forces of the tension pile foundation, analyze the safety in different scenarios and to analyze the potential failure mechanism of the entrances of the EHT.

Based on this aim and method, two main research questions for this thesis are posed as follows:

'What is the relevant potential failure mechanism for the tension pile foundation of the EHT and to what extent can its reliability be assessed?'

'How can a numerical model assist in the monitoring of a tunnel element, in order to assess possible detection levels of the progress of a failure mechanism?'

In order to answer this research question properly, a set of sub-questions are formulated.

'What types of corrosion are relevant for tension pile failure to what extent are they a relevant failure mechanism for tunnels?'

'To what extent can the type of failure mode of the incident be modelled/predicted using analytical models and or numerical methods?'

'What is the impact of changes in design methods of tension piles between time of construction of the EHT and design methods used currently?'

'What is the factor of safety against uplift failure for the EHT?'



‘What is the impact of the failure of tension pile(s) on the factor of safety against uplift?’

‘How does the current factor of safety obtained from current methods against uplift failure compared to the factor of safety as employed during the original design of the tunnel?’

‘To what extent can a warning mechanism that signals whether tension piles are failing be derived from the numerical model?’

‘How does the failure mechanism of the tunnel progress as tension piles are gradually failing?’

‘How many tension piles can fail in order for the whole foundation as constructed in the numerical model to fail?’

The numerical model is used to extract information of the failure mechanism of the EHT. This information could be used to define warning levels for monitoring the tunnel. This supports in the development of the preventive and corrective measures necessary to guarantee the structural safety of the tunnel and on a larger scale the infrastructural integrity of the Dutch transport network.

The model is limited to the section of the tunnel entrance ramp where tension piles are used, as here the most resultant upward force is present and thus the highest risk for heave is present. The geotechnical conditions and the design of the tension pile foundation are analyzed in order to formulate the model. The model will be limited to a static analysis to limit both the project scope and computational load of the numerical model solving.

The numerical model is used to simulate different loading scenarios on the geometry of the tunnel entrance and analyze the response of the tunnel in terms of unknowns, such as present deflections and stress. The factor of safety of the tension pile foundation based on different amounts of failed tension piles in the foundation is simulated. This information is used to perform a failure analysis on the tension pile foundation of EHT.

To validate the numerical model, known analytical calculation models for tension pile foundations can be used. Also settlement monitoring strategies such as total stations or satellite data can be used to measure actual deflections, with which the numerical model can be validated.

## 2. Pile foundations

Pile foundations are generally applied in construction projects where the bearing soil layers are situated relatively deep. The pile is cast or driven through the existing soil layer until the desired pile tip level. The pile bearing capacity is mobilized by the combination of pile tip resistance in the bearing soil layer and the shaft friction resistance between the soil and pile along the length of the pile.

Pile foundation can be loaded both in compression and tension. Compressive forces generally originate from downward forces such as self-weight of the structure resting on the foundation. Tensile forces generally originate from upward forces such as water pressures acting on the foundation or structure.

This research will focus on tension piles, as this is the scope of this specific research. This chapter will go over the practical application of tension piles and which methods/techniques are used most commonly in the application of a tension pile foundation in practice.

The capacity of a tension pile is mobilized through the friction between the shaft of the installed tension pile and the surrounding soil along the length of the pile. The pile tip resistance is mobilized for piles in compression, for tension piles there is no tip resistance mobilized.

Three main types of construction exist in geotechnical engineering for foundation piles. These are; driven concrete piles, auger piles and methods combining these two. Each of these alternatives have their own benefits and the different methods can be employed for different geotechnical challenges.

The bearing capacity of the pile is influenced by many factors such as shape of pile, type of installation and roughness of material used. Many different combinations of these factors exist and provide different capacities. This influence in bearing capacity is highly dependent on the soil disturbance that is happening during installation. For example installation methods which compact the soil lead to relatively higher bearing capacities than installation methods which loosen the soil.

Another structural object that is designed to resist tensile forces is the ground anchor. The main difference between a tension pile and an anchor is that the former is also able to resist compressive forces and the latter is only able to resist tensile forces. Tension piles are used when compressive and tensile forces are expected in the piles during their lifetime. This study will focus on different types of practically applicable tension piles.

### 2.1 Driven piles

These type of piles are driven into the ground using a hammer, vibrations or a pushing method.

With the driving of the pile, the compaction of the soil that is caused by the pile driving increases the stresses around the pile, which increase their total bearing capacity. The method is also relatively simple, cheap and not as time consuming as other methods.

As the pile tip level goes deeper, more force is needed to drive the pile due to the increased stresses at the tip. This limits the maximum depth of driven piles. Also driven piles are known to produce sounds and vibrations in the neighboring soil which results in possible settlements and/or damage to buildings/infrastructure.

For the driven piles both pre-cast concrete piles or steel profiles are used for driving. However, concrete is used more often due to its cheaper application and lower sensitivity to corrosion in comparison to steel. Steel however is able to resist more extreme loads. After installation these piles can be loaded under compression or tension.

## 2.2 Auger piles

Auger piles are types of piles that are constructed in-situ through the use of a soil auger. A hole with the desired pile diameter is dug out to desired depth. In some methods a steel casing is installed in the drill hole to prevent collapse of the hole. The reinforcement of the pile is lowered into the hole and concrete is poured into the hole. After the pouring of concrete, the steel casing is removed and the concrete is compacted and cured. This method is very flexible in both desired pile length and amount of piles. This installation method also causes very little nuisance in terms of vibrations and noise. The construction of the auger piles is more time consuming than driven piles due to construction process including the drilling and the need of in-situ curing of concrete.

As mentioned, the auger piles are more flexible in design such as pile length and amount of piles, but generally the bearing capacity of the pile is lower than driven piles because the soil is not compacted in the driving process and the stresses around the pile are generally lower.

## 2.3 Combined methods

Lastly there are methods for foundation piles that combine the driven and cast methods. Two methods that are commonly applied are the Vibro and Vibro-combination method. The Vibro method includes driving a steel tube with a detachable closed-end to a desired depth in the subsoil. In this steel tube, reinforcement steel is installed and concrete is poured. After the pouring of concrete, the closed end of the steel tube is detached from the steel tube and the tube is driven out of the ground. This assists in the compaction of concrete and guarantees a strong connection between the subsoil and concrete.

The Vibro and Vibro-combination methods are very similar. The main difference is that with the Vibro-combination method, instead of the reinforcement steel being installed in the steel tube, a prefab concrete pile is installed instead. High quality concrete is poured to fill the voids between the steel tube and concrete pile. This method guarantees a high quality core of the pile and is not as dependent on the quality of compaction and curing of the concrete.

This combined method profits from the benefits of both driven and cast piles. Due to the driving of the steel tube, the soil around the pile is compacted which results in higher bearing capacity of the pile. The option also exists to screw the steel tube, which results in little to no vibrations or noise during construction. This method offers a lot of flexibility in terms of pile design.

Figure 1 depicts the construction phases as explained for a tension pile according to the Vibro method.

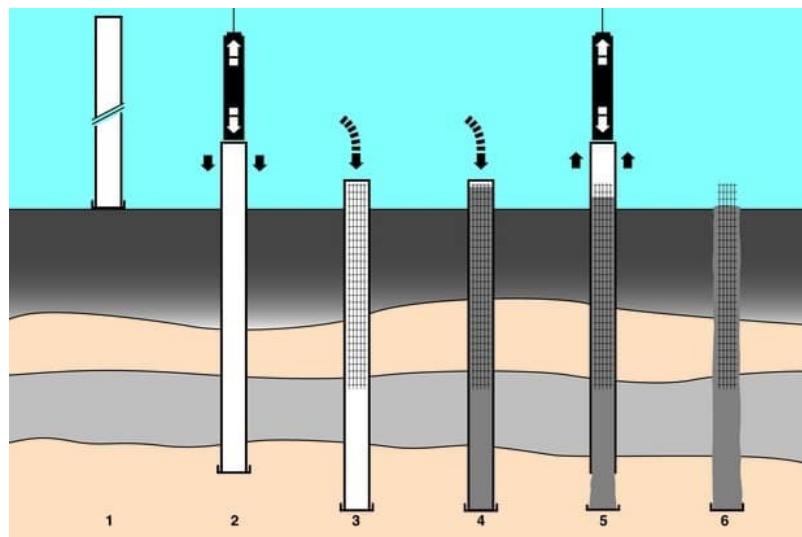


FIGURE 1: VIBRO INSTALLATION METHOD STEP-BY-STEP

### 3. Failure mechanism

The cause of the calamity that happened to the Prinses Margrietunnel was the loss of bearing capacity of the tension piles. The loss of bearing capacity happened due to the failure of the reinforcement of the tension piles caused by plastic deformation and fracture of the material. These tension piles are installed in the tunnel entrances to resist the water pressure on the tunnel. An extensive research was carried out by TNO and Deltares for Rijkswaterstaat in order to find the cause for the reinforcement of the tension piles breaking. The provisory result from this research was the occurrence of stress corrosion in the reinforcement steel of the tension piles, which ultimately led to brittle failure of the reinforcement rods.

The tension pile reinforcements installed for the Prinses Margriet tunnel have the same dimensions as those installed for the EHT. The tension piles are constructed according to the Vibro method with a steel rod as reinforcement a diameter ranging from 32 to 36 mm. The reinforcement consists of a high steel quality of QP 105 steel surrounded by concrete with a total diameter of 450 mm. (RWS directie sluizen & stuwen, 1962). The difference is the utilized corrosion protection for the steel. For the Prinses Margriet tunnel a grease coating was applied on the reinforcement, and for the EHT asphalt was used to coat the reinforcement.

#### 3.1 Background

After the calamity, it was found that some of the reinforcements of the tension piles had failed in both the northern and southern entrance of the Prinses Margrietunnel. This was discovered by uncovering the tension piles in the tunnel and loading them with a tensile force. Due to the failed reinforcements rods, the connection between the tension piles and the floor of the tunnel element vanished. Since only one rod was installed per tension pile, this meant that the total bearing capacity of the tension pile was lost due to the failure. The loss of tensile bearing capacity resulted in the uplift of tunnel elements.

Research has been carried out for the cause of the failure of the reinforcements by TNO and Rijkswaterstaat. This was done by removing the reinforcements from the tension piles and analyzing them in the laboratory of TNO. The rods have been inspected visually and the fracture surfaces in steel have been researched through fractography and metallography. This in order to find the cause of the breakage of the reinforcements.

Figure 2 shows an example of the fracture surface of a reinforcement. The darker areas of the surface in the figure show the initial corrosion areas of the section. It is expected that these corrosion areas eventually led up to the brittle fracture of the rod section.



FIGURE 2: FRACTURE SURFACE OF STEEL REINFORCEMENT (BORSJE & SCHURING, 2023)

Extensive research has been done on these fracture surfaces by TNO and it was stated that all the reinforcements showed a similar failure mechanism. Different factors that could have caused this failure mechanism have been considered by TNO.

The research showed that the probable cause for the breakage of the steel rod was stress corrosion induced by a base environment induced by lye. This conclusion was motivated by the nature of the development of the fracture in steel and the presence of secondary fractures in the rod above the fracture surface. (Borsje & Schuring, 2023) The next section will focus mainly on this phenomenon.

### 3.2 Corrosion in steel

When constructing in the subsurface, corrosion is a relevant failure mechanism. Corrosion in soils, or underground corrosion is applicable to a wide range of different components in civil engineering such as pipelines, steel sheet piles, storage tanks and most importantly for this research, the reinforcement of underground objects such as ground anchors and foundation piles. In the soil, the materials are exposed to a wide range of different conditions imposed by the soil which can result in different types of corrosion. The consideration of a civil engineering object subjected to corrosion must address the constituent of corrosion present in the soil site, which can either be induced by naturally present constituents or contaminated by human processes. Also the utilized material which is in the subsoil should be considered. (Martin & Bastidas, 2022)

This research will focus on one specific type of corrosion, namely stress corrosion. This type of corrosion is researched and assumed to be the constituent for the incident that happened to the Prinses Margriet tunnel as mentioned in the introduction. Added to the corrosive environment of the soil site and the utilized material of the object, stress corrosion is also caused by the presence of tensile stress in the material. This makes up a total of three main constituents of stress corrosion happening in civil engineering objects in the subsoil.

Stress corrosion in itself is a corrosion mechanism that can lead to unexpected failure of metal alloys subjected to a tensile stress when not monitored properly. The tensile stresses in the material cause very small cracks which propagate due to the presence of a corrosive environment in the subsoil. This process degrades the material. In the case of reinforcement rods applied in the tension piles, the propagation of cracks within the material causes a decrease of effective cross section. The decreasing cross section causes an increasing stress. This increase of stress could possibly reach above the designed resistance designed with the original cross section which could end up in the failure of the reinforcement rods such as brittle failure. (ASM international, 1997)

In this chapter the three main constituents of stress corrosion for underground tension piles applied are discussed. Also possible prevention and detection methods for the case of a tension pile installed in the subsoil are analyzed. For stress corrosion to initiate, the following constituents should all be present.

*Utilized material should be susceptible to corrosion*

There are many different materials that are susceptible to corrosion. Ferrous alloys such as various types of iron, steel, aluminum, etc. are subject to various types of corrosion in the subsoil.

For the type stress corrosion specifically, generally higher quality types of steel are more susceptible. This is due to the higher quality steel type allowing a higher tensile stress in the material, which in turn increases the amount of cracking in the steel, which in turn increases the chance of corrosion propagating. Also the microstructures of these types of steel are more sensitive to external influences causing corrosion, increasing the probability of corrosion happening in the material.

Generally tension piles exist of a reinforcement rod covered in concrete reaching into the subsoil. The reinforcement rod is connected to a construction which transfers its tension forces into the tension pile. In order for the reinforcement rod to resist high tensile forces, a high quality steel is used. This means that in the application of these tension piles, the material used is susceptible to corrosion and thus is a relevant failure mechanism to analyze.

*The environment of the subsoil should be able to enable corrosion*

Presence of corrosive environments in the subsoil where a material is installed is necessary for stress corrosion cracks to propagate. These environments are constituted by the presence of acidic or alkaline substances dissolved in the subsoil. Different types of environments are able to enable and increase probability of stress corrosion occurring.

The most common types of stress corrosion induced by the environment are acidic-, alkaline and chloride stress corrosion. The presence of a high concentration of either acidic or alkaline substances in the environment is able to induce their respective stress corrosion type. High concentrations of chlorides in the subsoil environment can cause salt intrusion in the utilized material which are able to induce and accelerate corrosion. (Bylapudi, Mondal, Spearing, & Bhagwat, 2015)

An extra type of environmental assisted corrosion which is relevant is hydrogen embrittlement. The hydrogen embrittlement is relevant when hydrogen atoms from the environment are able to migrate into the utilized material, which then cause the embrittlement of the material.

The consequence of the steel being present in an environment which enables corrosion is the expected material behavior of the steel changes. This change happens due to the composition of the steel being manipulated by the hostile environment. An example for this is the embrittlement of steel. Embrittlement was for example seen in the failure patterns of the steel researched of the Prinses Margrietunnel which showed failure. Here the steel rods showed a sudden brittle failure instead of the plastic yielding behavior which is generally expected upon loading steel. This makes it very important to take the environment of the subsoil into account.

In the case of the tension piles, both the cement present in the concrete surrounding the steel rods and water from its voids create an environment that enables stress corrosion due to their alkaline nature. For this reason, the steel rods are coated by a medium such as grease or asphalt to prevent this alkaline fluid from reaching the steel. However due to imperfections in the corrosion protection coating, this alkaline environment could still develop around the steel rods, eventually leading up to stress corrosion in the steel rods. (Martin & Bastidas, 2022)

Dependent on the environment around the tension piles, there could also be acidic substances present which increases the probability of corrosion initiating and propagating.

Also due to the presence of water, hydrogen atoms could migrate into the steel reinforcement rods causing hydrogen embrittlement. Hydrogen embrittlement of steel increases the hardness values of steel and thus reduces ductility. Upon loading, this could cause the steel to skip the yielding zone and experience brittle failure.

*Amount and variation of tensile stress in the material*

The cause and speed of propagation of stress corrosion cracking is influenced by the amount of tensile stress in the utilized material. The tensile stress is the constituent of the first cracks in the material. This tensile stress originates from external loading and residual stress in the material. For example the external loading could originate from the resistant force of a tension pile connected to a tunnel floor on which a buoyant force is imposed. An example of residual stress in the material is from plastic deformation or the prestressing of the material.

On top of the amount of tensile stress in the static situation, dynamic loading also has an influence on the development of stress corrosion. This dynamic loading causes stress variations in the material. The stress variations cause fatigue in the material, which enables the cracks in the material to propagate even further.

Corrosion fatigue is relevant when the utilized material is subjected to cyclic loading. The cyclic loading causes fatigue in the utilized material, which also causes embrittlement. This embrittlement makes it more susceptible to corrosion cracking or eventually corrosion failure (Giorgini, 2024). It depends on the share of stress variation compared to the total stress whether corrosion fatigue is a relevant failure mechanism.

For the case of tension piles installed in tunnel entrances, static tensile stresses are generally very high due to the large buoyant forces on the tunnel floor which are transferred to the tension piles. Also in case the reinforcement rods are prestressed, a residual tensile stress is present. Possible stress variations for these tension piles mainly exist out of three different sources, namely traffic loads, tidal loads and thermal expansion loads. It is analyzed further on what the amounts of static stresses and stress variations are and to what extent they can cause micro cracks in the material.

Also based on the cyclic nature of the stress variations, the mechanism of corrosion fatigue should be taken into account as a component of the corrosion failure mechanism. It will be analyzed further on in this thesis to what extent the quantity of stress variations cause an influence on the initiation and propagation of stress corrosion in steel. Research done on the expected strain level of steel at which stress corrosion crack initiation happens in environments where chlorides are abundantly present showed that a strain level as small as 0.4% is sufficient to initiate stress corrosion cracks (Miller, Mintz, He, Pabalan, & Pan, 2013). This number will be used in calculations in order to assess whether the stress variations have an influence on the initiation and propagation of stress corrosion cracking.

The material in which stress corrosion cracks are able to propagate is not always observable, it is important to utilize prevention methods to the material and environment. Also detection techniques should be put in place to prevent unforeseen failure due to this mechanism. In the case of the steel reinforcement rods installed in tension pile, the material is buried in the soil beneath the tunnel floor. This makes conventional detection methods such as visual inspection very impractical. However there are methods which make the detection of stress corrosion in the subsoil possible.

The three constituents of stress corrosion as discussed above all contribute to the probability of stress corrosion cracking initiating and/or propagating. A combination of all three constituents is required. However it depends to what extent the constituent is present in order to determine its effect on stress corrosion occurring. This means for stress corrosion to initiate; a susceptible material should be used, which is installed in a corrosive environment and is loaded with high tensile stress. A more susceptible material, or a more corrosive environment or a higher tensile stress will increase the probability of stress corrosion occurring.

### 3.2.1 Prevention & detection methods

The studies by TNO have shown that stress corrosion is a very probable cause for the failure of the tension piles. For the maintenance of the tunnels with a similar tension pile foundation method, it is relevant to research both prevention and detection methods for stress corrosion in the tension piles. This in order to control the risk of unexpected brittle failure of the steel rods by detecting the corrosion beforehand and putting prevention or mitigation in place before the failure takes place.

#### 3.2.1.1 Prevention

In materials engineering, stress corrosion is a known species of corrosion. Hence many ways to prevent this type of corrosion have been researched. The works by done on stress corrosion cracking (Jones, 2017) suggest various methods to prevent stress corrosion on steel elements. For each method, the feasibility for usage on the tension piles is analyzed.

##### *Preliminary design*

In the specific case of the tension piles a prevention method is to design the tension piles with materials that are not susceptible to stress corrosion in the given environment. For this the presence of stress corrosion agents in the environment should be researched. An alternative is to neutralize corrosive agents in the subsoil before the construction of the tension piles are initiated.

##### *Lowering/changing tensile stress*

In the case the tension piles with susceptible material are already installed in the subsoil and the corrosion agents are not able to be neutralized, a possible prevention method is to reduce the amount of static stress and stress variation on the material. The static stress can be reduced by creating extra support structures on the main construction which relieve the tension piles of their stress by for example installing more tension piles. The possibility of reducing of stress variations are dependent on the source of the dynamic loading. For the previously discussed main three dynamic loads on tunnel entrances, reduction methods are available but very costly. The magnitude of these dynamic loads should be determined first in order to conclude if reduction of these loads will be effective.

##### *Cathodic protection*

Cathodic protection is a method where corrosion of metals in the subsurface is prevented by obstructing the outflow of electrical current out of the anodic locations (Mink, 1975). In terms of the steel rods, it could be made fully cathodic by connecting an electrical circuit to a more base metal, which becomes the anode in the circuit. If it can be stated that a steel rod is still intact, cathodic protection could be a worthy measure to prevent or slow down stress corrosion from happening

##### *Inhibitors*

Inhibitors are mediums that are able to influence the environment around the steel rod to reduce stress corrosion cracking propagation of the steel. However it would be difficult to get the medium around the steel rod and keep it there, due to for example leakages in the concrete. The inhibitor is able to neutralize the acidic environment around the steel rod, which could prevent or slow down the propagation of stress corrosion.

##### *Coating*

To protect the utilized material from external corrosive agents, a protective coating may be used. For this coating, many different materials viable materials exist. Coating is achieved through applying a protective layer to the material sensitive to corrosion, effectively separating it from the environment. The coating method for corrosion protection is used in both the tension piles of the Prinses Margriet tunnel and the EHT. For the Prinses Margriet tunnel, grease was used to coat the prestressing rods. For the EHT asphalt was used. No big difference between the performance of these coating agents are known as of yet and it is assumed that they are able to protect from corrosion as long as they provide full coverage on the steel.

TNO expects that the stress corrosion in the steel rods took place through the coating because of imperfect application around the steel rods. It is recommended that this phenomenon is analyzed further (Borsje & Schuring, 2023).



These preventive measures could also be used as corrective measures to the existing tension piles in order to protect them from stress corrosion.

### 3.2.1.2 Detection

One of the bigger challenges in the research of the breakage of steel rods is the detection of stress corrosion before brittle failure has happened. This in order to be able to control the risk more. This chapter will go over some stress corrosion detection methods in steel. These methods could be used to gain insight into the amount of steel rods that have actually failed in the foundation of the tunnels.

Since visual inspection is quite impractical for the detection of stress corrosion cracking of underground tension piles, other detection methods are developed in order to do this inspection. These detection methods are either destructive or non-destructive.

The non-destructive methods are more interesting in existing construction as it does not require the tension piles to be destroyed.

#### *Pile load testing*

The most common destructive detection method for tension piles is performing a pile load test to its design pile load. If the pile would fail prematurely, it can be assumed that the early failure happened due to stress (or some other type of) corrosion cracking.

Further detection methods are considered that adhere to nondestructive evaluation.

#### *Ultrasonic detection*

The ultrasonic detection is a way to find cracks caused by stress corrosion in steel using high frequency loading. This method can either be carried out through the usage of a laser or sound waves. A transducer is used to send the high frequency waves through the material. These waves are reflected when they encounter an anomaly in the material such as a crack or void. By analyzing the return time of these waves, the presence of stress corrosion can be determined.

In research done on ultrasonic detection (Hernandez-Valle, Clough, & Edwards, 2014), an experiment was carried out which analyzed whether ultrasonic detection could be used for the detection of stress corrosion cracking in steel. In this experiment, a laser scans along the surface of the steel sample and through time-frequency analysis of the generated wave modes of the laser, it is determined whether stress corrosion cracks are present in the steel. Figure 3 shows the results of this experiment. It can be seen that the defect in the material is identified through this experiment. This shows the effectiveness of the method for very small cracks which are not observable by the naked eye.

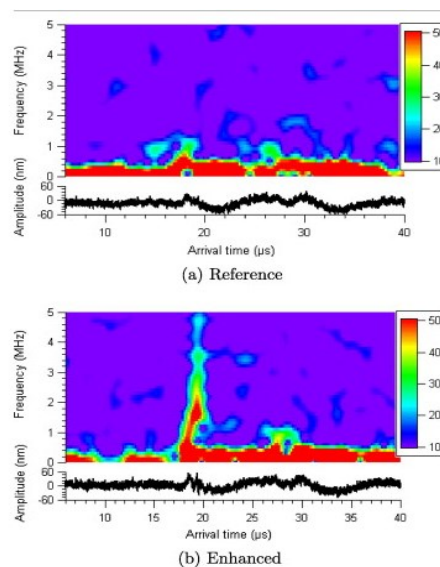


**FIGURE 3: CORROSION DETECTION USING ULTRASONIC DETECTION (HERNANDEZ-VALLE, CLOUGH, & EDWARDS, 2014)**

This detection method could be relevant as a use for detecting stress corrosion in the steel rods. However, a large downside is that the steel surface has to be analyzed, which means the steel rods have to be removed from the subsoil in order to analyze them. This detection method cannot be performed in situ, as the concrete and subsoil surround the steel rod which block the laser.

#### *Acoustic emission*

A method to detect stress corrosion in steel is the acoustic emission technique. This technique is defined as the class of phenomena whereby transient elastic waves are generated by the rapid release of energy from localized sources within a material' (Ramadan, Gaillet, Tessier, & Idrissi, 2008). The method involves detecting acoustic signals from a pre-stressed steel element undergoing stress corrosion. From the acoustic response can be detected whether there may be cracks forming. This method is a continuous method, and thus can be seen as a monitoring method.

An experiment was carried out on a pre-stressed steel cable in a highly alkaline environment. The goal was to analyze whether stress corrosion is detectable using acoustic emission. Figure 4 depicts the results of this experiment.

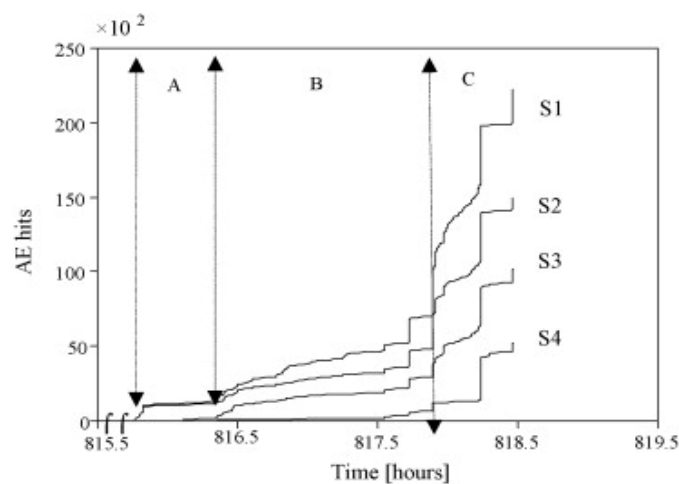


FIGURE 4: CORROSION CRACKING DETECTION USING ACOUSTIC EMISSION (RAMADAN, GAILLET, TESSIER, & IDRISSE, 2008)

After a total of 815 hours, significant change in accumulated acoustic activity was seen in the experiment. This acoustic activity is depicted on the y-axis. Zone A, B and C in the figure are depicted as the initiation, propagation and failure zone respectively. It can be seen that after 815 hours of no activity, the total failure of the sample took place in only three hours.

Because detection of the crack initiation to failure of the sample happens so suddenly, this method is not very suitable for monitoring tension piles continuously. However this method could be useful to detect whether a steel rod has failed already, but for this the acoustic emission must have been measured before the stress corrosion causes breakage of the steel rods (Djeddi, Khelif, Benmedakhene, & Favergeon, 2013).

#### *Electrochemical impedance*

Electrochemical impedance spectroscopy is a method which can be used to detect stress corrosion cracking in steel samples. Impedance is a measure of resistance and reactance of a circuit. It is used to characterize how a circuit responds to signals with alternating current. An electrical circuit can be set up with a steel element possibly subjected to tension corrosion included. Targeted research on electrochemical impedance on stress corrosion (Bosch, 2005) has made such a setup.

Their main findings were that the phase shift of two different similar samples at certain imposed frequencies could be related to the presence of stress corrosion cracking. For the steel rods of the tension piles, if it is able to be included in an electrical circuit, impedance measurements can be performed on it. This method could be used to locate stress corrosion cracks in the steel rods. More research should be done on how the impedance measurements could be used for the identification of stress corrosion cracking.

## 4. Capacity determination tension piles

Throughout the years, much research has been carried out in order to determine the geotechnical capacity of a tension pile in the world. For the Netherlands specifically, from 1991 onwards, the findings of this research have been collected in the form of the NEN-norms (NEN, 2023).

This chapter will give an overview of the development of the available design methodologies for the capacity of tension piles in the Netherlands. There are three main time periods. The first period is before the first geotechnical NEN-norm, in which the EHT was designed. The second period is when the first NEN norm came out. The third period is when the Eurocode 7 was published, with a national appendix for the Netherlands in which the previous knowledge from the NEN norms was applied. The overview includes a background summary of the applicable norm, the calculation method for tension pile capacity and applicable safety factors for calculated characteristic values.

Furthermore applicable tension pile capacity determination methodologies are touched upon, and their suitability for utilization in the Netherlands and especially the case study of EHT is discussed.

### 4.1 Dutch methods throughout the years

#### 4.1.1 Before 1991 – Grondmechanica Delft

In the period before 1991, there were no normative or publicly accepted calculation methods for determining the geotechnical capacity of a tension pile. There were models which could determine the capacity, but there was still a lot of uncertainty about the outcome as the models were not validated sufficiently. To solve this, generally a relatively high global safety factor was used on the calculated capacity of the tension pile in order to address this uncertainty (van Noortwijk, Everts, & Janse, 1994).

Grondmechanica Delft (now Deltares) was responsible for the calculation and design of the tension pile foundation of the EHT. Since the EHT is the relevant case for this research, the calculation method and applied safety factors for the tension piles used by GD at the time are reviewed.

A calculation method used for determining the geotechnical capacity of the tension piles in this period was the so called  $q_c$ -method. The  $q_c$  value is obtained by measuring the resistance on the cone tip of a cone penetration test (CPT). CPT's are relatively easy to carry out in Dutch subsoil. Because of this, the  $q_c$ -method was regularly used in this period in the Netherlands. The geotechnical capacity of the tension pile is obtained from this  $q_c$  value (van Noortwijk, Everts, & Janse, 1994).

$$T_{pile} = \alpha_s * q_c * O * L$$

Where  $T_{pile}$  is geotechnical capacity of a single pile and  $\alpha_s$  is an empirical value that is determined through the test loading of tension piles. The correction factor  $\alpha_s$  is dependent on the installed pile type and soil type.  $O$  is the circumference of the pile and  $L$  is the length of contact surface between pile and ground layer.

The effect of piles in a group was accounted for by taking into account the effective weight of the soil clod surrounding a single pile. The geotechnical capacity of a single pile should not exceed this value. The soil clod around the tension pile is assumed to be shaped as a silo. The effective weight of this shape is calculated through the following formula. (Stam & van der Poel, 1994)

$$G_{clod} = a * b * \sigma'_{v,z=h} - \frac{\gamma'_{sat} * a * b * (\sqrt{a * b} - 1.5 * d)}{3 * \tan(\varphi')}$$

Where  $a$  and  $b$  are the horizontal and vertical center-to-center distances of the pile plan,  $\sigma'_{v,z=h}$  is the vertical effective stress at the pile tip level,  $\gamma'_{sat}$  is the effective volumetric weight of the soil at the pile tip level,  $d$  is the diameter of the pile and  $\varphi'$  is the effective internal friction angle of the soil at pile tip level.

A partial safety factor of 1.2 is applied to the weight of the soil clod. This means the weight of the soil clod must be equal to at least 1.2 times the geotechnical capacity of a single tension pile in order to satisfy this condition.

The schematization of the silo shaped soil clod is shown in Figure 5.

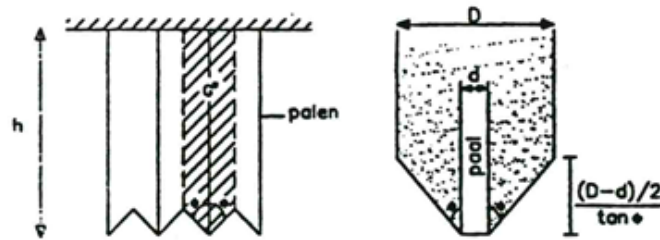


FIGURE 5: SILO SHAPED SOIL CLOG DIMENSIONS (VAN NOORTWIJK, EVERTS, & JANSE, 1994)

It is not known whether there were more influences accounted for in the calculation design of the tension piles of the EHT. The calculation reports of this tunnel have not been made publicly available.

It is known that for the tension pile design of the EHT an overall safety factor of 2.5 was used. The calculated capacity of the tension pile is divided by this overall safety factor in order to obtain the design value for the tension pile foundation (Stam & van der Poel, 1994).

In 1974, an installed tension pile foundation of Verolme-Dok in the Netherlands failed. The foundation capacity was recalculated and the overall safety factor was calculated to be 1.7. Still the foundation failed, this showed that the calculation models for tension pile foundations at the time were not adequate (van Noortwijk, Everts, & Janse, 1994).

The unexpected failure resulted in the initiative of more research in tension piles and possible influences on the calculated geotechnical capacity of the piles. In this period, a lot of extra research was carried out in geotechnical engineering. The findings of this research resulted in the development of the first norm relevant for geotechnical engineering in the Netherlands.

#### 4.1.2 1991-2005: TGB 1990 + NEN 6740 series + CUR 98-9

The first NEN-norm that was relevant for geotechnical engineering in the Netherlands was the NEN 6740:1991. This NEN norm was based on the 'TGB 1990 – Geotechnical engineering' norm, which is an abbreviation for 'Technische Grondslagen Bouwen (Technical basis for building)'. A supplement to the NEN6740 is the NEN6743, this NEN norm goes into detail on the design and safety philosophy of foundation piles in compression. There were no calculation rules or models available in the norm for the design of tension piles.

The NEN 6740 norm however, did give partial safety factors for the geotechnical capacity of tension piles. The norm also introduced a correction factor based on the amount of piles in the foundation and the amount of CPT-tests performed. This correction factor  $\xi$  should be multiplied with the calculated capacity of a single tension pile. Table 2.2.1 shows the distribution of quantities for this correction factor (NEN 6740, 1991).

TABLE 1: CORRELATION FACTOR BASED ON M TENSION PILES AND N CPT'S (NEN 6740, 1991)

M	N						
	1	2	3	4	5	10	>10
1	0,75	0,78	0,79	0,80	0,81	0,82	0,83
2	0,78	0,81	0,83	0,83	0,84	0,86	0,87
3-10	0,81	0,84	0,86	0,87	0,87	0,89	0,90
>10	0,82	0,86	0,87	0,88	0,89	0,91	0,92

The partial safety factor  $\gamma_{m,b}$  for a tension pile in the NEN6740 is equal to 1.4. This is a large decrease from the overall safety factor of 2.5 that were applied for the tension piles of the EHT in 1970.

The design geotechnical capacity of the tension pile is calculated using the following formula.

$$T_{pile,max,d} = \xi * \frac{T_{pile,max}}{\gamma_{m,b}}$$

In 2001, CUR 2001-4 – Design rules for tension piles was issued. In this report, a multi-step plan is proposed to design the geotechnical capacity of a tension pile. This design method builds on the earlier mentioned  $q_c$ -method. The updated version of the NEN 6740 that came out in 2006 refers to this CUR report to calculate the bearing capacity of tension piles (CUR98-9, 2001).

This report was issued because there was no consensus in the different available calculation methods for the geotechnical capacity of tension piles, while tension piles are commonly applied for foundations in the Netherlands. In the calculation model presented by the CUR 2001-4, two different criteria are tested. These two criteria are the mobilization of sleeve friction along the circumference of a single tension pile and the mobilization of self-weight of soil around the tension. (CUR98-9, 2001)

The calculation method for the geotechnical capacity of a tension pile following the CUR 2001-4 is derived from the proposed method for the capacity of a pile under compression from the NEN6743. The correction factor for shaft friction in compression  $\alpha_s$ , which is dependent on the pile installation method is used in the NEN6743 to calculate shaft friction in compression. In the CUR calculation model, a new correction factor  $\alpha_t$  is introduced, which is the same correction factor for shaft friction, but meant for shaft friction under tension. The  $\alpha_t$  value is generally lower than the original  $\alpha_s$  value. The values for  $\alpha_t$  were obtained by performing tension pile tests for different pile installation types. Table 2 shows some  $\alpha_t$  values for different pile installation types. The pile type used for the EHT is the ‘vibro- en vibrocombinatiepalen’.

TABLE 2: ALPHA VALUES FOR DIFFERENT PILE INSTALLATION TYPES (CUR98-9, 2001)

paaltype	gemiddelde $\alpha_t$	variatiecoëfficiënt
prefab beton	0,0071	0,33
stalen palen met gesloten punt	0,0082	0,38
vibro- en vibrocombinatiepalen	0,0148	0,25
stalen palen, weinig grondverdringend	0,0046	0,34
MV-palen	0,012	0,36

In the CUR 2001-4, the effects of installing piles in a group are incorporated in the formula for the geotechnical capacity of a tension pile. Here both the compaction of the soil due to installation and the decrease of vertical effective stress due to tensile stresses from the pile are taken into account. These effects are represented in the constants  $f_1$  and  $f_2$  respectively. The geotechnical capacity of a single tension pile following the CUR 2001-4 is done through the following formula.

In the CUR 2001-4, the effects of installing piles in a group are incorporated in the formula for the geotechnical capacity of a tension pile. Here both the compaction of the soil due to installation and the decrease of vertical effective stress due to tensile stresses from the pile are taken into account. These effects are represented in the constants  $f_1$  and  $f_2$  respectively. The geotechnical capacity of a single tension pile following the CUR 2001-4 is done through the following formula.

$$F_{r,trek,d} = \int_0^L q_{c,z,d} * f_1 * f_2 * O_{p,z} * \alpha_t dz$$

Where  $F_{r,trek,d}$  is the design value for the geotechnical capacity of a tension pile,  $L$  is the total length of the pile,  $q_{c,z,d}$  is the adjusted value for the cone resistance at relevant depth, constants  $f_1$  and  $f_2$  account for the influence of piles in a group,  $O_{p,z}$  is the circumference of the pile and  $\alpha_t$  is the correction factor based on pile installation type as earlier mentioned.

The constants  $f_1 * f_2$  are only relevant for sandy soils. For cohesive soils like clay or peat, these factors should be set equal to 1;  $f_1 = f_2 = 1$ .

The adjusted value for cone resistance is obtained by adjusting the measured cone resistance from a CPT. The first adjustment is based on the OCR value of a soil layer. The measured cone resistance  $q_{c,z}$  should be adjusted according to the following formula.

$$q_{c,z,NC} = q_{c,z,OC} * \sqrt{\frac{1}{OCR}}$$

Then, the newly obtained  $q_{c,z,NC}$  should be adjusted for the excavation of the structure, this adjustment is done through the following formula.

$$q_{c,z,ontgr} = q_{c,z,NC} * \frac{\sigma'_{v,z,ontgr}}{\sigma'_{v,z,0}}$$

The ratio of effective stresses is obtained by dividing the effective stress distribution in the soil after excavation by the original effective stress distribution in the soil before excavation. The  $q_{c,z,ontgr}$  should be limited at 15 MPa if a layer has a  $q_{c,z,ontgr}$  value larger than 15 MPa for more than 1 meter. The value should be limited at 12 MPa if it holds a value larger than 12 MPa for less than one meter.

The design value of  $q_{c,z,ontgr}$  is calculated by incorporating the safety and correlation factor using the following formula.

$$q_{c,z,d} = \xi * \frac{q_{c,z,ontgr}}{\gamma_{m,var,qc} * \gamma_{m,b}}$$

$\gamma_{m,var,qc}$  is a factor dependent on the nature of loading, for static loading, this factor is 1. For varying loads, this factor is calculated using the difference between acting varying forces on the soil. The values of the correlation and safety factors are the same as in the NEN 6740. Namely  $\gamma_{m,b} = 1.4$  and  $\xi$  is found using the Table 1 based on number of piles and CPT tests performed. The values of the factors are the same, but in the CUR the factors are applied on the measured and adjusted  $q_{c,z,ontgr}$ , not on the calculated geotechnical capacity of the tension pile  $T_{pile,max}$ . The application of the factors on the  $q_{c,z,ontgr}$  results in more accuracy approximating the eventual geotechnical capacity of the tension pile.

Factor  $f_1$  incorporates the effect of installation of the pile on the  $q_{c,z,d}$  value in sand. The factor is calculated through the change in relative density of the sand using the following formula.

$$f_1 = e^{3*\Delta Re} \text{ with } \Delta Re = \frac{\sum_1^n \Delta e}{(e_{max} - e_{min})} \text{ and } \sum_1^n \Delta e = -\frac{(r-6)}{5.5} * \frac{(1+e_0)}{50}$$

With  $\Delta Re$  being the change in relative density. This value is calculated through the relative change of void ratio in the soil sample. The value  $r$  is the center-to-center distance to the closest pile in a pile group.

Factor  $f_2$  incorporates the effect of the tension force exerted by the pile on the soil on the  $q_{c,z,d}$  value in sand. The factor is calculated per distinguished layer of the soil profile.

$$f_{2,i} = \frac{-M_i + \sqrt{M_i^2 + (2 * \sigma'_{v,d;j;0} + \gamma'_{d,i} * d_i) * (2 * \sigma'_{v,d;j;0} + \gamma'_{d,i} * d_i - 2 * \sum_{n=0}^{i-1} T_{d,n})}}{(2 * \sigma'_{v,d;j;0} + \gamma'_{d,i} * d_i)}$$

With  $M_i$  being a factor per layer calculated using the formula:

$$M_i = \frac{f_{1,i} * O_{p,i} * \alpha_t * q_{c,d,i} * 1000 * d_i}{A}$$

Once the factors  $f_{2,i}$  and  $M_i$  have been calculated per layer, the total geotechnical capacity of a single pile in a group can be calculated by summing up the shaft friction force per acting layer  $i$ .

$$F_{r,trek,d} = A * \sum_{i=1}^m M_i * f_{2,i}$$

In this formula,  $A$  is the effective area in which the tension pile acts. For a regularly spaced pile plan, this is the squared product of the center-to-center distance. The maximum value for  $F_{r,trek,d}$  is limited by the clod criterium as earlier mentioned in the directives by Grondmechanica Delft. The clod criterium in the CUR 2001-4 is calculated through the following formula. The volumes of the soil clod are schematized in Figure 5.

$$F_{r,trek,max} = (V_{cone} + V_{cylinder}) * \gamma'_d \text{ with } \gamma'_d = \frac{\gamma'}{\gamma_{m;g}}$$

Below excavation level, a partial safety factor is applied to the soil weight of  $\gamma_{m;g} = 1.1$ , because the soil weight has a favorable effect for the tension piles (CUR98-9, 2001).

Finally, the self-weight of the tension pile should be added to the total capacity of the pile  $F_{r,trek,d}$ . This self-weight is calculated through:

$$G_{pile} = V_{pile} * (\frac{\gamma_{pile}}{\gamma_{m;g}} - \gamma_{water})$$

Using this calculation scheme, the geotechnical capacity of a single tension pile standing alone or in a pile group can be calculated. The CUR report is used widely in the Netherlands for the calculation of tension piles. Because of this, an initiative was taken to combine the existing NEN 6740 norm with the CUR 2001-4 report. When the Eurocodes, which are building norms relevant for Europe, were set as normative in the Netherlands following Bouwbesluit 2012 (BWT, 2012) a Dutch annex for this Eurocode came out in which the NEN 6740 and CUR 2001-4 among some other reports were incorporated.

#### 4.1.3 2005 – present – Eurocode 7 + Dutch Annex NEN 9997-1

The Eurocode 7 for geotechnical engineering officially was released in 2005. But as earlier mentioned, was not implemented as normative for application in the Netherlands until the Bouwbesluit 2012. In the original Eurocode 7, no calculation method for the geotechnical capacity of a tension pile was included. However with the Dutch Annex of Eurocode 7 which first came out in 2009 called NEN 9997-1, the calculation method originating from the CUR 2001-4 report was included. This calculation method has not been changed from the original 2001-4 report in the current version of the NEN 9997-1 (NEN 9997-1, 2023).

In this norm, the definition of  $\alpha_t$  makes distinction between sandy soils and soft soils in addition to the used pile type. Table 3 contains the values of  $\alpha_t$  for sand and  $\alpha_t$  values of soft soils.

**TABLE 3: ALPHA VALUES FOR DIFFERENT TYPES OF INSTALLATION PILES AND SOILS (NEN 9997-1, 2023)**

Paalttype			Paalklassefactor <sup>a</sup>		
Type	Nadere specificatie	Wijze van installeren	$\alpha_p$	$\alpha_s$	$\alpha_t$
Beton-paal	Geprefabriceerd; met constante dwarsafmeting	Geheid	0,7	0,010	0,007
	In de grond gevormd met een gladde mantelbuis op een voetplaat, waarbij het beton direct tegen de grond drukt	Geheid; de mantelbuis wordt terugheind in combinatie met statisch trekken uit de grond verwijderd; de voetplaat blijft in de grond achter	0,7	0,014	0,012
	In de grond gevormd met een gladde mantelbuis op een voetplaat, waarbij het beton direct tegen de grond drukt	Geheid; de mantelbuis wordt trillend in combinatie met statisch trekken uit de grond verwijderd; de voetplaat blijft in de grond achter	0,7	0,012	0,010

Grondsoort	$q_{c,gem}$ MPa	$\alpha_s$ en $\alpha_t$
Klei	$\geq 2,5$	$\leq 0,03$ <sup>a</sup>
	$\geq 2,0$ en $< 2,5$	$0,02 \times (q_{c,gem} - 1)$
	$< 2$	$\leq 0,02$ <sup>a</sup>
Sterk zandige leem		Wrijvingsgetal <sup>b</sup> met een maximum van 0,025
Zwak zandige leem		0,025
Veen		0

In the original Eurocode 7, the partial safety factors are given in Annex A. These are sets of partial factors which are used for the assessment of a geotechnical structure. The partial safety factors for the tension pile capacity ( $\gamma_{m,b}$ ) of these sets range from 1.1 to 1.6. This is quite a broad range. In the latest Dutch version of the Eurocode 7, NEN 9997-1, this Annex containing partial factors is replaced by a Dutch version. In this case the partial safety factors for tension pile capacity ranges from 1.25 to 1.35. Where 1.25 is applicable for a tension pile which has been load-tested and 1.35 for a tension pile which geotechnical capacity has been determined using soil tests. This is a slight decrease from the partial safety factor of 1.4 from the previously applicable NEN 6740 series (CUR98-9, 2001) (NEN 6740, 1991) (NEN 9997-1, 2023) (Eurocode7, 2006).

Furthermore application the correlation factor  $\xi$  is changed compared to the CUR 2001-4. The value  $q_{c,z,d}$  is calculated in the NEN 9997-1 as follows:

$$q_{c,z,d} = \frac{q_{c,z,ontgr}}{\gamma_{m,var,qc} * \gamma_{m,b} * \xi_4}$$

Here the correlation factor  $\xi_4$  is relevant for the determination of geotechnical capacity of a tension pile based on soil tests. This value is dependent on the amount of performed CPT tests. The values can be found in Table 4, where  $n$  is the number of CPT tests performed.

TABLE 4: CORRELATION FACTORS FOR N CPT'S (NEN 9997-1, 2023)

<b>Correlatiefactoren <math>\xi</math> voor een stijf bouwwerk</b>							
<b><math>\xi</math> voor <math>n =</math></b>	<b>1</b>	<b>2</b>	<b>3</b>	<b>4</b>	<b>5</b>	<b>7</b>	<b>10</b>
$\xi_3^a$	1,26	1,20	1,18	1,17	1,17	1,15	1,14
$\xi_4^a$	1,26	0,96	0,94	0,93	0,93	0,92	0,91
<sup>a</sup> De factor 1,1 volgens NEN-EN 1997-1+C1+A1:2016, 7.6.2.3 (7) is al verwerkt in de factoren van tabel A.10b.							

A timeline of the applicable global, partial and correlation factors throughout the years is shown in Table 5.

TABLE 5: HISTORICAL TIMELINE OF GLOBAL AND PARTIAL SAFETY FACTORS IN DUTCH NORMS

Type	Before 1991 (GD)	1991-2005 (NEN 6740)	2001-2005 (CUR 2001-4)	2005-present (NEN 9997-1)	
Global safety factor		3	1.4	-	-
Partial safety factor		-	-	1.4	1.35
Partial safety factor		1.2	1.1	1.1	1.1
Correlation factor for $N_{\text{cpt}} = 10$		-	0.83-0.92	0.83-0.92	0.91

Using the latest mentioned calculation model for the geotechnical capacity of a tension pile and its and safety factors, the tension pile foundation of the EHT is recalculated. The results of this analytical method will follow in the Chapter 7.2. This capacity of a single tension pile alone and in a group is recalculated using the newest available code applicable for the Netherlands, which is the NEN9997-1.

This calculation scheme to obtain the pull out resistance for a single tension pile or tension piles in a group is incorporated in the software DFoundation made available by Deltares. This software could be used in order to determine the pull out resistance relevant for the chosen case study following the latest applicable norms relevant for the Netherlands.



## 4.2 Other methods

In Europe generally the Eurocodes with respective national annexes are used to design and assay different kinds of constructions as explained in the previous chapter. Outside of the Eurocodes however, different methods exist for design of a tension pile. This chapter will delve into alternative design methods for the capacity of a tension pile that are used in practice. Their applicability is also analyzed for the situation in the Netherlands.

### 4.3.1 Empirical methods

Empirical methods for determination of pull out capacity of tension piles are based on observed data originating from performed experiments and/or field tests.

The most straightforward empirical method that is used is the pull-out test for tension piles. In this test, a tension pile is installed in the ground and it is loaded in tension by for example a hydraulic jack. The exerted tension force is measured and if the pile tip reaches a certain heave, the tension loading is stopped and the pull out capacity is determined by the exerted tension loading on the tension pile.

This is a quite simple and effective method to get an idea of the pull-out resistance of tension piles, as long as the pull out tests are performed at the projected location of the to-be installed tension piles. A limitation of this method however is that it is quite time consuming and expensive. For the case study EHT, these pull-out tests were performed on the relevant site. This information will be used in the parametric study of the calculated capacity of the tension piles in a further chapter.

### 4.3.2 Semi-empirical methods

By combining empirical research and correlations through theory, semi-empirical methods are developed. As the name suggests, these semi-empirical methods combine existing correlations between soil-pile parameters with empirical data performed on the capacity of the tension pile. The empirical data is generally represented in the formula as a factor. Two known examples of semi-empirical methods in tension pile practice are the  $\alpha$  and  $\beta$  methods.

This semi empirical method uses of correlation between parameters relevant to the tension pile capacity to be calculated. The  $\alpha$  and  $\beta$  methods are relevant for piles in cohesive and granular soils respectively (Tomlinson & Woodward, 2008);

$$F_{r,trek,max} = \alpha * c_u * A \text{ (cohesive soils)}$$

$$F_{r,trek,max} = \beta * \sigma'_v * A \text{ (granular soils)}$$

An advantage of using this method is that it is easy to calculate as long as the  $\alpha$  and  $\beta$  parameters are estimated correctly and the other soil parameters are known. Different proposals have been done in order to estimate the empirical parameters  $\alpha$  and  $\beta$ . This is however out of scope for this research, as the methods are deemed too simple to model pile soil interaction compared to the method described in Chapter 4.1

The outcome of the formulas are easy to interpret and does not consume a lot of time. A limitation however is also its simplicity. In the design of a tension pile plan more complexity is generally desired to model the soil-pile interaction more accurately. The simplicity of this method is a limitation.

A more rigorous method to accurately model pile-soil interaction and the pull out capacity of the pile is the use of a numerical method. The possibility of applying numerical methods to determine pull out capacity of a tension pile is explained in the following chapter.

## 5. Numerical design

In addition to the analytical, empirical and semi-empirical methods discussed in the previous chapter, another more accurate but rigorous method exists to estimate the axial capacity of a tension pile. This method is the numerical method. The most common numerical analysis methods are Finite Element Method (FEM) and the Finite Difference Method (FDM). The main difference between one another is that the FEM is regarded as superior for handling complex geometries and non-linear material behavior. FDM is more suitable for time-dependent or dynamic problems and performs best when the geometry of the problem is relatively simple. (Zienkiewicz, Taylor, & Zhu, 2013)

Regarding the scope of this specific research, where the complex geometry of the tunnel element and its tension pile foundation is modelled, FEM seems more suitable than FDM. Also the main interest of this specific research scope is the pull-out resistance of the tension piles in the static domain. Time dependency and dynamic effects are assumed to be neglected for the simplicity of modelling purposes. For this research, the application of the FEM to perform a numerical analysis on the tunnel element and its foundation piles is analyzed.

The FEM is used to model soil-structure reactions through stress-strain relationships in complex geometries such as a tunnel element with a tension pile foundation. The finite element method is a numerical calculation method which takes into account complex geometry and more complex stress strain relationships of soil-structure interaction, as opposed to the analytical methods which are simplified to make calculation by hand possible. Also the analytical methods are not able to encompass the interaction of the different elements that make up a structure, instead the different components of the structure are discretized and treated as separate components. Their interaction of the different components are not taken into account in the analytical method. The numerical method however, is able to do this and thus is able to give a better approximation in the simulation of the actual behavior of a structure.

The FEM is incorporated in many different software packages which are able to carry out the analysis on a defined geometry and soil stratigraphy. The most commonly used software packages in research based on the modelling of the pull-out capacity of tension piles are DIANA, ABAQUS and PLAXIS. These packages are very similar in their use. In literature and past research, ABAQUS and PLAXIS are the most commonly used FEM software in the modelling of pull out capacity of tension piles.

The geometry of a real-world problem to be modelled numerically using FEM, is defined in three dimensions. In the available FEM-software, there is the possibility to model geometries in 3D. The benefit of this is that the unknown values are calculated for each different direction. A drawback however, is that the calculation time & power generally are very high when modelling in 3D. To limit the amount of computation time, the model could be simplified to either a 2D or 2D – axisymmetric problem. The model is simplified to 2D by assuming plane strain along the axis of the geometry where the strains are expected to be very small, such as a long retaining wall. The 2D – axisymmetric model is used when the 3D geometry is rotationally symmetric around an axis. This is for example the case of round tension piles. The decision of reducing the problem from 3D to lesser dimensions is a tradeoff between computation time and result accuracy. However, for simpler geometries, reducing the amount of dimensions could have no effect on result accuracy. Therefore it is important to define the geometry correctly and evaluate what amount of dimensions are necessary in order to reach satisfactory result accuracy.

Due to the expected complex geometry of the tunnel element to be modelled, it is decided not to reduce the amount of dimensions of the geometry. Hence a 3D formulation will be done. For this research, PLAXIS 3D is made available to use as a software. The possibilities of the software are discussed in the next section. After the possibilities of the software are analyzed, literature is used to examine the knowledge on using FEM for modelling tension piles.

## 5.2 Tension piles with the Finite Element Method

In this chapter information is shared regarding modelling tension piles using the Finite Element Method. The goal of this chapter is to get an idea of what the possible methodologies are for designing tension piles numerically and determining the geotechnical capacity using this numerical modelling software.

In the master dissertation by Ryltenius (2011) a piled raft foundation with an uniform load was analyzed in PLAXIS 2D and 3D. The 2D model was made by assuming plane strain along the z-axis. Furthermore analytical models were used to calculate settlements and structural forces. A parametric study was done to judge on the outcomes of the different models. This pile raft was modelled in a uniform soft clay layer and the modelling software was used to analyze the stress and deformation distribution in the piled raft and in the surrounding soil.

The geometry of the PLAXIS 3D model is depicted in Figure 6.

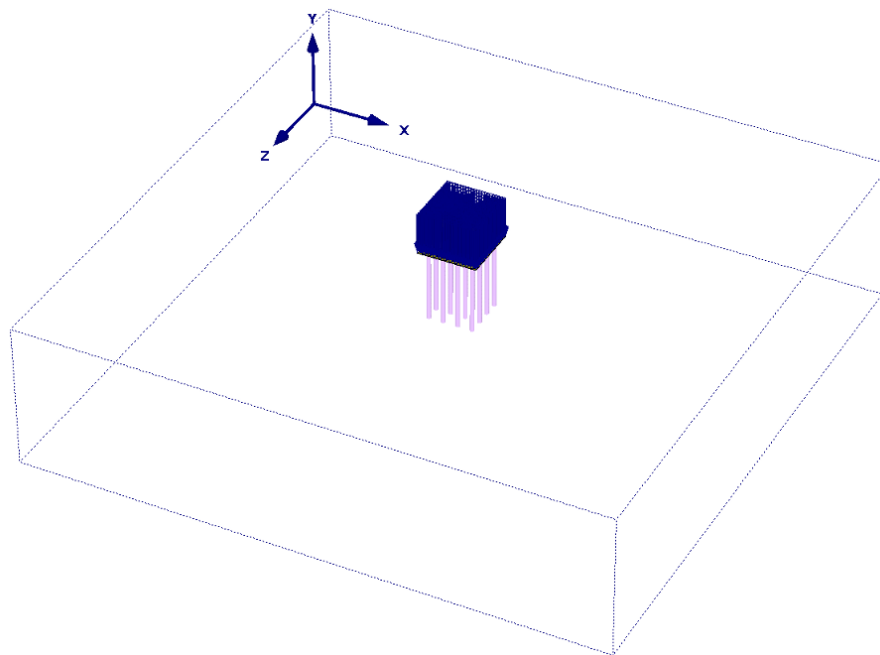


**FIGURE 6: GEOMETRY OF A PILED RAFT FOUNDATION AS A PLAXIS 3D MODEL (RYLTENIUS, 2011)**

In this model the soil was modelled as a volume elements, the raft was modelled as a floor element and the piles are modelled as embedded beams. As previously explained, the embedded beams automatically have interface elements modelled around them to model the interaction between embedded beams and the soil. The uniform load was modelled on top of the raft plate.

The uniform clay layer was modelled using the Mohr-Coulomb model. For the interfaces, the strength reduction factor  $R_{inter}$  of 0.8 as advised by PLAXIS for cohesive soil was used for the interface elements.

The initial stress state of the model was calculated with the K0 procedure and initial water condition was calculated by the direct method in PLAXIS, using the defined phreatic water level. The calculation was performed as a plastic calculation, as this model was defined for calculating final settlements and structural force distribution along the geometry. To model this, one calculation phase was defined, including activation of all elements and the load.

The results of the PLAXIS 3D calculation was compared with similar plane-strain 2D analyses and analytical methods. The findings were that 2D or other simplified models generally over-estimate the settlements and structural forces and thus estimate the structure to be weaker than it actually is. In this dissertation, it is advised to use 3D models as geotechnical problems get more complex for more accurate results through less simplification of models (Ryltenius, 2011).

van Baars and van Niekerk (1999) analyzed the numerical modelling of tension piles to calculate the ultimate tension capacity using PLAXIS 2D. The results of the numerical model are compared with actual pile tests results and analytical models to judge their respective performance. The assumed installation type of the tension piles are according to the 'Vibro' system as touched upon before.

The report proposes to model tension piles by modelling their skin only. This skin is modelled using a beam element. This method is discussed to be more effective than modelling tension piles as volume soil elements, as a large part of the tensile bearing capacity originates from the skin friction between the pile and soil. The main advantage is faster calculation due to reduction of number of elements. Furthermore it makes it possible to apply a load or interface on the boundary of the beam element such as in-situ soil stress which is not possible using volume elements to model the pile.

The installation of the tension pile is incorporated in the model by simulating pile driving effects and curing effects of the concrete. This is done by introducing a boundary pressure along the pile length. This boundary pressure initially consists of the in-situ soil stress, this pressure is increased from in-situ stresses to a pile driving stress consisting of four times the in-situ stress and finally the boundary pressure is equal to the curing pressure of the concrete. Finally a pull-out test is simulated by introducing a pile head displacement at the top of the pile.

In this research was concluded that the numerical modelling of tension piles assessed the measured bearing capacity more closely than analytical models which results in lower acceptable factors of safety. The behavior of the interface between pile and soil has the most influence on the modelled bearing capacity of the tension pile. This report suggest a strength reduction factor of 0.8 to 1.0 for the modelling of interfaces.

The numerical model generally under-estimates the tension bearing capacity compared to the pile load tests by 10%. This in contrary to analytical models which over-estimates the tension bearing capacity for up to 100%. This means the factors of safety applied on calculations can be reduced, decreasing number and/or size of tension piles in design (van Baars & van Niekerk, 1999).

Engin & Brinkgreve (2009) introduce and test the embedded pile model as an applicable element for modelling piles in PLAXIS 3D. The embedded pile elements are used to model a single pile load test and a case study of a piled raft foundation. The surrounding soil was modelled using the Hardening Soil model. The results are compared to actual pile test results in order to determine the applicability of the embedded pile element for foundation piles.

In this study it was found that the embedded pile element in combination with the Hardening soil model to model the interface is a very efficient yet accurate formulation to model piles. The applicability in practical cases was validated and the results of the modelled embedded piles performed very well for both single and large groups of piles. It is recommended to use the embedded pile element when modelling foundation piles both in tension and compression (Engin & Brinkgreve, 2009).

Sheil and McCabe (2012) researched the performance of friction pile group responses using embedded pile elements in PLAXIS. The friction pile groups are modelled numerically in PLAXIS 3D to analyze their group effects on settlements. For this research, both a linear elastic soil model (Mohr-Coulomb) and a nonlinear soil model (Hardening soil) was used. The results are compared with field tests in order to judge on their performance. The first stage of analysis of the pile group consists of initial stress generation in the soil by the K0 procedure. The second step is to activate the embedded pile elements in the soil. The third step is to install a floor element that is connected with the embedded piles to represent the foundation slab. The fourth step is to apply a compressive uniform load on top of the floor. Pile installation effects were not modelled. The interaction of floor and soil was not modelled, a certain gap was maintained between the floor element and ground level. This study found that this method of installing a tension pile group reproduced satisfactory results compared to field tests and experimental data. Predictions of two-pile interaction factors using embedded piles together with the HS model agree well to the field data reported by McCabe and Lehan (2006) and can be considered a significant improvement on existing approaches that idealize the soil as a LE soil medium (Sheil & McCabe, 2012). Therefore it is opted that when the geotechnical research is available, a more complex soil model such as Hardening soil is issued to reach better results using FEM compared to simpler models such as Mohr-Coulomb.

Research carried out on the deformation model of sand around short tension piles in a pull-out test used ABAQUS to model the test for verification. The sand was modelled using the Mohr-Coulomb model, which means an isotropic, linear elastic perfectly plastic material. This model was used due to the limited availability of soil parameters for the sand. Due to the simplicity of the pull-out test and to limit the calculation time necessary, the test was modelled in a 2D axisymmetric plane with symmetry around the axis through the center of the pile. This type of modelling is done in ABAQUS. The initial step consisted of determining the initial stresses in the soil. Then the friction interface between soil and pile was defined with a friction coefficient of 0.28. Then the prescribed displacement was imposed on the top of the pile. This means no installation effects of the pile have been included in the model. The model results, consisting of the time required to pull out the pile for 25 mm, were compared with experimental results and field data and were concluded to have minimum and maximum errors of 0.6% and 11%. It is concluded that ABAQUS software can simulate and verify the experimental results of the pull out test with a high degree of accuracy (Faizi, Armaghani, Sohaei, Rashid, & Nazir, 2014). The main findings are that both the extent of failure surface and failure mechanisms had a good agreement between the ABAQUS model and the pull-out test.

Further research carried out on the pull-out load performance of piles in clay validated the numerical model made using PLAXIS 3D. The research included the simulation of underreamed tension piles compared to the standard tension piles. Before the comparison, the PLAXIS 3D model was validated with experimental data. It was concluded that the PLAXIS 3D software analysis demonstrates excellent agreement with experimental data of nearly 99%. This concludes that the use of PLAXIS 3D is suitable for modelling the pull-out capacity of tension piles. (Al-Bayati, Al-Neami, & Rahil, 2023) In the model, the soil was modelled using the Mohr-Coulomb model. This type of soil model is often used when limited geotechnical parameters are available. The pile was modelled as a linear elastic volume element with interfaces to model the friction between pile and soil. The interfaces were modelled using a friction coefficient of 0.6. Installation effects of the pile were not taken into account in this research. The results of the numerical model were satisfactory and could be compared to experimental tests.

The main takeaways from the literature on modelling tension piles using FEM is that the procedure often consists of using volume elements to model the tension pile with an interface along the skin of the pile to model the friction between the pile elements and soil elements. The Mohr-Coulomb model was often used to model the soil. However it was mentioned regularly that this was due to limited availability of soil parameters. The validation of the embedded beam elements in PLAXIS for example, are modelled using the more complex Hardening soil model taking stress history into account. Also research suggested that the usage of the Hardening Soil model compared to the Mohr-Coulomb model showed significant improvements in the results. This embedded beam element is especially usable when many piles have to be modelled in the geometry, mainly because they have less computation time compared to the standard volume element with interfaces modelling. A consensus for friction reduction coefficients between pile and soil was not found in the literature. It is best found through validation with experimental results. Pile installation effects were included in very few research reports. In the ones that did, it was concluded that including pile installation effects such as excavating the hole and the curing of the concrete had little effect on the eventual results of the model. The models run without pile installation effects still show good results compared to experimental results. Therefore pile installation effects are assumed to be negligible when using FEM to model tension piles.

Based on previous research mentioned, PLAXIS 3D and ABAQUS are both suitable software's to model tension piles using FEM. PLAXIS 3D is used for this research due to familiarity and availability of the software for this research.

## 6. Case: EHT

In this chapter information is gathered on the relevant case study: the EHT. This will include an introduction to the tunnel, the design of the tunnel and its entrances along with the geotechnical longitudinal and cross section. In the design analysis the focus is on the applied tension pile foundations, as these are relevant for the case study. The failure mechanism of the tension pile foundation is analyzed and the critical location for this failure mechanism in the tension pile foundation is analyzed. Then the design of the tunnel at this critical location is analyzed with available technical drawings.

### 6.1 Background

The EHT is an immersed tunnel located in the province of Zuid-Holland, located between Barendrecht and Heinenoord. The highway A29 goes through this tunnel and is constructed underneath the waterway Oude Maas. The tunnel was opened on 22th of July 1969. The tunnel has a total length of 1064 meters and has three lanes going in each direction. The traffic intensity of this tunnel is estimated at around 111000 vehicles per day (Wegenwiki, 2023). Rijkswaterstaat is responsible for the maintenance of this tunnel.

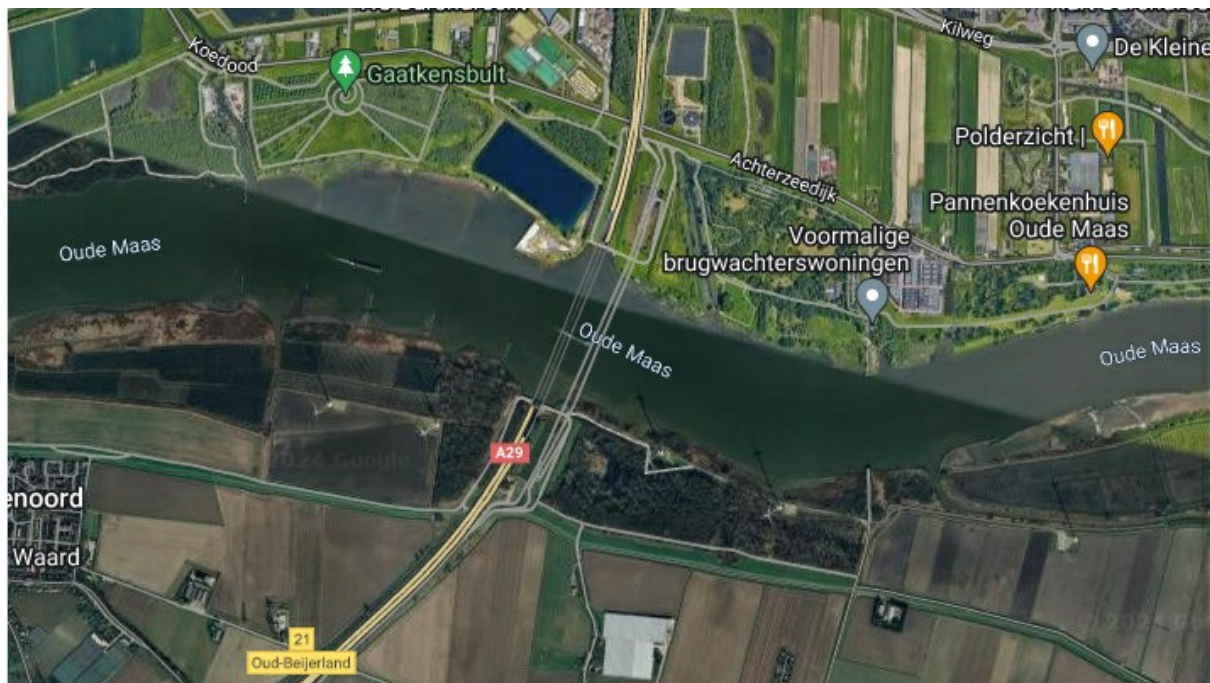


FIGURE 7: OVERVIEW OF THE LOCATION EHT (GOOGLE MAPS, 2024)

The tunnel is an immersed tunnel and thus was constructed through immersing tunnel elements in the waterway, and connecting them to the entrances of the tunnel which are constructed in advance. The entrances of the tunnel were constructed in a dry dock with an open drainage, keeping the water levels low during construction. During construction, the entrances of the tunnel are founded on the tension piles mentioned in the introduction. By applying the tension piles in the foundation of the entrances, the open drainage of the construction pit could be halted, restoring the water levels to their levels before construction. The restoration of water level causes the tunnel entrance to be submerged, which exerts an upward force on the tunnel entrance. The tension piles give resistance to this upward force, making vertical equilibrium and keeping the tunnel entrance in place.

The immersed elements of the tunnel are each made up of six concrete parts which are connected through joint strips of rubber and metal, with the purpose of waterproof connection. The immersed part of this tunnel however, is out of the scope for this thesis. The focus is on the entrances of the tunnel, where the tension piles are applied.

Figure 8 shows a schematic overview of the longitudinal section of the EHT. The northern and southern tunnel entrance along with the immersed part in the middle can be seen in the figure.

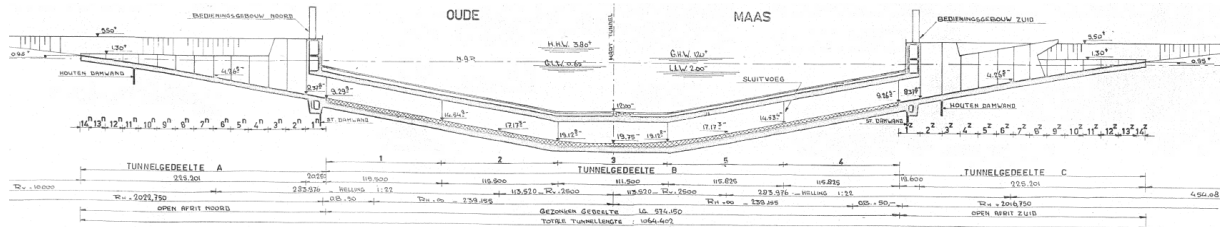


FIGURE 8: LONGITUDINAL SECTION OF EHT (TEK HE757)

The tunnel entrances are divided into fourteen different elements. They are numbered 1N to 14N and 1Z to 14Z respectively. Here 1N & 1Z are the deepest elements and 14N to 14Z are the most shallow elements. Each element has a length of approximately 18 meters. (RWS directie sluisen & stuwen, 1962)

Judging from the longitudinal section, the deepest parts of the entrances are situated at NAP – 8.38 m for both the northern and southern entrance. This level is taking into account the concrete floor of the tunnel entrances.

Figure 9 shows a top view of the tunnel. Here the alignment of the road inside the tunnel and various dimensions are shown.

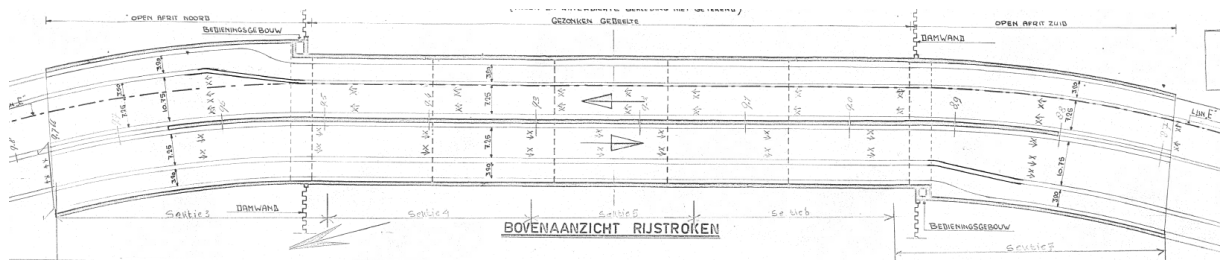
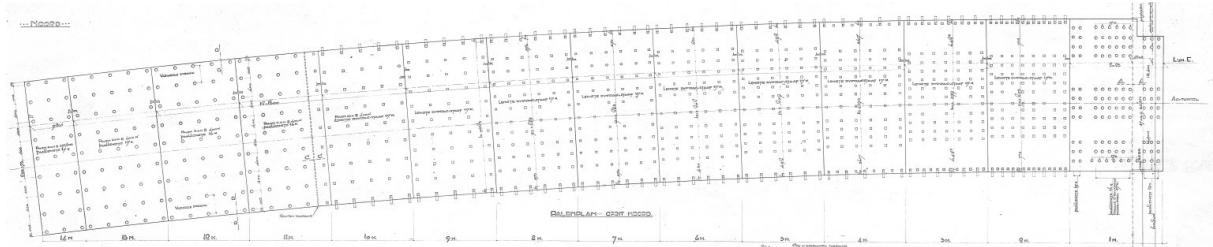


FIGURE 9: TOP VIEW OF THE EHT (TEK HE757)



## 6.2 Tension pile foundation

The schematic overview of the tension pile foundation of both the northern and southern entrance are shown below. The figures show a top view of the foundation, including installed piles and their respective length of reinforcements. The numbering of the different elements from 1N to 14N and 1Z to 14Z respectively can be seen on the figures.



**FIGURE 10: TENSION PILE FOUNDATION NORTHERN ENTRANCE (TEK HE759, 1962)**

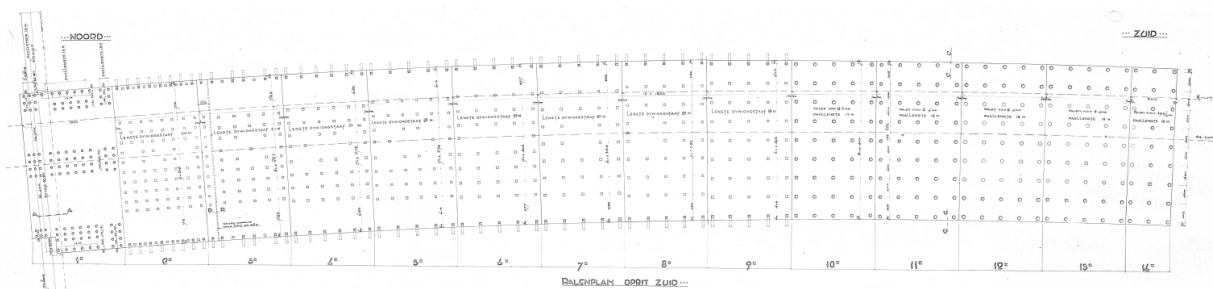


**FIGURE 11: TENSION PILE FOUNDATION SOUTHERN ENTRANCE (TEK HE765, 1962)**

In both figures, the circles resemble foundation piles under compression, and the squares resemble foundation piles under tension. It can be seen that there are some differences in the foundation methods between north and south. Namely the northern entrance has installed tension piles from element 11N till 2N while the southern entrance has them installed from element 9Z till 2Z. In both the deepest elements, no tension piles are installed. Instead foundation piles under compression are installed. In Figure 10 & 11 it can be seen that the control buildings of the tunnel are constructed on the elements 1N and 1Z. The extra applied self-weight of this building on the foundation is enough to resist the upward force on the element. Hence no tension piles are installed in both the deepest elements.

The tables below show an overview of the amount of tension piles installed per element for each tunnel entrance. As seen in the figures, the tension piles are distributed over the area of the floor of each element. On the outskirts of the element, the tension piles have been installed under a slope of 1:10. This gives a horizontal component of resistance to water pressures on the side of the element. The deeper elements are expected to have a larger number of tension piles due to the higher upward force the tension piles have to withstand.

**TABLE 6: AMOUNT OF TENSION PILES PER TUNNEL ELEMENT (TEK HE759 & HE765, 1962)**

Element	1N	2N	3N	4N	5N	6N	7N	8N	9N	10N	11N	12N	13N	14N
No.	0	104	95	84	78	72	66	69	55	45	9	0	0	0
tension piles [-]														
Length piles [m]	-	17	17	17	17	17	17	17	17	17	16	-	-	-
Element	1Z	2Z	3Z	4Z	5Z	6Z	7Z	8Z	9Z	10Z	11Z	12Z	13Z	14Z
No.	0	104	67	54	52	47	43	44	45	0	0	0	0	0
tension piles [-]														
Length piles [m]	-	20	21	21	21	21	21	21	21	-	-	-	-	-



The tables show that both 2N and 2Z have the most tension piles installed. This is as expected due to their deeper position compared to the other element and thus having to resist more upward force.

The tension piles are installed according to the Vibro system as described in Section 2.3. In the case of the EHT specifically, the tension piles are designed as cast-in-place concrete piles reinforced with a single high quality steel rod, also known as a Dywidagstaaf. The steel rod is coated with asphalt as a measure of corrosion protection. The rod is prestressed with a stress of 55 tons or 550 kN in order to impose a compressive force in the concrete surrounding the rod, eventually increasing the tensile capacity of the concrete surrounding the steel rod. In the initial design, the piles were designed to be a 45-ton tension pile. In other words, the projected capacity for a single tension pile was designed to be 450 kN for the EHT (Wolsink, 2024).

The tension piles applied in the EHT are circular and have a diameter of 450 mm. The steel rod has a diameter of 32 mm and has a steel quality of QP 105. This steel quality has a yield strength of 1030 N/mm<sup>2</sup> and a tensile strength of 1050 N/mm<sup>2</sup>. A schematic of the applied tension pile is shown in Figure 12.

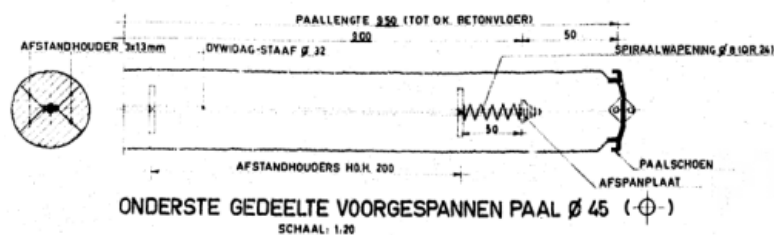


FIGURE 12: TENSION PILE SCHEMATIC (RWS DIRECTIE SLUIZEN & STUWEN, 1962)

The connection of such a tension pile with the floor of an element is shown in Figure 13. This type of connection is similar for every tension pile in both northern and southern entrances. It is also shown that the steel rod, shown in the middle of the schematic, is coated with asphalt for protection against corrosion.

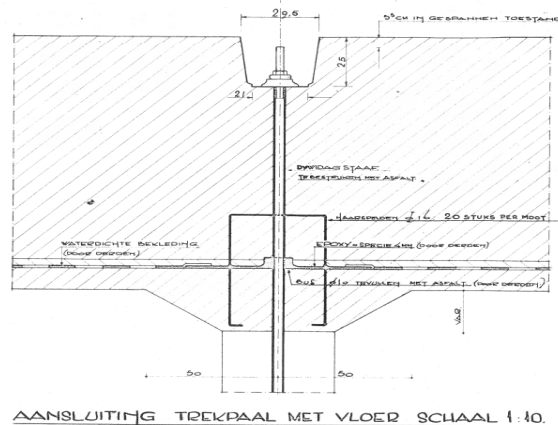


FIGURE 13: TENSION PILE CONNECTION TO TUNNEL FLOOR (TEK HE759, 1962)

The figure shows that the steel rod is installed at the top of the concrete floor of the tunnel entrance. To obtain the final depth of the tension piles, the length of the steel rod should be subtracted from the level at the top of the concrete floor. For the deepest tunnel element with a concrete floor situated at NAP – 8.38 m and a steel rod with a length of 17 m for north and 21 m for south, the level of the bottom of the deepest installed tension pile is at NAP – 25.38 m and NAP – 29.38 m respectively.

### 6.3 Geotechnical & hydrological situation

To model the entrances of the tunnel correctly, information about the geotechnical cross section and geohydrological information such as water levels are necessary. Prior to the construction of the tunnel entrances, a total of three cone penetration tests and one borehole have been carried out as soil investigation for both the northern and southern entrance of the tunnel. This information will be used along with geotechnical information originating from the analysis that was done in order to build the bored tunnel, the Second Heinenoordtunnel, which is located next to the EHT. This geotechnical information includes a multitude of CPT-tests and boreholes, along with laboratory tests to determine geotechnical parameters.

For general monitoring of water levels, Rijkswaterstaat put monitoring wells in place around the entrances of the EHT since 2022. These monitoring wells have been measuring phreatic water levels and head heights in the deeper sand layer beneath the tunnel entrances. This data is used to get the actual governing water levels of the northern and southern entrance of the tunnel respectively. These water levels are used to calculate the uplift force on the tension pile foundation.

### 6.3.1 Geohydrological

Both the phreatic and deeper water levels at the location of the northern and southern entrance were measured from November 2023 and are still ongoing. The measurements of water levels are done through monitoring wells. This data is used to create an actual view of the hydrological situation around the tunnel.

Figure 14 shows the layout of the installed monitoring wells of the northern entrance (left side of figure) and the southern entrance (right side of figure). The wells are not installed in the deepest parts of the tunnel entrances. However it is assumed that the measured water levels in the well are uniform due to the relatively short distance to the deepest part of the tunnel entrance.

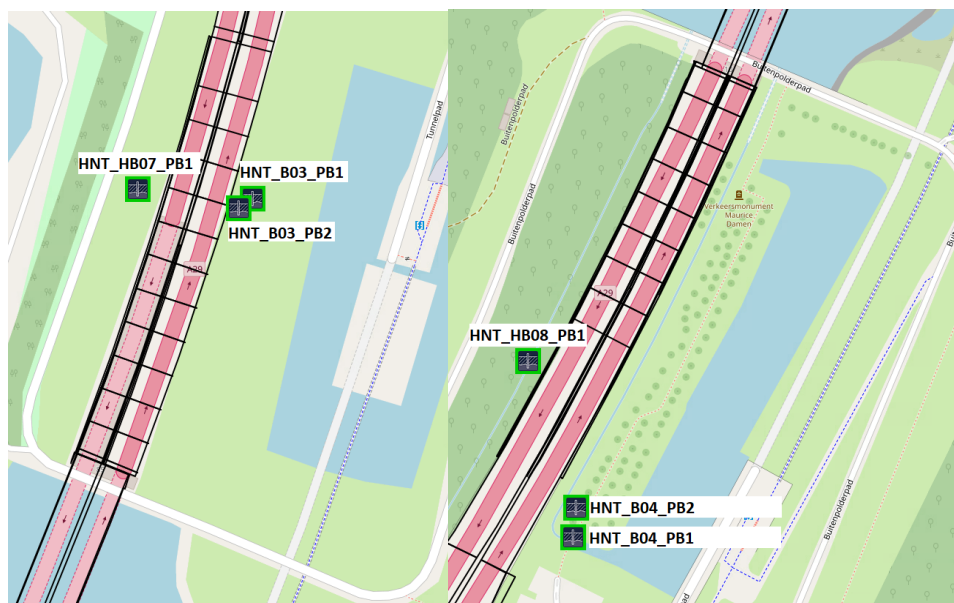


**FIGURE 14: LOCATIONS OF INSTALLED PIEZOMETERS (FUGRO, 2024)**

The yearly water level profile of the phreatic layers are shown in Figure 15. The water levels are measured from 13 February 2023 until 13 February 2025.

Grondwaterstand ondiepe peilbuizen

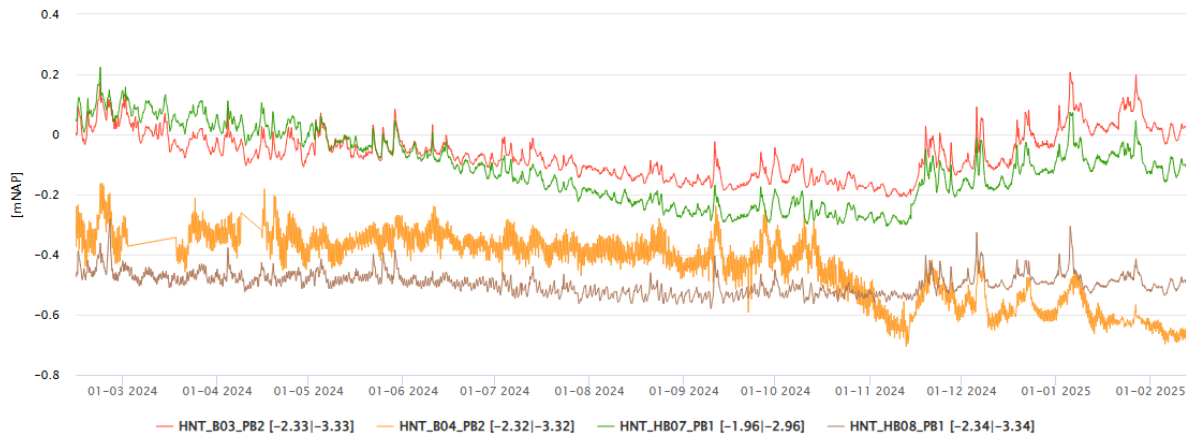


**FIGURE 15: EVOLUTION OF PHREATIC WATER LEVELS THROUGH TIME (FUGRO, 2024)**

Judging from the water level profile, the phreatic level at the location of the northern entrance fluctuates around a mean of NAP + 0 m with a maximum water level of NAP + 0.2 m and a minimum of NAP - 0.2 m. The phreatic level at the location of the southern entrance fluctuates around a mean of NAP - 0.3 m with a maximum water level of NAP - 0.2 m and a minimum of NAP - 0.4 m.

The yearly water level profile for the deeper water levels are shown in Figure 16. The water levels are measured from 13 February 2024 until 13 February 2025.

Grondwaterstand diepe peilbuizen

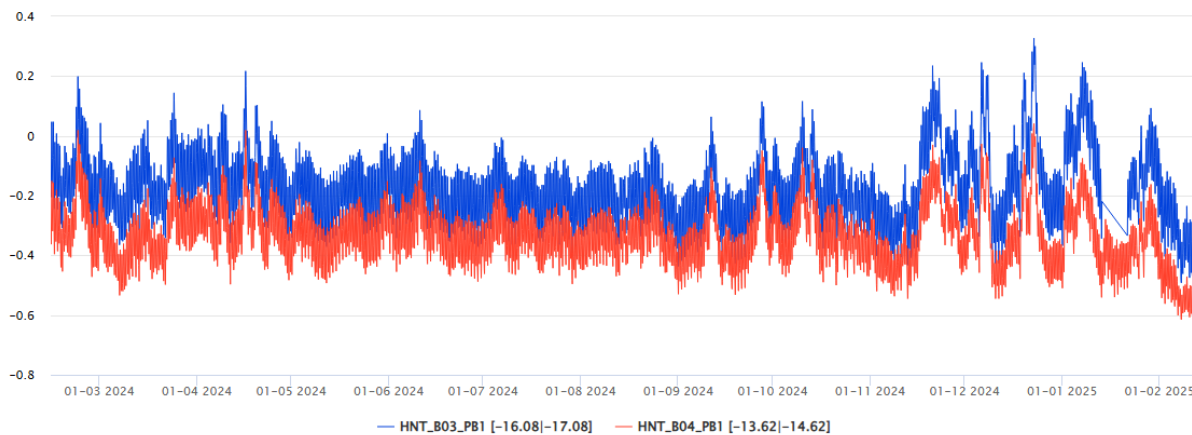


**FIGURE 16: EVOLUTION OF DEEP WATER LEVELS THROUGH TIME (FUGRO, 2024)**

The northern monitoring well measures water levels which fluctuate around NAP - 0.15 m with a maximum of NAP + 0.40 m and a minimum of NAP - 0.40 m. The southern monitoring well measures water levels which fluctuate around NAP - 0.30 m with a maximum of NAP + 0.20 m and a minimum of NAP - 0.5 m.

Also in both deep wells, a tidal movement can be seen. It is assumed that the tidal movement originates from the connection waterway to the deeper permeable sand layers. This also explains the higher variability in deep water levels compared to the phreatic water levels. Also in the right part of the graph, amplitude of the water level seem to get stronger. This could be due to rainfall in winter, or more extreme tides. The amplitude of the tidal movement in the first period is approximately 0.2 meters. In the second period it increases to 0.4 meters. The cyclic nature of the water level impose stress variations on the tunnel and the tension piles. This phenomenon is analyzed further in the report.

The seasonal effects on the water levels can be seen in the graph. In the winter period (November - December - January) it can be seen that the water level fluctuates more heavily and has a higher mean than in warmer and dryer periods (March - April - May).

The different measured water levels are collected in Table 8.

**TABLE 7: PHREATIC AND DEEP WATER LEVELS FOR BOTH NORTH & SOUTH**

<b>Water levels</b>	<b>North phreatic</b>	<b>North deep</b>	<b>South phreatic</b>	<b>South deep</b>
<b>Minimum</b>	NAP - 0.3 m	NAP - 0.5 m	NAP - 0.6 m	NAP - 0.6 m
<b>Maximum</b>	NAP + 0.3 m	NAP + 0.3 m	NAP - 0.2 m	NAP + 0.0 m
<b>Average</b>	NAP + 0 m	NAP - 0.1 m	NAP - 0.4 m	NAP - 0.3 m

There is not much difference between the water phreatic and deep water levels for both north and south respectively. For the southern part, the deeper water level is a bit higher than the phreatic water level. This means there is water seepage from the deeper layer to the phreatic level. This can be explained by the presence of soft layers with low permeability near the surface of the southern entrance, causing an increase in water pressure in the deeper layers.

From the graphs it can also be seen that there is a slight downward trend in the shallow and deep water levels. To confirm this data trend, a wider timespan than the current year should be analyzed.

### 6.3.2 Geotechnical

To obtain the required geotechnical information for this case study, a desk study on publicly available information is carried out. Also a specialized report of geotechnical site investigation of the Second EHT, constructed 20 years later, is analyzed. Since the First and Second EHT are located closely together, it is assumed that this geotechnical research is also relevant for the EHT. The sources are used to construct the governing geotechnical situation of the tunnel.

In the period from 20 April 1994 to 8 June 1994 the definitive geotechnical site investigation was carried out for the Second EHT. This tunnel was going to be a bored tunnel, hence very detailed geotechnical site investigation was required in order to determine the alignment of the tunnel along length and depth. Due to the location of the Second EHT being so close to the EHT, it is assumed that this geotechnical site investigation can be interpreted as relevant for this tunnel.

The geotechnical site investigation included both field work, such as CPT's and boreholes and laboratory tests in order to determine geotechnical parameters of the subsoil. This information is used to construct the governing geotechnical soil profile along with their respective parameters for the EHT.

#### 6.3.2.1 Geotechnical profile

For this research, a total of 66 CPT-tests and 10 boreholes were carried out. Soil samples of the different layers were also taken during these tests in order to perform laboratory tests. The research was used to construct the geotechnical section as seen in Figure 17 (Grondmechanica Delft, 1994).

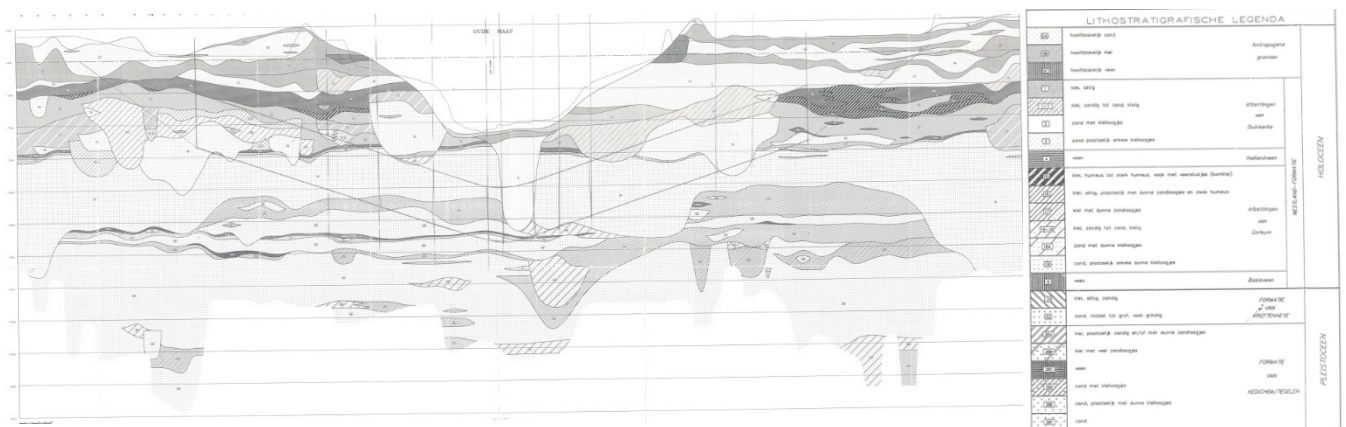


FIGURE 17: GEOTECHNICAL LONGITUDINAL SECTION OF THE TUNNEL (GRONDMECHANICA DELFT, 1994)

The figure shows a very distinct difference between the northern entrance (right on figure) and the southern entrance (left on figure) which is also seen in the CPT's. The northern entrance is shown to be an almost uniform sand layer, while the southern entrance is mostly made up of soft soils like clay and peat, with a sand layer from NAP - 16 m to NAP - 22m

The soil profile shows high local soil variability along the length of the tunnel. The CPT's are chosen to be as close to the deepest parts of the entrances as possible, because this is where the uplift force is expected to be largest and thus be the critical soil conditions for modelling the tunnel entrances. The governing CPT is chosen for both northern and southern entrances respectively.

Laboratory tests were performed on the samples taken from the performed boreholes. This in order to determine their geotechnical parameters. The laboratory tests performed on the previously defined layers are collected in this chapter in order to get an overview of their respective geotechnical parameters. The geotechnical parameters such as friction angle, cohesion, volumetric weight and stiffness values are collected from the laboratory tests performed on soil samples with the same classification and in-situ depth. Where there are no laboratory tests performed on a defined soil, a representative parameter value is assumed according to NEN 9997-1 standards.

### 6.3.2.1.1 Northern entrance

The figure below shows an overview of the geographical locations of the boreholes and CPT-tests that were carried out for the northern entrance of the tunnel. The CPT-tests are denoted by triangles and boreholes are denoted by circles.



FIGURE 18: LOCATIONS BOREHOLES & CPT'S NORTH (DINO-LOKET, 2024)

The CPT-tests, boreholes and matching laboratory tests are used to make the governing geotechnical cross section for the northern entrance of the EHT. It is assumed that this governing geotechnical cross section is uniform for the complete area of the tunnel entrances

For each layer, the soil type, top layer level and the geotechnical parameters resulting from the performed laboratory tests are shown in the table below.

TABLE 8: GOVERNING GEOTECHNICAL CROSS SECTION NORTH

Layer	Level top layer [m]	Friction angle [°]	Cohesion [kPa]	Volumetric weight [kN/m <sup>3</sup> ]	E50 [MPa]	Soil classification
N1	NAP + 0	22.5	15	17.2	-	Clay, weak silty to silty
N2	NAP – 1.5	36	2	17.7	8 - 30	Sand, silty to silt
N3	NAP – 5.75	28	2	13.1	20 - 36	Sand, silty to silt
N4	NAP – 10	34	2	17.7	10 - 75	Sand, moderate dense
N5	NAP – 17.25	36	0	19.6	32 - 66	Sand, clean
N6	NAP – 20.75	26	20	20.1	5 - 15	Clay, weak silty to silty
N7	NAP – 25	34	0	19.7	17 - 60	Sand, clean
N8	NAP – 26.5	26	20	20.8	5 - 15	Clay, weak silty to silt

The range of the E50 stiffness values are quite broad for the soil layers. As a first guess for modelling purposes, the mean of the range will be taken. Through validation methods, the stiffness values will be changed in the given range in order to obtain the validated soil parameters which can be used for modelling this soil profile.

### 6.3.2.1.2 Southern entrance

The figure below shows an overview of the geographical locations of the boreholes and CPT-tests that were carried out for the southern entrance of the tunnel. The CPT-tests are denoted by triangles and boreholes are denoted by circles.

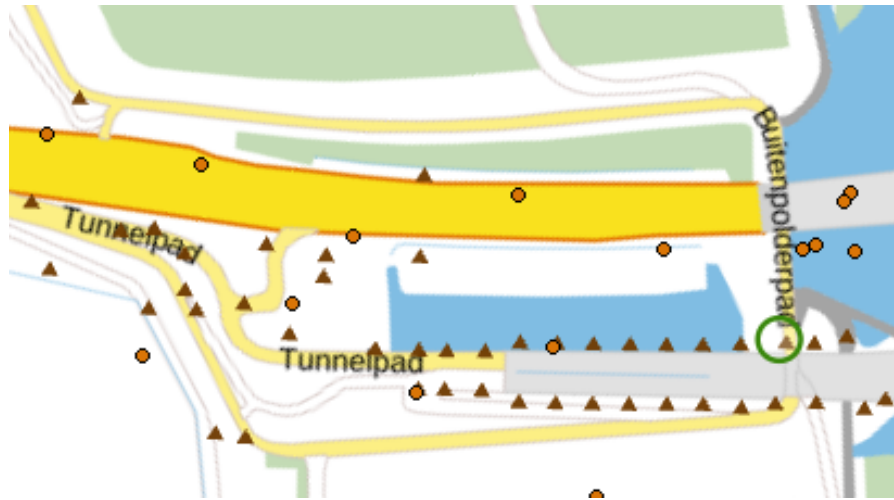


FIGURE 19: LOCATIONS BOREHOLES AND CPT'S SOUTH (DINO-LOKET, 2024)

The CPT-tests, boreholes and matching laboratory tests were used to make the governing geotechnical cross section for the northern entrance of the EHT. It is assumed that this governing geotechnical cross section is uniform for the complete area of the tunnel entrances

For each layer, the soil type, top layer level and the geotechnical parameters resulting from the performs laboratory tests are shown in the table below.

TABLE 9: GOVERNING GEOTECHNICAL CROSS SECTION SOUTH

Layer	Level top layer [m]	Friction angle [°]	Cohesion [kPa]	Volumetric weight [kN/m <sup>3</sup> ]	E50 [MPa]	Soil classification
<b>Z1</b>	NAP + 1	22.5	15	18	-	Clay, weak silty to silty
<b>Z2</b>	NAP – 3.25	36	2	20	8 - 30	Sand, weak silty to silty
<b>Z3</b>	NAP – 4.5	30	4	13	1 - 4	Peat, organic soil
<b>Z4</b>	NAP – 7.25	25	10	17	6 - 26	Clay, weak silty to silty
<b>Z5</b>	NAP – 10.5	29	0	20.5	2 - 10	Sand, silty to silt
<b>Z6</b>	NAP – 14.75	39	1	20.5	15 - 60	Sand, clean
<b>Z7</b>	NAP – 21.5	29	25	20	6 - 14	Clay, weak silty to silt
<b>Z8</b>	NAP – 24.5	34	0	20.5	17 - 60	Sand, clean

The range of the E50 stiffness values are quite large for the soil layers. As a first guess for modelling purposes, the mean of the range will be taken. Through validation methods, the stiffness values will be changed in the given range in order to obtain the validated soil parameters which can be used for modelling this soil profile.



## 6.4 Failure mechanism & Critical element

In order to make a failure analysis of the entrances of the EHT the failure mechanism and its respective critical element(s) are determined. The failure mechanism of the installed tension piles itself is initiated due to the brittle failure of the tension pile reinforcements due to corrosion. A failed tension pile loses its connection to the floor of the tunnel element and thus makes it lose all its geotechnical capacity. The reduction of capacity of the full foundation results in a reduced resistance against upward force from the water. The failure mechanism of the whole tunnel element due to the breakage of the tension piles is the uplift of the critical element(s).

The upward pressure exerted by the water on the is determined using the formula for uplift pressure.

Here  $\rho_w$  is the density of the water,  $g$  is the gravity acceleration. The hydraulic head  $h$  is the difference in height between water level and the bottom of the tunnel element. (White, 2016)

Multiplying the calculated water pressure  $P$  with the area of the tunnel element floor, the total upward force exerted by the water pressure can be calculated.

The upward pressure exerted by the water on the is determined using the formula for uplift pressure.

$$P = \rho_w * g * h$$

Here  $\rho_w$  is the density of the water,  $g$  is the gravity acceleration. The hydraulic head  $h$  is the difference in height between water level and the bottom of the tunnel element. (White, 2016)

Multiplying the calculated water pressure  $P$  with the area of the tunnel element floor, the total upward force exerted by the water pressure can be calculated.

$$F_{water} = P * A_{elem}$$

The upward pressure is dependent on variable  $h$ , which is the hydraulic head. The total area of each tunnel element is assumed to be equal for every element. This shows that the highest upward force from the water pressure is highest for the deepest elements of the construction.

To prevent uplift from happening, the resistance of the tunnel element should be larger than the upward force exerted on it. In other words the vertical equilibrium must be satisfied.

$$R_d \geq F_{water}$$

In this formula,  $R_d$  resembles the design value of the total resistance to uplift forces. This resistance consists of the self-weight of the tunnel element and the geotechnical capacity of the tension pile foundation. Following the actual normative calculation rules in the NEN9997-1,  $R_d$  is calculated as follows.

$$R_d = V_{elem} * \gamma_c * \gamma_{G;stb} + \sum_{i=0}^n T_{i,d,pile}$$

The volume of concrete in a tunnel element is denoted as  $V_{elem}$ . The parameter  $\gamma_c$  is the weight of the concrete used. This value is assumed to be 24 kN/m<sup>3</sup>. The safety factor for favorable self-weight  $\gamma_{G;stb}$  holds a value of 0.9 (NEN 9997-1, 2023). The design value for capacity of a single pile  $T_{i,d,pile}$  is summed over the amount of installed piles to obtain the capacity of the tension pile foundation.

Since the water levels are assumed to be uniform, the critical tunnel element where the failure mechanism occurs is determined through the vertical position of the tunnel element ( $h$ ), the amount of functioning tension piles of the specific tension pile foundation ( $n$ ) and the volume of concrete used for the tunnel element ( $V_{elem}$ ).

Another factor that is taken into account is the friction of the tunnel elements against each other. If the friction would be present, the element is able to mobilize resistance from the neighboring elements and could result in a clamped connection. The friction between tunnel elements is approached as either present, which results in a clamped connection between the elements. The other option is that friction is not present, and the tunnel elements are free to move vertically.



Judging from Figures 10 & 11, elements 1N & 1Z are the deepest elements and thus have the largest hydraulic head ( $h$ ). However, these elements have a very large volume of concrete applied due to the control building situated on top of it ( $V_{elem}$ ). Due to this, the foundation piles are assumed to be loaded in compression and not relevant for the tension pile research. Elements 2N & 2Z are the deepest elements with tension piles installed with relatively less volume of concrete compared to elements 1N & 1Z.

Elements 2N & 2Z initially are assumed to be the critical tunnel elements for the uplift failure mechanism taking into account the vertical equilibrium. However, from schematic tunnel drawing HE-401 (Rijkswaterstaat, 1967) it is seen that elements 2N & 2Z are designed to be connected to the heavy elements 1N & 1Z using dowels. This greatly increases the uplift resistance given that elements 2N & 2Z share the uplift load with elements 1N & 1Z. The rest of the elements of the tunnel are not connected with each other, so it is assumed that there is no vertical friction between element walls.

Therefore elements 3N & 3Z are assumed to be the critical elements for uplift failure due to having the highest expected resultant upward force in combination with the least expected resistant downward force.

## 6.5 Model choice

For this research, an advanced soil model will be chosen based upon the available information of the soil. Since there is laboratory data available on the in-situ geotechnical parameters of the EHT, a matching advanced model is chosen. When required, a simpler model is chosen to simplify calculations and reduce runtime in order to get results quickly. It will be analyzed whether the performance of the simple model is sufficient compared to a more advanced model. The model choice for this case study is also based on the literature research carried out on numerical modelling in practice. The main takeaway is that a more complex model is able to model soil-structure interaction more precisely, but at the cost of more calculation time. Balance should be found between each other.

Sandy soils are modelled using the Hardening Soil model as this model holds sufficient complexity and is suitable for modelling sandy soils (Engin & Brinkgreve, 2009). Also the literature study showed that using the nonlinear Hardening soil model over linear elastic models such as the frequently used Mohr-Coulomb model resulted in significant improvement in validation results (Sheil & McCabe, 2012). As most of the tension pile capacity is gathered from the sandy soils, it is important to model their behavior as accurate as possible. The model parameters for this advanced model are based on the volumetric weights, friction angle, cohesion and various stress-dependent stiffness values of the soil which are provided by the performed laboratory tests.

The soft soils do not provide as much skin friction capacity for the tension piles. But since the laboratory tests for determining the required parameters for the Hardening soil model are also performed on the soft soil layers, the Hardening Soil model will also be used for these layers. Generally it can be seen that the mean stiffness values are quite lower, this explains the decreased capacity for softer soils.

## 6.6 Pile load tests

In two different instances, tension pile load tests have been performed for the EHT. The first pile load test was performed by Grondmechanica Delft (GD) in 1968. The goal of this research was to analyze the influence of the shape of tension pile tip on its geotechnical capacity. This research includes installing a single tension pile similar to the ones to be used in the construction of the EHT and loading it in tension using hydraulic jack until failure. Different types of loading such as static and cyclic were performed and the settlement of the pile was measured.

The second pile load test was performed by Heijmans under commission of Rijkswaterstaat in 2018. This test was carried out in order to explore whether the tension piles in the foundation of the EHT had failed. A total of 20 piles have been tested non-destructively in tunnel elements 3N, 3Z, 7N & 7Z. The testing procedure included freeing up the top of the tension pile in the tunnel floor and loading the pile using a hydraulic jack.

The mentioned pile load tests by GeoDelft are modelled numerically in PLAXIS 3D for this research. This in order to evaluate the performance of modelling tension piles in PLAXIS 3D. The relevant information on the pile load tests regarding modelling purposes is highlighted in this chapter.

### 6.6.1 Pile load test GD (1968)

This test was performed on the northern side of the EHT.

In total eight different tension piles with three different types of footing were tested. The first one is a truncated footing, the second one a flat footing and the third one a sharp footing. Figure 20 shows the shapes of the tension pile footings. From top to bottom; sharp footing, truncated footing and lastly the flat footing.

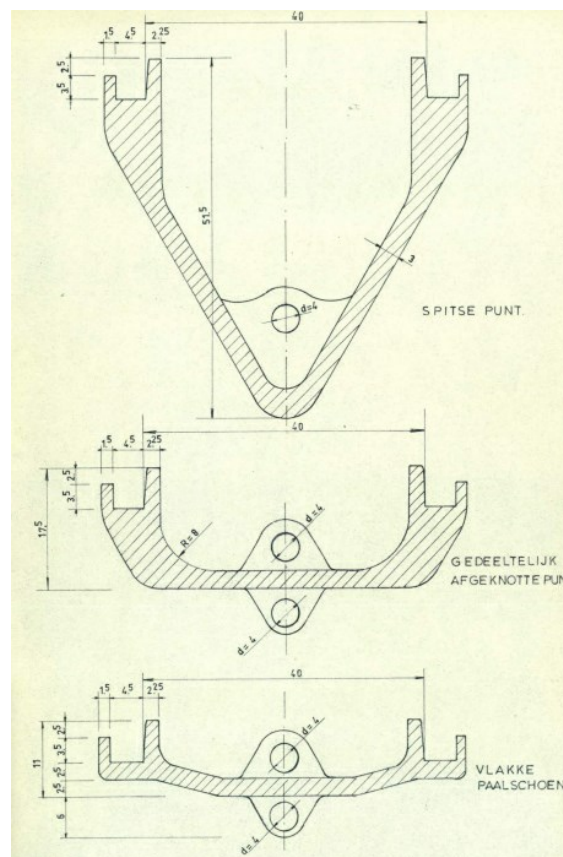


FIGURE 20: DIFFERENT TENSION PILE FOOTING SHAPES (1994)

It is expected that the footings will have a notable effect on installation speed and compaction of the soil along the shaft during installation. The report focusses more on determining the determination of the limit carrying capacities of the installed tension piles and less on the effect of the footing.

The tension piles dimensions are designed to have a diameter of 450 mm and reach 20 meters in the subsoil, similar to the tension pile design for the EHT. The piles were prestressed with a stress of 60 tons or 600 kN, this

is slightly more than the prestressing of 45 tons which was applied on the tension piles of the EHT. Another major difference between these piles and the piles used in the EHT is that a total of three steel rods were used as reinforcement as opposed to the single steel rod used for the EHT. This increases the material capacity threefold and is put in place in order to make sure that if the pile does fail, it is due to geotechnical failure along the shaft of the pile and not due to failure of the steel material itself upon loading in tension. After installation of these different types of tension piles, they are loaded in tension through different loading schemes per tension pile. During loading, the displacement of the tension pile was measured. The goal of this pile load test is to determine the limit carrying capacity of the tension pile by imposing a pull-out force of 200 tons or 2000 kN on each pile.

Figure 21 shows the load displacement curves of the eight tested tension piles. Different loading schemes and pile tips resulted in different shapes of load displacement curves. The horizontal axis represents force in tons and the vertical axis represents settlement in mm. All the piles were loaded to the planned load of 2000 kN, and none of the piles showed total failure, which is expected to be the pile being pulled out of the soil.

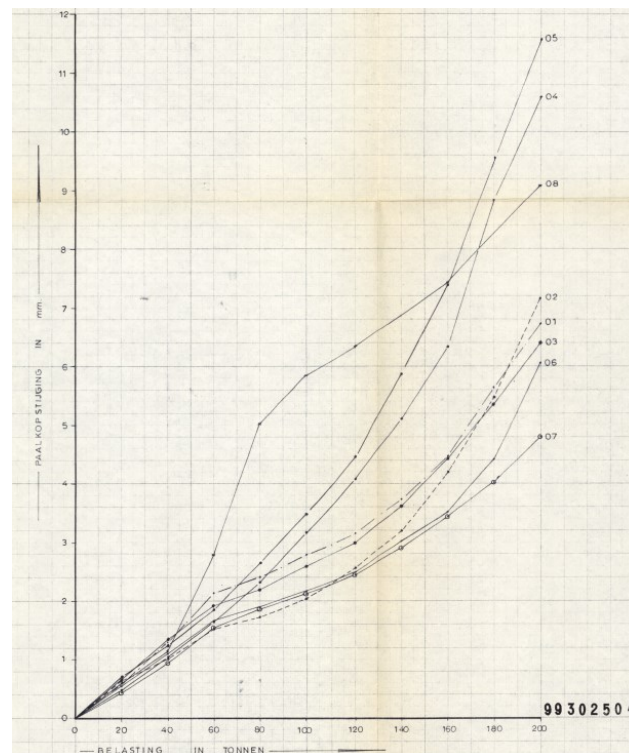


**FIGURE 21: LOAD-DISPLACEMENT CURVES OF VARIOUS PERFORMED PILE LOAD TESTS (1968)**

The tension piles are numbered from 1 to 8. Two different loading schemes have been applied along with three different pile footing for the tension piles.

Tension pile tests 1, 3, 4, 5 & 6 are similar, having a total loading duration of 40 hours, where every 4 hours 20 tons are added to the total load which starts at 20 tons. This results in a maximal load of 200 tons. The total displacements of the tension piles during this loading are measured to be 6.6 mm, 6.4 mm, 10.5 mm, 11.5 mm and 6.1 mm respectively for tension pile tests 1, 3, 4, 5 & 6.

Tension pile test 2, 7 & 8 are similar too, having a total loading duration of 80 hours, where every 8 hours 20 tons are added to the total load which starts at 20 tons. The total displacements of the tension piles during this loading are measured to be 9 mm, 4.8 mm and 9.1 mm respectively for tension pile tests 2, 7 & 8.

Tension pile tests 1 & 8 pile footings are truncated, tension pile tests 2, 5 & 6 pile footings are sharp and tension pile tests 3, 4 & 7 are flat. Looking at the measured displacements, the type of footing used does not show significant differences.

The range of measured displacement of the first loading scheme is from 6.1 mm to 11.5 mm. For the second one this is 5.8 mm to 9.1 mm. The ranges between similar tests are quite large, this can be attributed to possible measurement errors, soil heterogeneity, installation effects and such.

None of the tested piles were pulled out of the soil. Therefore it was concluded from the pile load tests that the limit carrying capacity is at least 200 tons or 2000 kN for this tension pile type. The actual geotechnical limit carrying capacity for the tension piles were estimated to be around 3000 to 3500 kN by Grondmechanica Delft based on the tension pile tests (1968).

This tension pile test are simulated numerically in PLAXIS 3D and the displacement ranges of the executed pile load tests will be used as a validation method of the model.

#### 6.6.2 Pile load test Heijmans (2018)

The pile load test performed by Heijmans was mainly to analyze whether some tension piles had failed and if action had to be taken in order to guarantee the safety of the tunnel. After imposing a tensile force equal to the design capacity on a total of 20 piles in tunnel elements 3N, 3Z, 7N & 7Z, it was concluded that none of them showed behavior that suggested that a tension pile had failed.

The tension piles were loaded with a maximum tension force of 420 kN, which is slightly below their original design capacity of 450 kN. These pile load tests show that the tested tension piles of the EHT still function correctly according to their design capacity, which is at least 420 kN. However the test gave no indication of what the limit capacity is of the installed tension piles.

Judging from this non-destructive pull-out test, the tunnel entrance of the EHT seems to function as intended with no failed tension piles.

However it must be taken into account that the sample size of 20 tension piles is quite small, as the northern tunnel entrance has a total of 677 tension piles installed. Also the corrosion could still be forming in the steel, but the cracks might not have propagated yet. This is why it is still important to monitor the tunnel entrance and to make sure the tension pile foundation does not fail unexpectedly.

## 7. Geotechnical capacity of a tension pile

The analytical and numerical methods to model the geotechnical capacity tension piles have been highlighted in previous chapters. The different models are used to calculate the theoretical geotechnical capacity of a tension pile installed in the soil stratigraphy of the EHT.

The goal of this is to get a feel for the modelling of a tension piles, and to evaluate the difference in outcomes between the available methods. This chapter is seen as a stepping stone in order to be able to model the critical section of the EHT and to be able to assess their results correctly.

First of all the pile load test as performed by Grondmechanica Delft (1968) and the estimated limit carrying capacity is shown. Then the theoretical capacity of a tension pile from the available calculation models at the time of construction, which is before 1991, is calculated for the single tension pile. This value is compared to the given 450 kN capacity that was said to be the design value for the tension piles of the EHT.

On top of that the pile load tests are re-calculated using the relevant calculation methods throughout the years. The latest available method is that of the NEN 9997-1. This calculation method along with the other calculation methods are described in Chapter 4.1. This serves to compare the current Dutch design method for tension piles. The influence of the proposed safety factors are evaluated as well. To do this efficiently, the single pile is modelled in DFoundation, which is a program that is able to calculate the capacity of a tension pile based on the relevant Dutch norms.

The pile load tests are simulated using PLAXIS 3D. The outcomes of the numerical model are compared to the measured displacements of the pile load tests as validation of the model. Also the limit carrying capacity according to PLAXIS is analyzed by continuing the loading scheme as carried out by in the pile load test until the model fails numerically. The tension force at which this failure occurs, is assumed to be the limit carrying capacity of the tension pile according to PLAXIS.

Once the modelling outcomes of a tension pile in PLAXIS 3D are validated with these methods, the critical tunnel element with the applied tension pile foundation can be modelled correctly.

The soil profile is in accordance to the determined soil profile of the northern entrance of the EHT along with its determined parameters, as the pile load tests were carried out at this location. This soil profile is used for the calculations and modelling in this chapter.

The relevant soil profile with soil parameters is shown in Table 11 below.

**TABLE 10: UTILIZED GEOTECHNICAL CROSS SECTION FOR MODELS**

Layer	Level top layer [m]	$q_{c, \text{gem}}$ [MPa]	Friction angle [°]	Cohesion [kPa]	Volumetric weight [kN/m <sup>3</sup> ]	E50 [MPa]	Soil classification
N1	NAP + 0	0.71	22.5	15	17.2	-	Clay, weak silty to silty
N2	NAP – 1.5	10.15	36	2	17.7	20	Sand, silty to silt
N3	NAP – 5.75	6.54	28	2	13.1	28	Sand, silty to silt
N4	NAP – 10	11.75	34	2	17.7	50	Sand, moderate dense
N5	NAP – 17.25	19.35	36	0	19.6	60	Sand, clean
N6	NAP – 20.75	2.8	26	20	20.1	10	Clay, weak silty to silty
N7	NAP – 25	5.54	34	0	19.7	60	Sand, clean
N8	NAP – 26.5	2.8	26	20	20.8	10	Clay, weak silty to silt

## 7.1 Pile load tests GeoDelft

From the performed pile load tests, three tests are chosen as validation for the modelling purposes of a tension pile. The set of three tests are chosen due to their similarity and the loading scheme is able to be modelled in the different types of software that are to be used. The figures below show the time-displacement diagram of the tests.

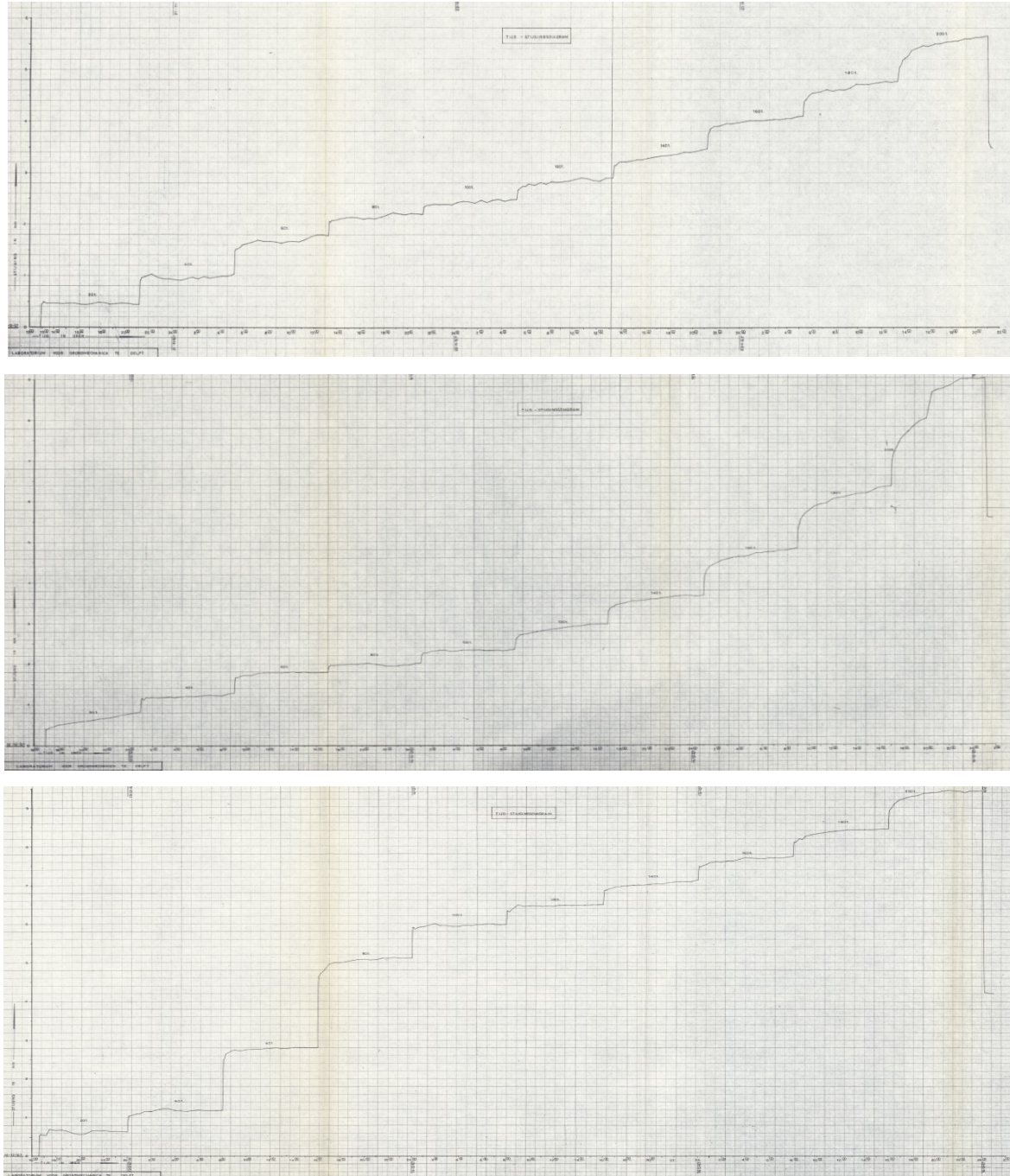


**FIGURE 22: PILE LOAD TESTS 2,7 & 8 PERFORMED BY GRONDMECHANICA DELFT (1968)**

In these three load tests, a total of 20 tons or 200 kN was added to the total load every 8 hours for a total of 80 hours. It can be seen that there is still a lot of variability in between the different tests even though they were performed in a similar way. The total displacement after the loading tests 5.8 mm, 9 mm and 9.2 mm respectively for the three different tests. It can be seen that failure is not yet achieved after the loading scheme. In the report by Grondmechanica Delft (1968), it is estimated from these profiles that the geotechnical limit carrying capacity is equal to around 300 to 350 tons or 3000 to 3500 kN of tensile force.



## 7.2 Theoretical capacity calculation

The methods used to calculate geotechnical capacity of the tension pile are described in Section 4.1. For each method, two different calculations are done. A calculation with applied safety factors as proposed by the calculation methods, and a calculation where these safety factors are all kept equal to 1.

The applicable method for the calculation of the geotechnical capacity of a tension pile at the time of construction of the EHT, which is before 1991, is calculated. The safety factor employed for this design is a global safety factor of 3.

Using the calculation scheme relevant before 1991 results in a geotechnical capacity of 1683.17 kN. Applying the global safety factor as discussed results in a capacity of 561.06 kN. This is a slight overestimation of the capacity which was used for the design of the tension piles of the EHT, which is equal to 450 kN with a deployed safety factor of 3 on the calculations.

The first relevant norm which included a tension pile capacity calculation scheme, which is the NEN 6740, gives a geotechnical capacity of 3049.21 kN with safety applied and 3927.39 kN without safety applied. Compared to the previous method the calculated capacities are substantially larger. It is expected that this is due to the availability of more research in tension pile modelling and thus the ability to estimate the capacities more accurately and thus with lower safety- and correction factors.

The CUR98-9 method gives a geotechnical capacity of 3572.98 kN with safety applied and a capacity of 4151.81 kN without safety applied. Compared to the previous method it seems that the impact of the safety factors have decreased. This could be due to uncertainty decreasing through the availability of more research and soil data.

The following calculation is in line with the calculation example of limit carrying capacity for a single tension pile as shown in the NEN 9997-1. The latest formula for calculating the geotechnical limit carrying capacity following the NEN 9997-1 norm is as follows.

$$F_{r,trek,d} = \int_0^L q_{c,z,d} * f_1 * f_2 * O_{p,z} * \alpha_t dz$$

with:

$$q_{c,z,d} = \xi * \frac{q_{c,z,ontgr}}{\gamma_{m,var,qc} * \gamma_{m,b}}$$

In the calculation example in the NEN 9997-1, it is shown that for the capacity calculation of a single pile, the installation and tensile effects on the soil are neglected. For the single pile it is assumed that  $f_1=f_2=1$ . The  $\alpha_t$  values are chosen according Table 3. The circumference of the pile and the surrounding soil layers and their depth are known. The value  $\xi$  is based on Table 4. Since for the geotechnical research a total of 25 CPT-tests were performed, a value of 0.91 can be maintained. There are no dynamic effects on the pile so  $\gamma_{m,var,qc}$  is set to 1. The safety factor  $\gamma_{m,b}$  is equal to 1.35 as previously discussed.

Using the NEN 9997-1 calculation scheme, the geotechnical limit carrying capacity for this specific single pile in the soil profile of the northern entrance of the EHT is equal to 1734.35 kN. Without safety factors this capacity increases to 3265.09 kN. This means the partial safety factors applied in the capacity calculation result in a global safety factor of approximately 1.9. Compared to the previously applicable method, it is seen that there is a decrease in capacity. One could argue that the safety was increased to appropriate to more strict safety norms in construction which are generally applicable through NEN-norms for the Netherlands and Eurocodes for Europe.

When performing a calculation using the scheme as shown in Chapter 6.4 for the different acting vertical forces for the critical section 3N of the EHT, it can be calculated that approximately a total of 3500 tons or 35000 kN upward force has to be resisted by the tension pile foundation. In Table 7 it can be found that a total of 95 tension piles were installed in the foundation of this tunnel element. This design shows that the tension piles for this tunnel element were designed to resist 367.39 kN force per tension pile. The applicable safety factor at that time for the tension pile capacity is equal to 3. This design without additional safety applied would result in a capacity of 1102.17 kN. The calculated design value through equilibrium is a slight underestimation of the original design value of the EHT which is equal to 450 kN or 1350 kN without additional safety.

For this specific type of tension pile, the steel quality used for the reinforcement is of QP 105 steel (Borsje & Schuring, 2023). It is assumed that when the yield stress is reached, the carrying capacity is nearly exceeded for the tension pile. In the code NEN-EN 1992 code, both the characteristic and design values for strength of this steel type have been given (RBK, 2021). These values are 1030 N/mm<sup>2</sup> and 936 N/mm<sup>2</sup> respectively. With a diameter of 32 mm, this results in a total capacity of 828.38 kN without safety and 752.78 kN with safety for every tension pile based on material properties.

On top of the design capacity and the steel strength capacity, the methods and safety factors in the relevant codes for the design of tension piles as mentioned in Chapter 4.1 are used to calculate the theoretical geotechnical capacity throughout the years. The results are included in Table 14.

**TABLE 11: CALCULATED CAPACITIES USING DIFFERENT METHODS**

	Capacity with safety applied [kN]	Capacity without safety applied [kN]
<b>Original design value EHT</b>	450	1350
<b>Grondmechanica Delft (Before 1991)</b>	561.06	1683.17
<b>NEN 6740 (1991-2001)</b>	3049.21	3927.39
<b>CUR 98-9 (2001-2005)</b>	3572.98	4151.81
<b>NEN 9997-1 (2005-present)</b>	2420.26	3265.09
<b>Calculated equilibrium capacity EHT</b>	367.39	1102.17
<b>Steel strength capacity EHT</b>	752.78	828.38

The first row shows the original design value of the tension pile capacity for the EHT. Row two to five of the table show the evolution of theoretical geotechnical capacity of a tension pile throughout the years. It can be seen that the calculated values increased greatly as time went on. This is due to pile and safety factors changing due to more empirical research available. Generally the pile factors became larger over the periods, increasing the theoretical capacity. The safety factors decreased every periods, also the way they are applied have changed, influencing the theoretical capacity.

The table shows a similarity between the design method before 1991 and the calculated design capacity for EHT. If the EHT would be designed with present methods, the capacity calculated per tension pile would be almost 5 times larger, reducing the amount of tension piles needed for the foundation drastically. So generally it can be said that calculations became more efficient and substantiated by research throughout the years.

Something that is not taken into account in this chapter is the change to how pile groups are calculated differently throughout the years. In the NEN 6740 and the CUR 98-9, the correction factors for both installation and stressing of pile factors were first introduced. However because this is a single pile, they are not represented in the calculation. These factors will be used when analyzing the actual tension pile foundation of the EHT.

Lastly the steel strength capacity of the tension piles applied for the EHT should be noted. The capacity is below the design value of the EHT, but if the applicable norms are used, the geotechnical capacity is way larger than the steel strength capacity. This would result in a failure of the steel before the geotechnical failure of the tension pile. In the pile load tests, this was prevented by installing three different steel rods in each tension pile, increasing the steel strength capacity threefold. For the EHT however, only one steel rod was installed per tension pile.



## 7.3 Numerical simulation

In the PLAXIS model the soil layers are modelled using the Hardening soil model. The model parameters for the soil layers are derived using laboratory tests that were carried out on the borehole samples in the site investigation that was performed for the Second Heinenoordtunnel as discussed in Section 6.3.2.

In order to get a feel for using PLAXIS 3D, the single tension pile is modelled using two different methods. The first one is modelling the tension pile as a ‘volume pile’, comprised of volume elements in the Finite Element mesh. This method is the regular, most broadly used method to model piles in PLAXIS. The second method is using the ‘embedded pile’ which is a structure element made especially to model the behavior of piles. The embedded beams were introduced to limit the amount of elements necessary in a mesh to reach satisfactory accuracy conditions for larger groups of piles. The two PLAXIS pile model variants will be judged based on their performance by comparing them to the results of the pile load tests mentioned in Section 7.1. Hence the construction phases of the PLAXIS 3D model are based on the pile load test by Grondmechanica Delft (1968), where 200 kN tensile force is added every 8 hours for a total of 80 hours.

After judging the performance of the PLAXIS 3D models, they are used to approximate the geotechnical capacity of the tension pile numerically. This value is found by steadily increasing the tension force in distinct construction phases. The amount of tension force at which the model numerically fails, is assumed to be the geotechnical capacity of the tension pile according to the numerical evaluation of PLAXIS 3D.

### 7.3.1 Volume pile

The volume pile is constructed by creating a volume element with a similar shape to the pile. On the skin of the volume element, interfaces are added to simulate pile-soil interaction. The stiffness of the volume pile is assumed to be that of uncracked concrete, which is roughly 30 GPa. The pile load is simulated as a surface load located on top of the volume pile. The pile load test was successfully simulated on this model and showed no numerical failure. The final distribution of deformation of the soil after the pile load test as simulated is shown below.

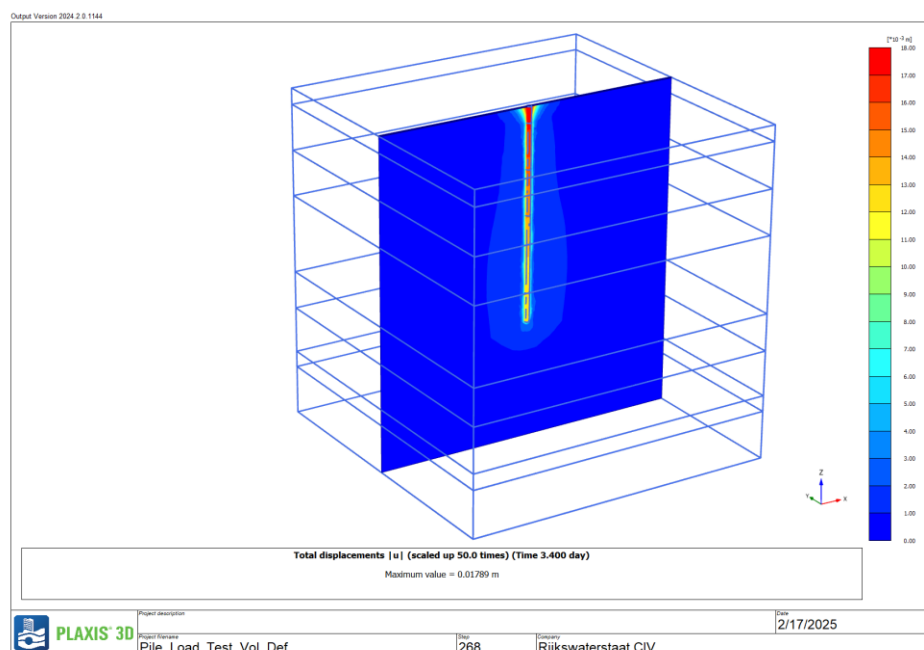
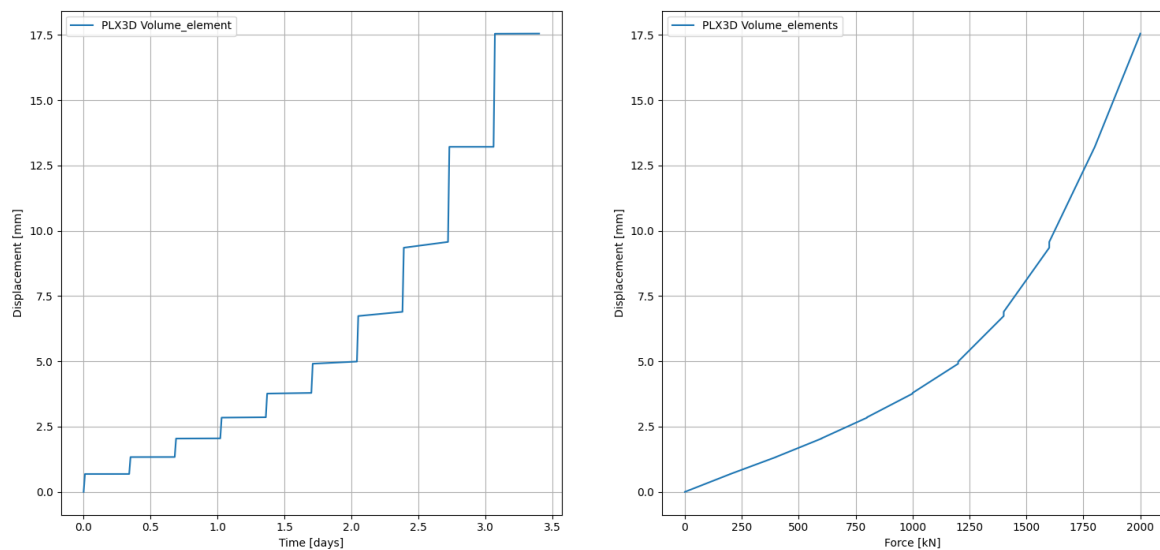


FIGURE 23: DISPLACEMENT DISTRIBUTION FOR VOLUME PILE

The output shows a maximum total displacement of 17.89 mm localized at the skin of the pile. The total calculation time to obtain the model results was equal to two hours. This is quite an inefficient model judging from the calculation time, especially taking into account the increase in calculation time if more piles would be used in the model.

The time-displacement and force-displacement profiles of the simulated pile load test are shown in Figure 24.



**FIGURE 24: TIME-DISPLACEMENT AND FORCE-DISPLACEMENT DIAGRAM FOR VOLUME PILE**

In the graph is seen that the development of the displacement of the pile along the duration of the pile load test is rather small in the beginning, and as the pile load test duration/force increases, the displacement of the pile per step increases as well. In the first few loading steps the displacement of the pile increases with 0.5 to 1 mm per step, and for the last few loading steps this ramps up to a maximum of 5 mm in the last step.

The tensile bearing capacity of the volume pile according to the numerical simulation is found by further increasing the loading on the volume pile until numerical failure in PLAXIS 3D is achieved. However it was found that the numerical failure did not occur in the model, even when the tensile load was increased up to 6000 kN. The displacement at this tensile force is equal to 0.25 m.

At the maximum displacement of 17.89 mm at 2000 kN the tension piles are assumed to be ‘failed’ due to the magnitude of the displacement. Upon load increase beyond 2000 kN, the maximum displacement will increase even faster as seen in Figure 24. Hence the bearing capacity of the volume pile is assumed to be 2000 kN.

### 7.3.2 Embedded beam

The tension pile is modelled as an embedded beam. The pile load is simulated as a point load on top of the embedded pile. The stiffness of the embedded beam is assumed to be that of concrete, which is 30 GPa. The pile load test was simulated using the embedded beam. In contrary to the volume pile test, the embedded beam model numerically failed halfway the pile load test. It is expected that this is due to the way the embedded beams are designed in PLAXIS 3D. The embedded beams are not actually part of the Finite Element mesh, which means their values are interpolated from the nearest known nodal values. It is expected that the numerical failure happens because the accuracy condition is not reached due to the large interpolation errors for the embedded beam. In the PLAXIS manuals the following information is found.

Embedded beam elements have demonstrated particularly good results for serviceability states of pile groups under axial loading. It is important to note that the calculation time and the number of elements required to analyze a certain pile–soil interaction problem are sufficiently reduced by using embedded piles compared to using volume piles. (Bentley, 2021)

From this, it is concluded that the embedded beam element is able to perform better numerically when used in a pile group, and thus is not fully suitable for the simulation of a single pile load test.

The final distribution of the displacement of the pile after the completed load test steps as simulated is shown below. The numerical failure occurred after approximately 1.35 days at 900 kN force.

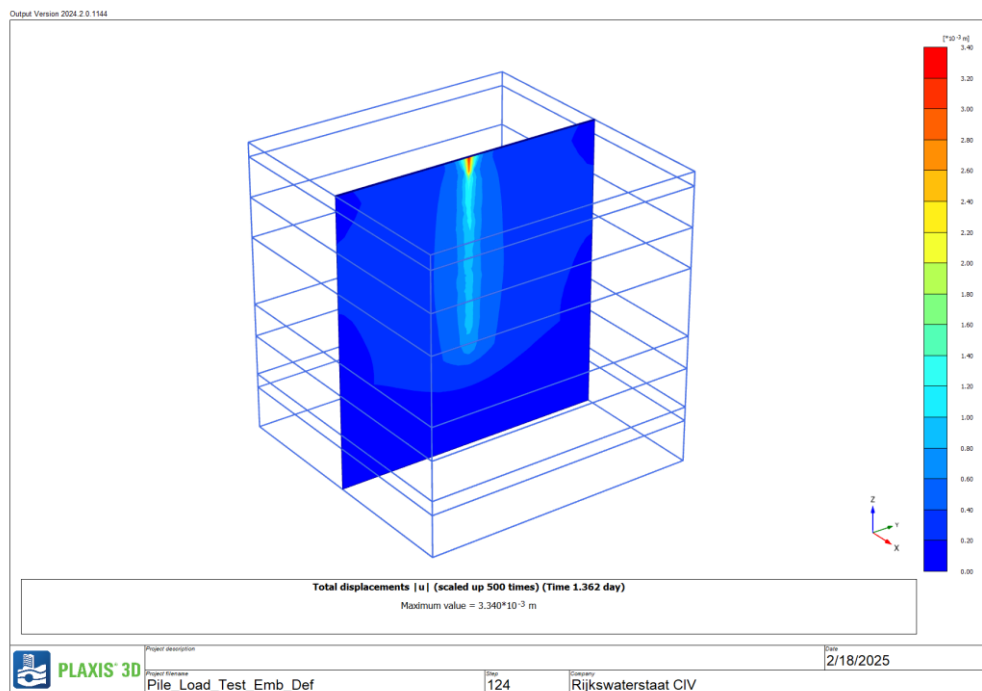


**FIGURE 25: DISPLACEMENT DISTRIBUTION FOR EMBEDDED BEAM**

The output shows that the maximum value of displacement is equal to 3.34 mm. The total calculation time for this model is equal to around 20 minutes, which as expected is much faster than the volume pile model in the previous section. The development of the time displacement and force displacement of the pile load test modelled as an embedded beam is shown below.

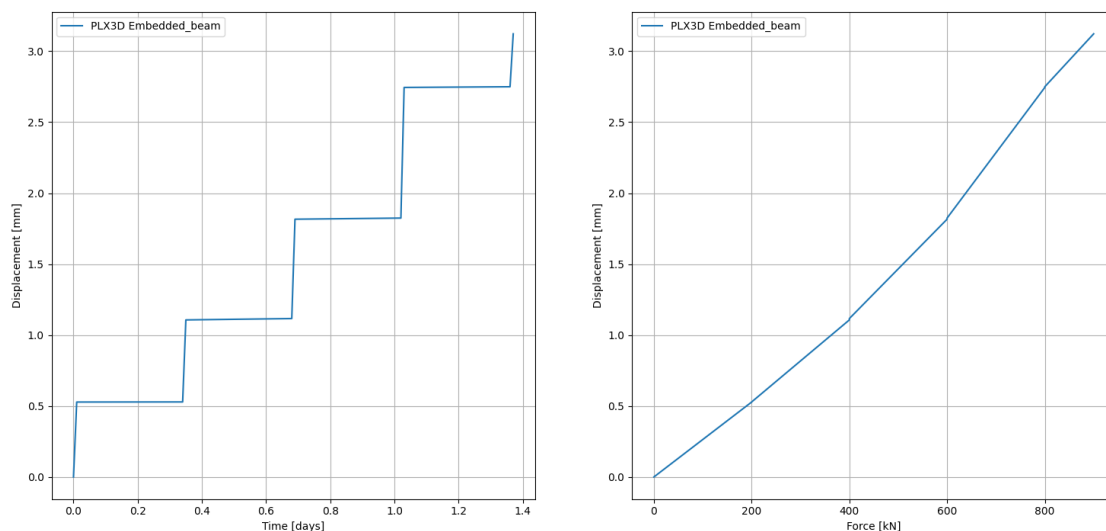


**FIGURE 26: TIME-DISPLACEMENT DIAGRAM FOR EMBEDDED BEAM**

The graph shows that the development of displacements of the pile are quite constant for every loading step, which is in line with the results from the pile load tests. Where the graph stops, the numerical failure occurred. In the profile of the displacement, no increase in reaction can be seen as time/force increases. No signs of geotechnical failure were shown before numerical failure happened. As earlier said it is expected that this is due to interpolation error within PLAXIS 3D. The geotechnical capacity of the single tension pile in PLAXIS 3D as an embedded beam is modelled to be 900 kN.

### 7.3.3 Comparison of numerical models

The volume pile model is seen as computationally inefficient since the calculation time for the simulated pile load test is around three hours. From the graph it can be seen that the displacement profile is in line with that of the pile load tests for the first five loading steps. For the remaining loading steps however, the volume pile model overestimates the displacements. The volume pile models' shows greater displacement at higher loads compared to the performed pile load tests.

The embedded pile model is computationally efficient, the calculation time for this model is only 20 minutes. This makes it a much more scalable option when more tension piles are modelled. The numerical failure occurred after a tensile force of 900 kN. The graphs of the embedded beam model are compared with the volume pile model graphs below.

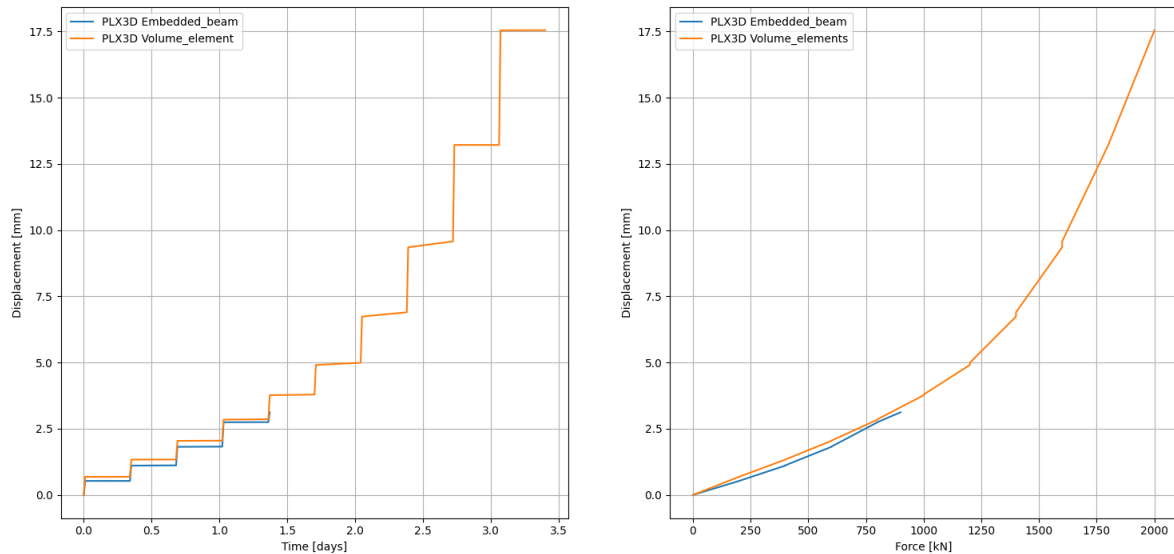


**FIGURE 27: COMPARISON DISPLACEMENT VOLUME & EMBEDDED PILE PLAXIS3D**

It can be seen that the graphs are very similar, up until the numerical failure occurs for the embedded beam model. From this similarity it is concluded that the volume pile and embedded beam show similar behavior upon tensile loading to the numerical capacity of 900 kN. The embedded beam model is a lot more efficient in computation time and is regarded as the optimal model as long as the axial loads imposed on the embedded beams are less than 900 kN. When modelled in a group, it is expected that numerical failure will not occur as early as the single pile and show behavior similar to the volume pile.

The performance of the single tension pile model is judged based on similarity in displacements between the pile load test and simulation. The graph below shows the time-displacement diagram of the three pile load tests as performed by GeoDelft (1968) and the two PLAXIS 3D tension pile models.

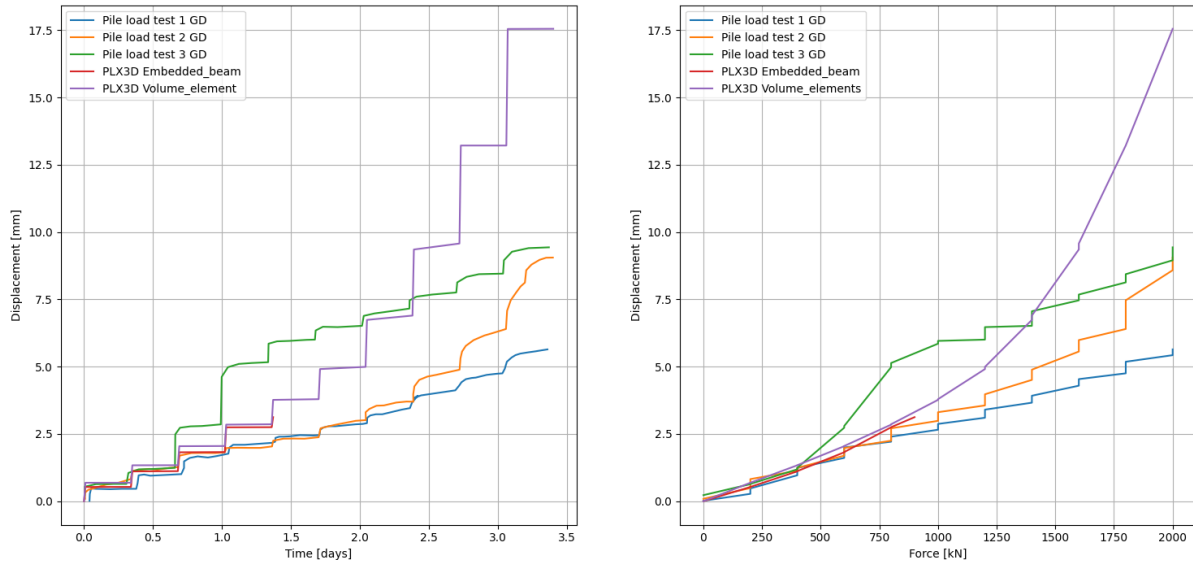


**FIGURE 28: TIME-DISPLACEMENT DIAGRAMS OF PULL-OUT TESTS AND PLAXIS 3D MODELS**

It can be seen that especially in tensile forces below 1000 kN, the pile load tests and numerical models show very similar behavior. This is seen as a satisfactory performance as the relevant design capacities as calculated in Table 12 are either close or below this value. The next step is to model the tunnel element with the tension pile foundation installed.

The embedded pile model is regarded as a suitable method for modelling tension piles in PLAXIS 3D for computational efficiency. In further PLAXIS 3D modelling for this research, tension piles are modelled as embedded beams. Since the critical tunnel element has a multitude of tension piles installed in its foundation, the embedded beams will be modelled in a group. Because of this, the numerical performance is expected to increase.

## 7.4 Comparison of limit carrying capacities

The obtained geotechnical limit carrying capacities from different sources for a single tension pile are compared in this chapter.

The pile load tests graphs in Figure 28 show that at 2000 kN of tensile force, failure is not yet achieved in the displacement profile. In the report the geotechnical limit carrying capacity was estimated to be around 3000 kN.

The modelled tension piles in PLAXIS 3D have a different calculated capacity. It is expected that this is due to numerical instability in the embedded beam model when modelling the pile load tests. The embedded beam model is expected to have better numerical stability when used in groups. In this case it is assumed that the embedded beam capacity is similar to the volume pile capacity.

From the calculation results following the model proposed in the relevant Dutch NEN 9997-1 norm it was calculated that the geotechnical limit carrying capacity of the tension pile is equal to 1734.35 kN with safety and 3265.09 kN without safety. In the DFoundation manual it is found that these capacities are based on an upward displacement of 10 mm. Judging from Figure 28, especially if the embedded beam behavior is assumed similar to that of the volume pile, it can be seen that at a displacement of 10 mm, the volume pile has a force of 1650 kN. This is slightly lower than the capacity calculated by DFoundation with safety factors but still very similar. The graphs from PLAXIS 3D are a slight overestimation of the graphs from the pile load tests, but still regarded as satisfactory. Given that PLAXIS 3D, DFoundation and the pile load tests give similar results, the software's are to model the critical tunnel element of the EHT. Only the latest applicable calculation norm is taken into consideration in this chapter.

The capacity of the steel prestressing rods of the tension piles have been calculated using the steel quality and relevant safety factors. This resulted in 752.78 kN with safety and 828.38 kN without safety.

The results are collected in Table 13.

**TABLE 12: LIMIT CARRYING CAPACITIES FOR TENSION PILES FROM DIFFERENT SOURCES**

	Capacity with safety applied [kN]	Capacity without safety applied [kN]
<b>Original design value EHT</b>	450	1350
<b>Pile load tests</b>	3000	3000
<b>NEN 9997-1 (2005-present)</b>	1734.35	3265.09
<b>Steel strength capacity EHT</b>	752.78	828.38
<b>PLAXIS 3D Volume pile</b>	2000	2000
<b>PLAXIS 3D Embedded pile</b>	900	900

It can be seen that the geotechnical capacities as determined by the pile load tests and the NEN 9997-1 norm are generally way higher than the material capacity given by the steel and the design value of the EHT. It is expected that due to limited geotechnical research in this period around 1960, a large safety factor was chosen in the design of the EHT to account for the large uncertainty due to absence of knowledge.

The steel strength capacity is substantially lower than the capacities from the pile load tests, PLAXIS 3D and the NEN 9997-1. However this is explainable due to the fact that the utilized amount of steel in the tension pile was based on the design value of 450 kN at the time of the design phase of the tunnel. In this case the steel design material strength amounts to 1.67 times the design value. The possibility of material failure before geotechnical failure should be considered in further models.

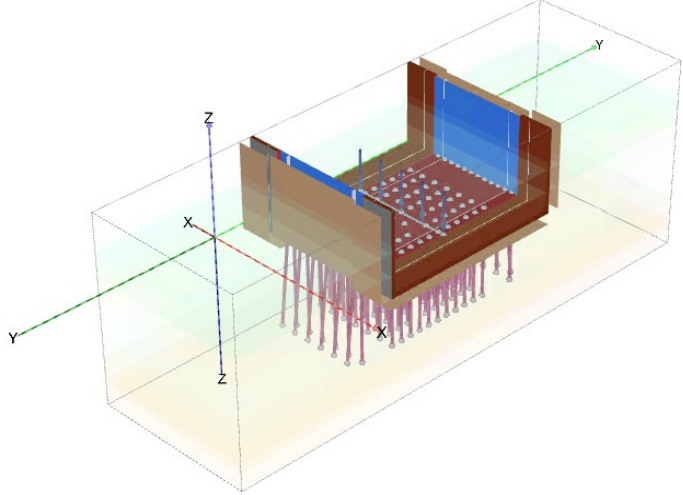
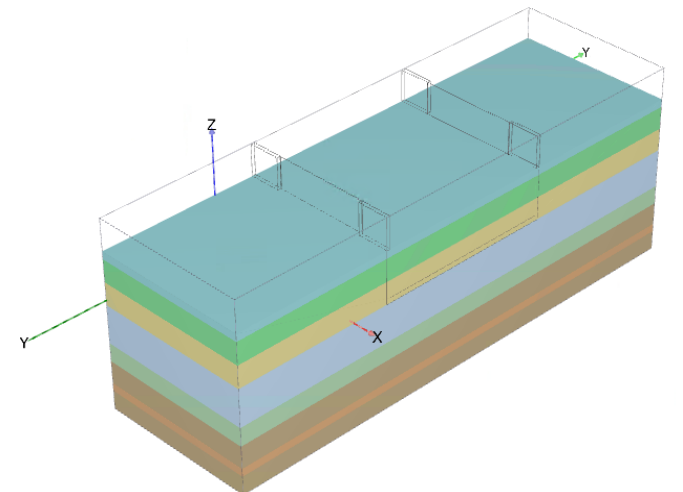
Since the tension piles for the EHT are installed at a deeper level due to the excavation, approximately 10 meters under surface level, the soil layers from which the geotechnical capacity is calculated is different. In the next chapter the geotechnical capacity following the NEN 9997-1 is recalculated based on the soil layers surrounding the tension piles installed. The tension pile foundation of the EHT is installed as a multitude of pile groups. The factors to account pile group effects have a large influence on the geotechnical carrying capacity. Also the clod criterium has to be checked for each pile group as earlier discussed. The critical tunnel elements on both sides of the tunnel are modelled for the analysis in both DFoundation and PLAXIS 3D to determine their tensile capacity.

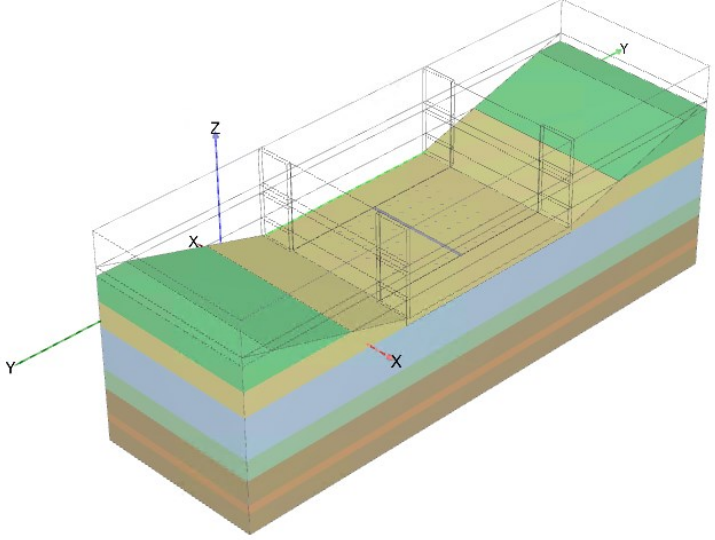
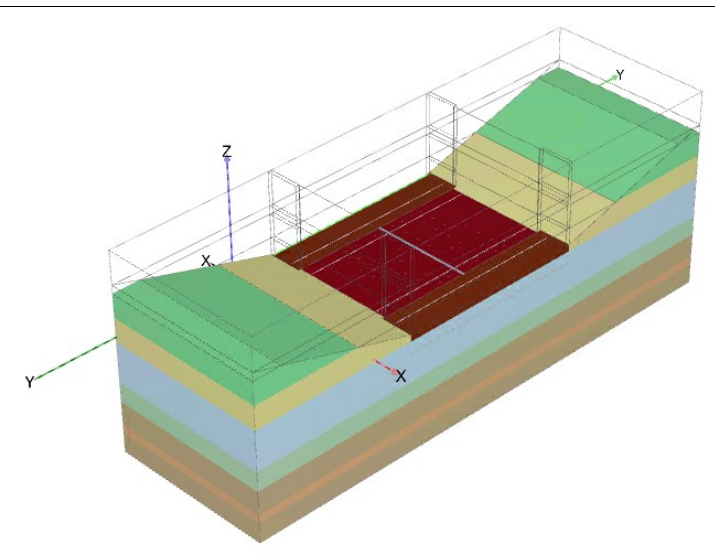
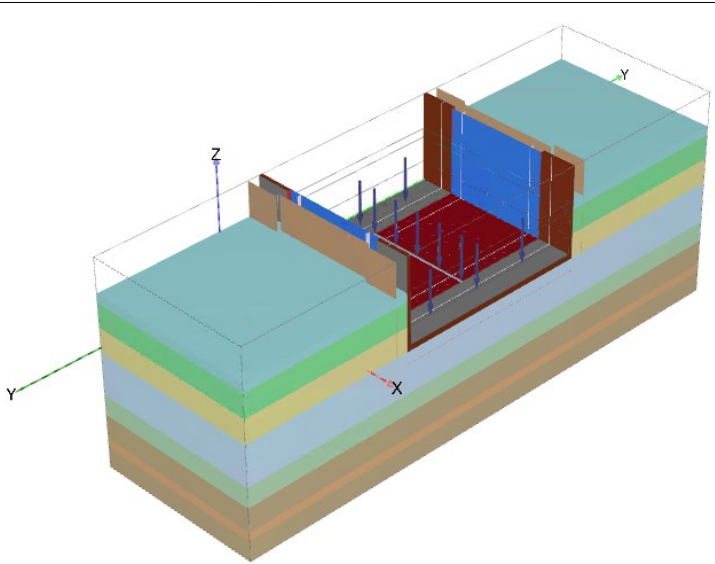
## 8. Capacity of the critical elements

As previously mentioned, the tension pile foundation of the critical tunnel element of the EHT is analyzed based on their capacity and the reaction based on the tension piles failing. To do this correctly, multiple software's are used; DFoundation is used as a validation of the numerical analysis, PLAXIS 3D and Python software are used to do the numerical geotechnical analysis, automate data collection and show its results.

The geometries of the critical tunnel elements 3N & 3Z along with their tension pile foundations are defined in PLAXIS 3D. In this model, the floor and walls of the tunnel are modelled as plates. Interface elements are added where the plates are adjacent to the soil. The wall in the middle of the tunnel element is modelled as a line load to reduce the amount of elements needed in the mesh. This is possible since this wall is not resisting any load. Only the self-weight is relevant for the formulation of the model. The tension pile foundation is modelled as a multitude of embedded beam elements, which are connected to the floor plate element. For the correct boundary effects on either side of the tunnel element, a part of the neighboring elements are modelled as well. However, they are not modelled with tension piles and buoyant force. Instead they are simulated as static tunnel elements with an interface element towards the critical tunnel element to simulate the friction between the neighboring tunnel element walls. This in order to limit computation time and focus mainly on the modelling of the critical tunnel element. In this original formulation of the model, the friction between tunnel walls is set to zero. This means it is assumed that the tunnel elements are kept separate from each other and can deform independently. The buoyant force from the water is generated in the model by defining the correct water levels and impermeable elements. The construction phases of the tunnel element are defined in the table below;

**TABLE 13: STRUCTURES MODEL AND CONSTRUCTION PHASES OF TUNNEL ELEMENT AS IN PLAXIS 3D**

<b>Structure model</b>	Definition of the structural elements, interfaces & embedded beams	
<b>Initial phase</b>	Soil is activated in its initial state	

<b>Phase 1</b>	Excavation of the building pit and reduction of water levels to excavation level	
<b>Phase 2</b>	Installation of floor & embedded beam elements and activation of their interfaces with the soil	
<b>Phase 3</b>	Installation of walls elements and activation of the remaining interfaces and backfill of excavation soil	



To validate the numerical model based on relevant construction norms, the information from Chapter 7.4 is used. In this chapter it was seen that the capacity of a tension pile can be calculated in various ways. The most representative method is chosen to be the NEN 9997-1 method, since it is the most relevant and actual geotechnical norm applicable in the Netherlands for geotechnical design and has a realistic safety factor when comparing to the pile load tests. Since the tension pile foundation is regarded as a pile group, the pile group effects and soil clod criterium should be taken into account when calculating the geotechnical capacities of the tension piles. Using DFoundation with the determined soil profiles, the geotechnical capacity of the tension piles in a group are calculated. The total capacity of the tension pile foundation is found by taking the sum of the capacities of the different pile groups. In DFoundation, the calculated capacity of the pile groups are calculated assuming failure at an upward displacement of 10 mm. This capacity at 10 mm displacement can be used to validate the numerical PLAXIS 3D models of the tunnel elements. This is done by checking the tensile forces in the piles in the PLAXIS 3D model when the maximum vertical displacement exceeds 10 mm. Validation with the NEN 9997-1 norm is seen as highly necessary in PLAXIS 3D is very prone to incorrect input which results in incorrect output which might be interpreted the wrong way.

The relevant soil profiles for the northern and southern elements respectively as used in DFoundation and PLAXIS 3D is shown in the tables below, which are extracted and repeated from Section 6.3.2.

**TABLE 14: REPETITION GOVERNING GEOTECHNICAL CROSS SECTION NORTH**

Layer	Level top layer [m]	$q_{c, \text{gem}}$ [MPa]	Friction angle [°]	Cohesion [kPa]	Volumetric weight [kN/m <sup>3</sup> ]	E50 [MPa]	Soil classification
N1	NAP + 0	0.71	22.5	15	17.2	-	Clay, weak silty to silty
N2	NAP – 1.5	10.15	30	2	17.7	20	Sand, silty to silt
N3	NAP – 5.75	6.54	28	2	13.1	28	Sand, silty to silt
N4	NAP – 10	11.75	34	2	17.7	40	Sand, moderate dense
N5	NAP – 17.25	19.35	36	0	19.6	50	Sand, clean
N6	NAP – 20.75	2.8	26	20	20.1	10	Clay, weak silty to silty
N7	NAP – 25	5.54	36	0	19.7	60	Sand, clean
N8	NAP – 26.5	2.8	26	20	20.8	10	Clay, weak silty to silt

**TABLE 15: REPETITION GOVERNING GEOTECHNICAL CROSS SECTION SOUTH**

Layer	Level top layer [m]	$q_{c, \text{gem}}$ [MPa]	Friction angle [°]	Cohesion [kPa]	Volumetric weight [kN/m <sup>3</sup> ]	E50 [MPa]	Soil classification
Z1	NAP + 1	0.72	22.5	15	18	-	Clay, weak silty to silty
Z2	NAP – 3.25	10.49	32	2	20	12	Sand, weak silty to silty
Z3	NAP – 4.5	0.42	30	4	13	2	Peat, organic soil
Z4	NAP – 7.25	1	25	10	17	12	Clay, weak silty to silty
Z5	NAP – 10.5	3.6	29	0	20	28	Sand, silty to silt
Z6	NAP – 14.75	13.6	36	0	20.5	55	Sand, clean
Z7	NAP – 21.5	3	29	25	20	10	Clay, weak silty to silt
Z8	NAP – 24.5	13.02	36	0	20.5	60	Sand, clean

## 8.1 Modelling northern element 3N

The capacity of the tension piles is based on their geotechnical capacity based on pile groups following the NEN 9997-1 model using DFoundation. The input in the model is the soil profile as shown on the previous page together with the tension pile properties and the tension pile foundation layout. DFoundation creates pile groups based on this layout. Then for each pile group, the capacity is calculated with safety factors applied as posed in the Dutch norm. The output of the model is shown below.

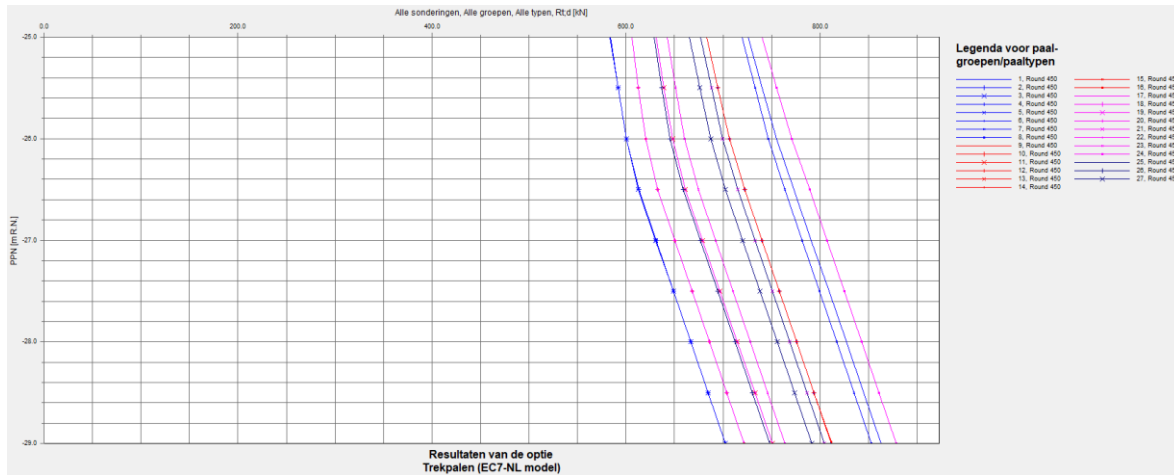


FIGURE 29: DFOUNDATION OUTPUT ELEMENT 3N WITH SAFETY FACTORS

Due to the asymmetry in the tension pile foundation layout, many pile groups are created by DFoundation represented by the different lines. The output shows the capacity of each tension pile group in kN at their respective depth. In the output, the depth ranges from -25 to -29 m. The total excavation of the tunnel element is equal to 10 m. The length of the tension piles for the northern side are equal to 17 m. This results in a tension pile tip level of 27 m which is the relevant depth in the output graph. At this depth, the single pile capacities of different pile groups range from 650 kN to 810 kN.

The same model run as above is done, except with all safety factors reduced to 1. The output is shown below.

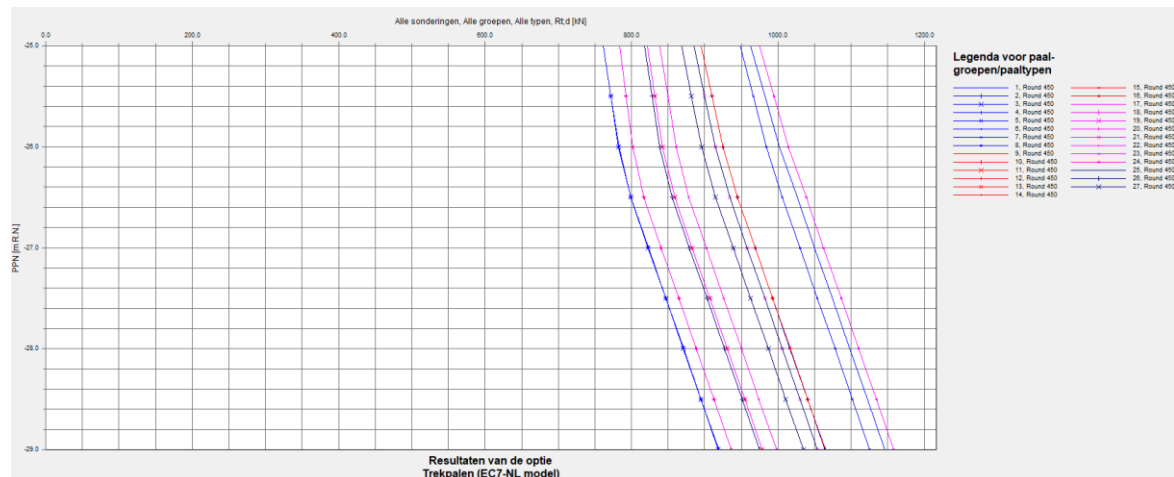


FIGURE 30: DFOUNDATION OUTPUT ELEMENT 3N WITHOUT SAFETY FACTORS

In this model run without safety factors applied, it can be seen that the single pile capacities of different pile groups range from 825 kN to 1010 kN. This is roughly an increase of 20% in capacity by removing the safety factors from the calculation. By taking the sum of these calculated single pile capacities for their respective pile groups, the total capacity of the tension pile foundation according to the Dutch norm is calculated for the northern entrance.

The DFoundation model run with safety factors results in a total capacity of 65534.9 kN with 95 piles.

The DFoundation model run without safety factors results in a total capacity of 84560.6 kN with 95 piles.

Using PLAXIS 3D, the capacity was found by increasing the upward pressure on the critical tunnel element until the model shows numerical failure. However, prior to reaching numerical failure, the PLAXIS 3D model can be validated with DFoundation by checking the force in the tension pile foundation when the maximum displacement in the floor exceeds 10 mm. If the force is similar to the calculated capacity from DFoundation, the PLAXIS 3D model can be regarded as validated using the most actual Dutch norm.

The numerical model of tunnel element 3N reaches a maximum vertical displacement of 10 mm of the tunnel floor at a buoyant pressure of  $153 \text{ kN/m}^2$  which is a 70% increase of the original buoyant pressure on the tunnel floor. The original buoyant pressure is equal to  $90 \text{ kN/m}^2$ . By multiplying this pressure with the floor area, the total buoyant force on the tunnel floor is found. By subtracting the self-weight of the tunnel from this force, the tension capacity of the tension pile foundation is found. Performing this calculation results in a force of 66644.6 kN. When comparing this to the capacity found in the DFoundation model, this value is almost identical to the capacity from DFoundation with safety applied. The numerical model underestimates the capacity without additional safety by 21%. The capacity from PLAXIS 3D falls within the range of the capacity determined using DFoundation. The PLAXIS 3D model of the critical tunnel element 3N of the EHT therefore is validated with the NEN9997-1 norm. The displacement of the floor plate element at an upward pressure of  $153 \text{ kN/m}^2$  and a maximum displacement of 10 mm is shown below. It can be seen that the displacement is at a maximum in the middle of the floor element. The circular shape is caused by the layout of the tension pile foundation.

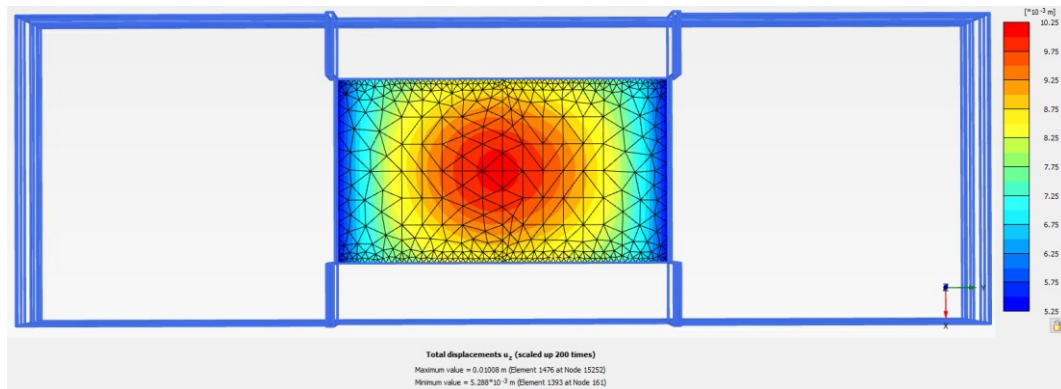


FIGURE 31: DISPLACEMENT OF FLOOR PLATE ELEMENT SLS 3N

The deformed mesh of the soil model is shown below.

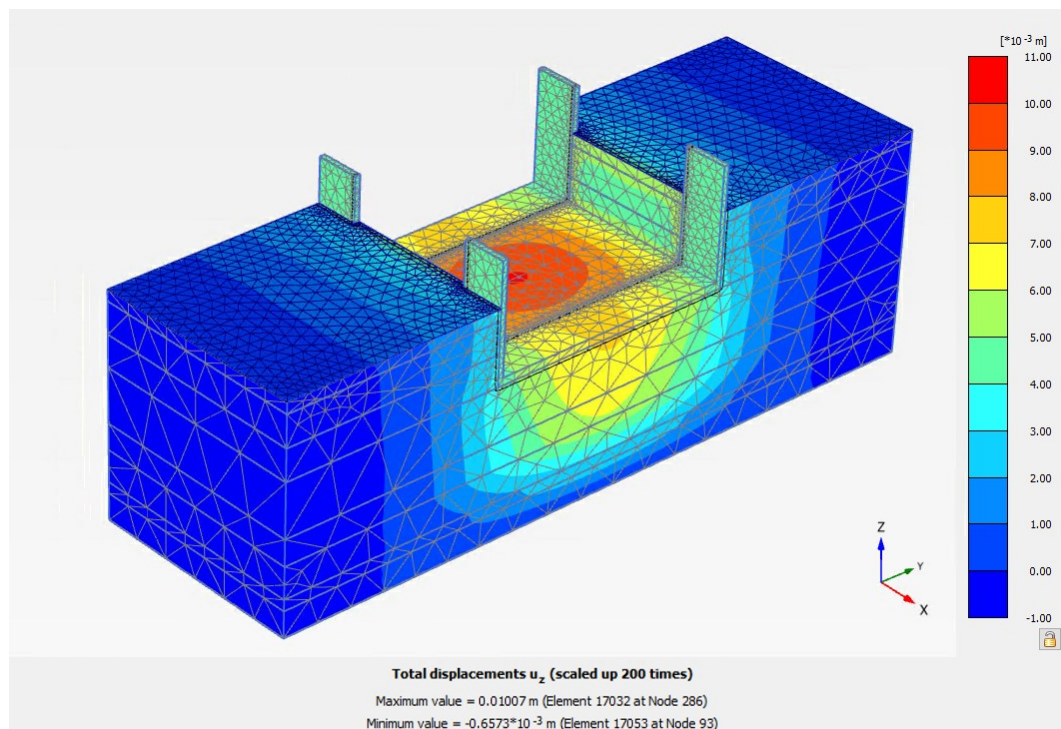


FIGURE 32: DEFORMATION OF SOIL BODY ELEMENT 3Z

Numerical failure of the PLAXIS 3D model of tunnel element 3N occurred at an applied upward pressure of 241 kN/m<sup>2</sup>. This is an increase of 168% from the original buoyant pressure. This means the factor of safety for the tunnel for numerical failure regarding the current situation is equal to 2.68. The water level could theoretically rise to 16.8 m above the surface prior to the tunnel element failing. This of course is an unlikely scenario. This capacity is an ultimate limit state (ULS) as the tunnel is expected to fully collapse if the upward pressure of 241 kN/m<sup>2</sup> is exceeded. The serviceability limit state (SLS) displacement for the tunnel element is assumed to be around 10 mm as it is expected that the tunnel will not be suitable for facilitating traffic safely anymore. The assumption is backed by the prescribed failure condition in DFoundation of 10 mm.

The maximum displacement in the tunnel floor at numerical failure is equal to 31.17 mm. The floor plate element is shown in the figure below. The maximum displacement of the tunnel floor is localized in the middle, where some tension piles are removed from the grid as seen in Figure 10.

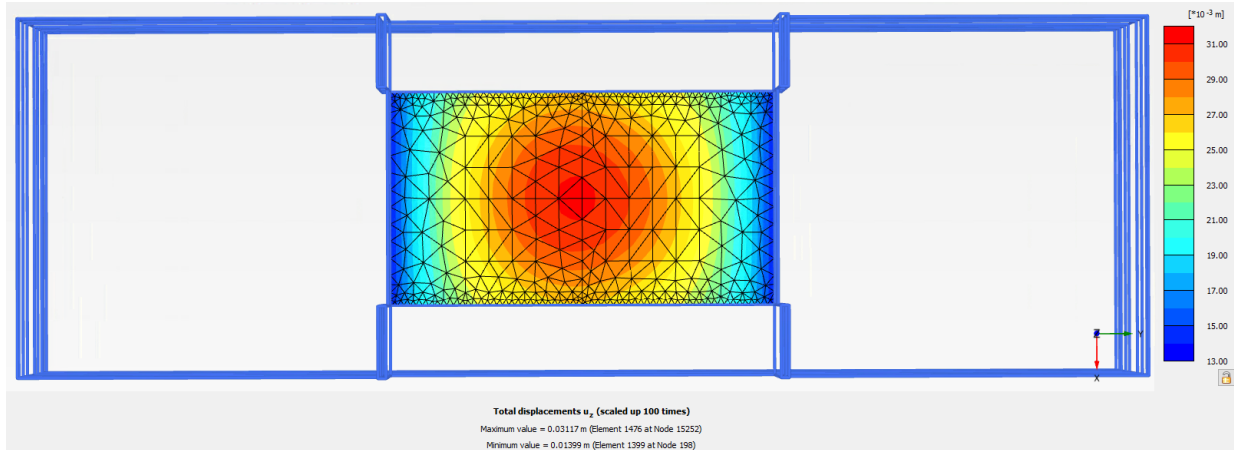


FIGURE 33: DISPLACEMENT OF FLOOR PLATE ELEMENT ULS 3N

The deformed mesh of the soil model is shown below.

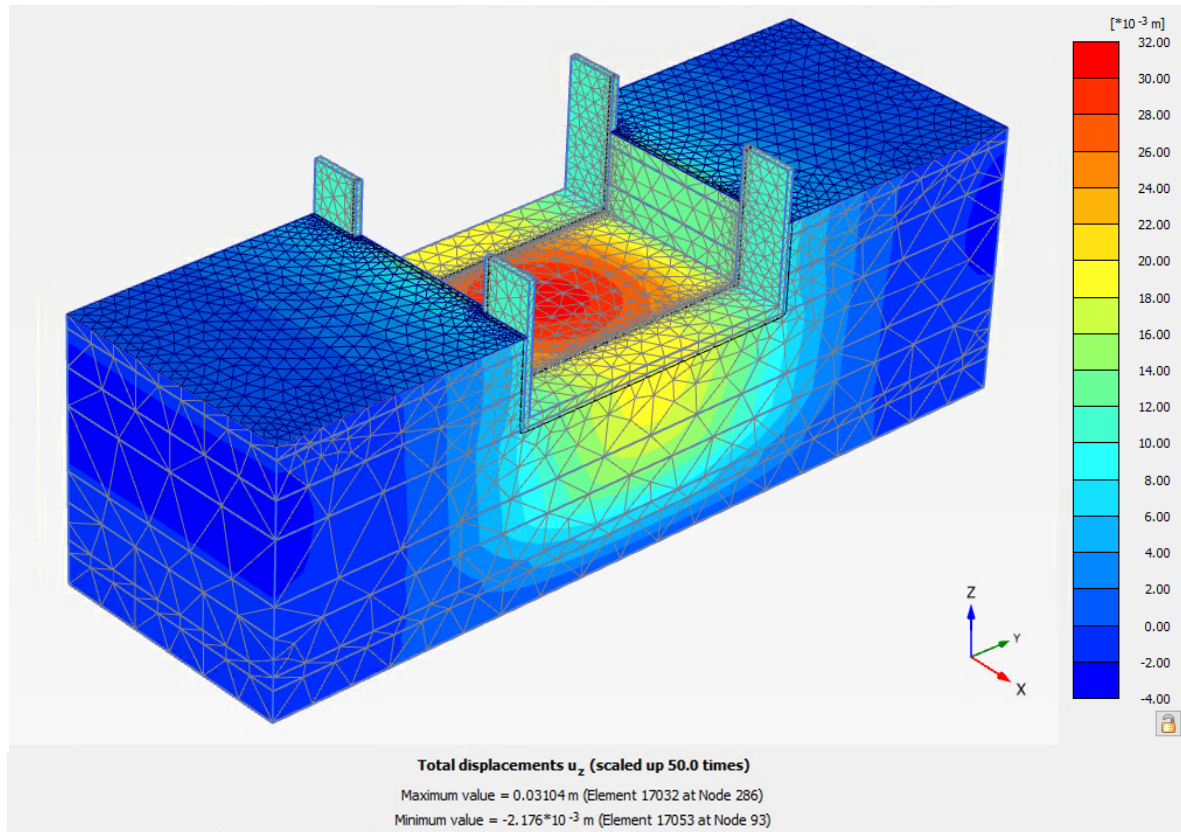


FIGURE 34: DEFORMATION OF SOIL BODY ULS 3N

An identical analysis is done for the southern element 3Z in the next section of this chapter.

## 8.2 Modelling southern element 3Z

Similarly to the calculation of tension pile foundation capacity according to DFoundation for the northern entrance in the previous section, the capacity of the southern entrance is determined.

The output of the DFoundation model with safety factors applied for the southern entrance is shown below.

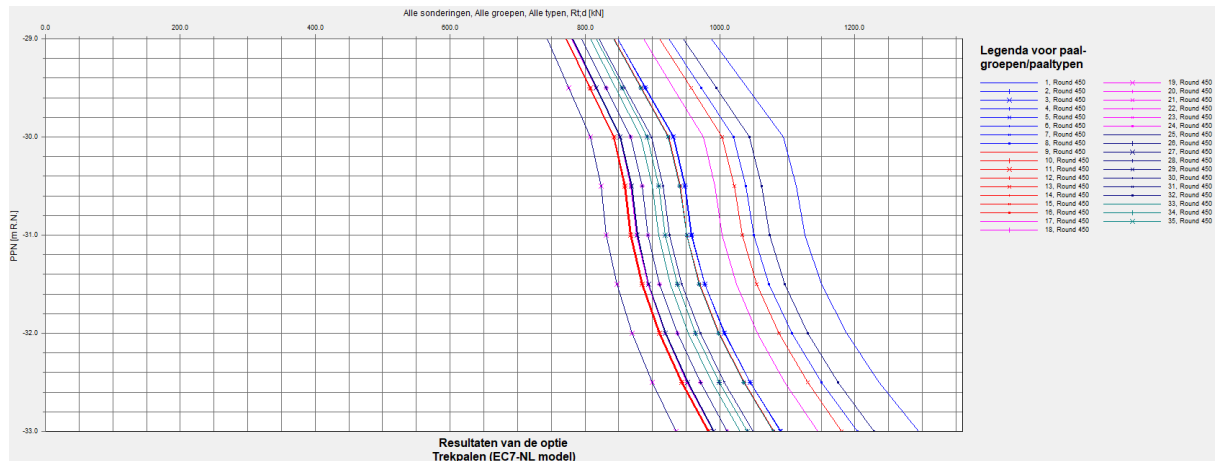


**FIGURE 35: DFOUNDATION OUTPUT ELEMENT 3Z WITH SAFETY FACTORS**

Similarly to the northern entrance, due to the asymmetry in the tension pile foundation layout, many pile groups are created by DFoundation represented by the different lines. The depth ranges from -29 to -33 m. The total excavation of the tunnel element is equal to 10 m. The length of the tension piles for the southern side are equal to 21 m. This results in a tension pile tip level of 31 m which is the relevant depth in the output graph. At this depth, the single pile capacities of different pile groups range from 830 kN to 1125 kN.

The resulting capacities are higher than those of the northern entrance. This is both due to the increase in length of 4 m of the tension piles compared to 3N and the presence of stronger & stiffer soil layers such as Z7.

The output of the DFoundation model for the southern entrance without safety factors applied is shown below.

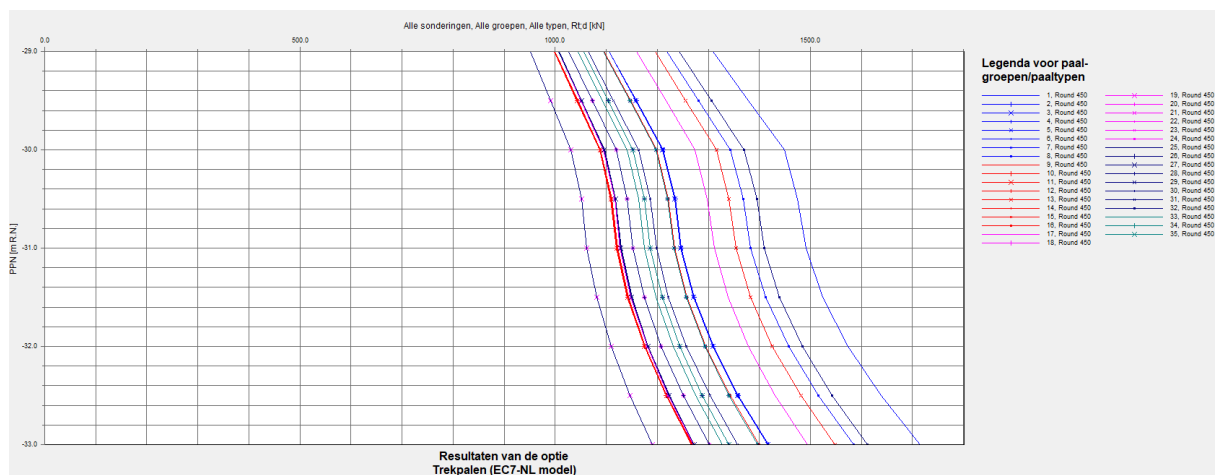


**FIGURE 36: DFOUNDATION OUTPUT ELEMENT 3Z WITHOUT SAFETY FACTORS**

In this model run without safety factors applied, it is seen that the single pile capacities of different pile groups range from 1050 kN to 1490 kN. This is roughly an increase of 20% in capacity by removing the safety factors from the calculation. By taking the sum of these calculated single pile capacities for their respective pile groups, the total capacity of the tension pile foundation according to the Dutch norm is calculated for the southern entrance.

The model run with safety factors results in a total tension capacity of 62302.9 kN with 67 piles.

The model run without safety factors results in a total tension capacity of 80492.6 kN with 67 piles.



Similarly to the analysis of tunnel element 3N in the previous section, the PLAXIS 3D model is validated using DFoundation.

The numerical model of tunnel element 3Z reaches a maximum upward displacement of 10 mm of the tunnel floor at a buoyant pressure of  $162 \text{ kN/m}^2$  which is an 80% increase of the original buoyant pressure on the tunnel. Assuming failure at this maximum displacement similar to DFoundation, the tension pile foundation capacity of element 3Z is equal to 72152.6 kN.

The numerical model underestimates the capacity determined using DFoundation without additional safety by 10%. The capacity according to PLAXIS 3D falls within the range of the capacity determined using DFoundation. The PLAXIS 3D model of the critical tunnel element 3Z of the EHT therefore is validated with the NEN9997-1 norm. The displacement of the floor plate element at an upward pressure of  $162 \text{ kN/m}^2$  and a maximum displacement of 10 mm is shown below. It can be seen that the displacement is maximum in the center of the plate, the elliptic shape of the displacement profile is caused by the layout of the tension pile foundation.

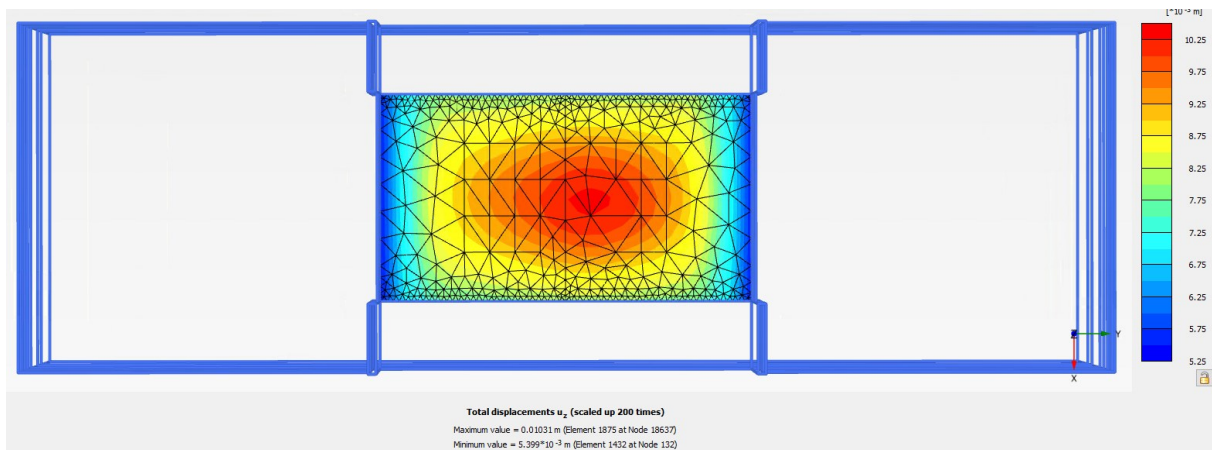


FIGURE 37: DISPLACEMENT OF FLOOR PLATE ELEMENT SLS 3Z

The deformed mesh of the soil model is shown below.

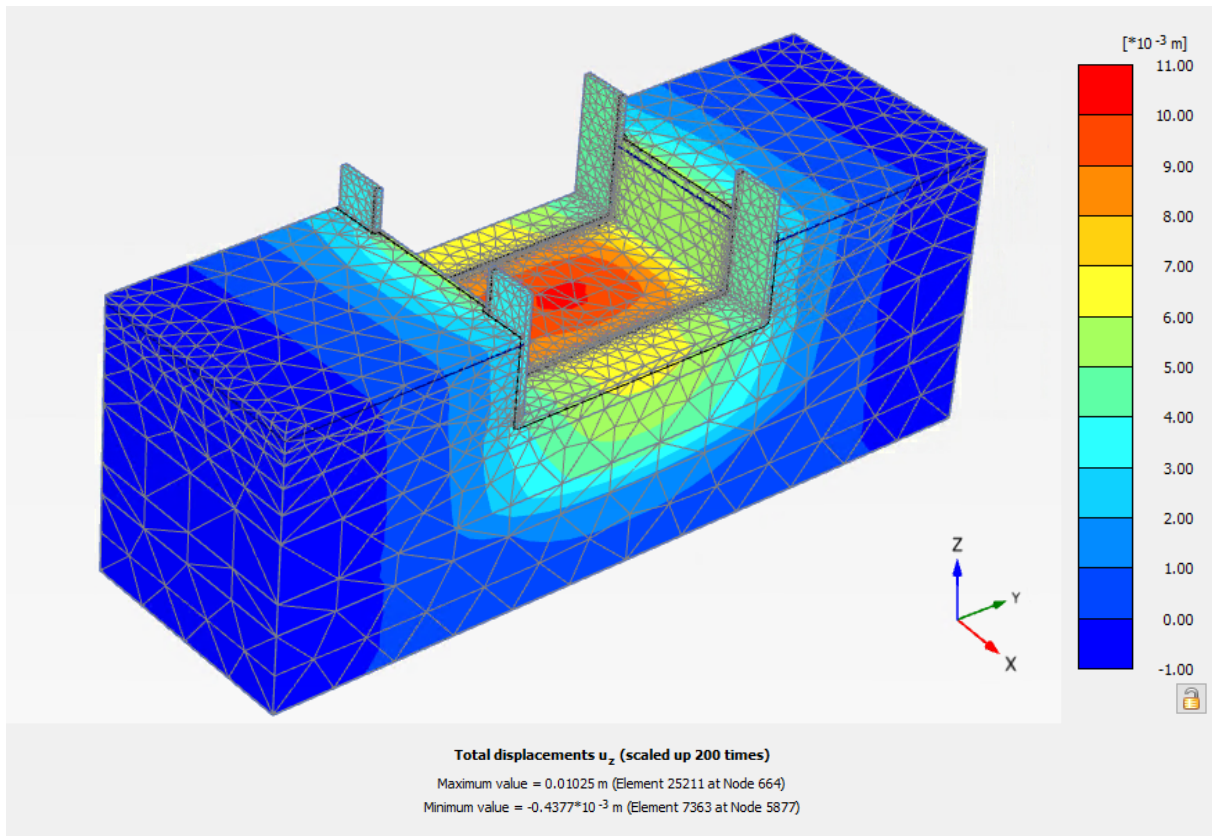


FIGURE 38: DEFORMATION OF SOIL BODY SLS 3Z

Numerical failure of the PLAXIS 3D model of tunnel element 3Z occurred at an applied upward pressure of 189 kN/m<sup>2</sup>. This is an increase of 110% from the original buoyant pressure. This means the factor of safety for the tunnel for numerical failure regarding the current situation is equal to 3.1. The water level could theoretically rise to 21 m above the surface prior to the tunnel element failing. This of course is an unlikely scenario. This capacity is an ultimate limit state (ULS) as the tunnel is expected to fully collapse if the upward pressure of 189 kN/m<sup>2</sup> is exceeded. The serviceability limit state (SLS) displacement for the tunnel element is assumed to be around 10 mm as it is expected that the tunnel will not be suitable for facilitating traffic safely anymore. The assumption is backed by the prescribed failure condition in DFoundation of 10 mm.

The maximum displacement in the tunnel floor at numerical failure is equal to 19.37 mm. The floor plate element is shown in the figure below. The maximum displacement distribution has an inhomogeneous shape, this is explainable due to the inconsistency in tension pile layout. On the right side of the tension pile foundation of element 3Z there are 4 tension piles removed from the grid as can be seen on Figure 11. This is where the maximum displacement is localized.

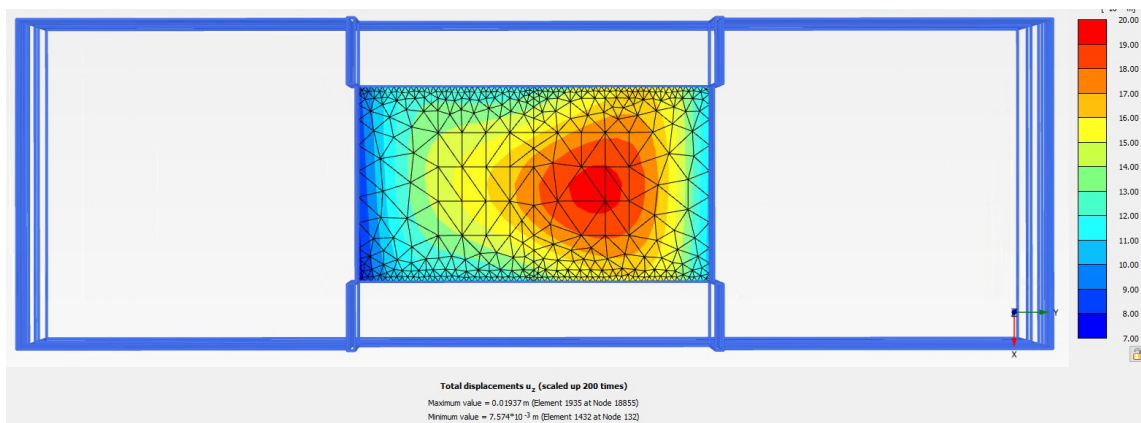


FIGURE 39: DISPLACEMENT OF FLOOR PLATE ELEMENT ULS 3Z

The deformed mesh of the soil model is shown below.

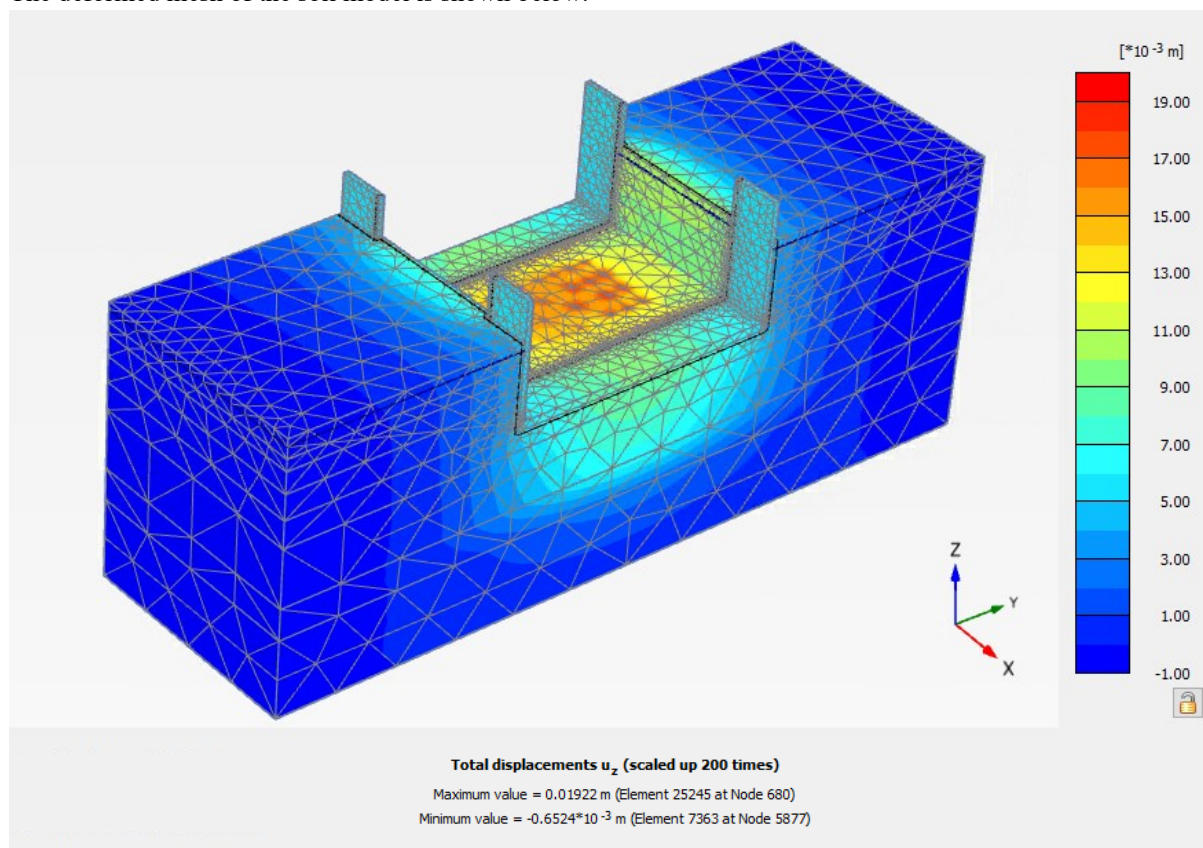


FIGURE 40: DEFORMATION OF SOIL BODY SLS 3Z

### 8.3 Comparison of results

If tension piles would lose function due to corrosion failure, this capacity could decrease drastically. In the next chapter the influence of corrosion failure is researched in more detail.

The results of the capacity analysis of element 3N & 3Z are collected in Table 17.

**TABLE 16: COMPARISON OF ELEMENT 3N & 3Z**

	<b>DFoundation safety included</b>		<b>DFoundation safety excluded</b>		<b>Plaxis3D SLS</b>		<b>Plaxis3D ULS</b>	
	Capacity [kN]	Displacement [mm]	Capacity [kN]	Displacement [mm]	Capacity [kN]	Displacement [mm]	Capacity [kN]	Displacement [mm]
<b>Element 3N</b>	65534.9	10	84560.6	10	66644.6	10	120500.6	31.2
<b>Element 3Z</b>	62302.9	10	80492.6	10	72152.6	10	88676.6	19.4

From the results is found that tunnel entrance elements 3N & 3Z have similar capacities. The outcomes of both Plaxis3D models are verified with their respective DFoundation results by checking the capacity at a maximum displacement of 10 mm. Both numerical models resulted in a slight overestimation of the DFoundation with applied safety factors. The results of determined ultimate capacity upon failure using Plaxis3D were slightly different. The ultimate capacity of element 3N is 36% higher than that of element 3Z. However, it is expected that at these rather large loads the numerical stability decreases which causes the model to fail. Since the capacity at SLS is roughly the same of the elements, it is more likely that their behavior is similar.

In this chapter the capacity of the element was found by increasing the buoyant pressure. However in order to model the failure mechanism of uplift due to stress corrosion, the buoyant pressure stays the same and the tension piles are failing subsequently due to corrosion. The capacity of buoyant pressure was mostly used to validate the numerical model. Now that the validation of the numerical models is done, they are used to model the failure mechanism of uplift due to stress corrosion. This is included in the next chapter.



## 9. Analysis of corrosion failure

As earlier described, the cause of the tension pile failure in the case of the Prinses Margriet tunnel is found to be stress corrosion. In Chapter 2.2, the combination of circumstances that enable types of corrosion are determined through literature.

### 9.1 Stress corrosion

In the PLAXIS 3D modelling of this research, the failure of a tension pile due to stress corrosion is modelled through the deactivation of that pile, losing full capacity. In research it was found that the presence of stress corrosion was distributed randomly among the tension piles, no pattern of tension pile failure could be identified. Because of this, a Monte Carlo analysis is done on the tension piles failing in randomly generated patterns. The expected outcome is an envelope of the heave of the tunnel element as more tension piles fail. This chapter will analyze the possibility of stress corrosion occurring for the EHT. The circumstances for stress corrosion to occur are as follows. For each circumstance the situation of the EHT is analyzed.

#### *Utilized material should be susceptible to corrosion*

The utilized steel quality in the steel rods is QP 105 steel. The relatively high steel quality is mostly applied for prestressing purposes. The quality is a carbon class type C steel quality which has poor resistance to corrosion compared to lesser strength steel qualities (Ideal-tek, 2012). The steel rods used for the Prinses Margriet tunnel are the same as those of the EHT. It is therefore expected that the steel rods used in the tension piles of the EHT are susceptible to stress corrosion.

#### *The environment of the subsoil should be able to enable corrosion*

Stress corrosion occurs in both acidic and alkaline environments. These environments are constituted by the presence of acidic or alkaline substances dissolved in the subsoil. The presence of chlorides specifically in the subsoil might cause salt intrusion to occur, which also enables stress corrosion. Such an environment with substances is likely to appear in the subsoil due to the groundwater and soil compositions. This assumption is based on the stress corrosion happening in a relatively similar subsoil composition of the Prinses Margriet tunnel. The composition of the subsoil and groundwater around the EHT are not measured. This research would be an opportunity to analyze whether the environment around the tension piles is able to induce stress corrosion.

The tension piles of the EHT were coated in asphalt as a measure for corrosion protection. This is different from the protection used for the Prinses Margriet tunnel, where grease was applied. It is expected that in time the coatings protective capacity reduces and since the tunnel exists for almost 55 years, it can be expected that the quality of the coatings have reduced greatly over this time period. Also during installation, the steel rods might have gotten imperfect coverage of the coating on the steel, resulting in reduced protection. As time goes on, it can be expected that the steel becomes more vulnerable to corrosion due to the coating wearing off even more. If this happens, the corrosive agents present in the soil will be able to reach the steel more easily and increase the risk of stress corrosion cracking and propagation.

#### *Amount and variation of tensile stress in the material*

The steel rods are both prestressed and loaded in tension. This results in a high amount of tensile stress in the material. As the stress increases, the susceptibility to stress corrosion increases too due to an increased crack propagation velocity. The models to calculate the critical tunnel elements show that the forces in the tension piles in some cases go up to the applied steel ultimate tensile strength. This proves that due to the buoyant force, there is a high tensile stress imposed on the tension piles which enables the risk of the cause and propagation of stress corrosion cracking in the steel. In literature it was found that for stress corrosion to occur in steel rods, a minimum strain level of 0.4% is required. This strain level is reached at a force of 675.57 kN taking into account the steel quality of the steel rods of the EHT. The capacity calculations of the numerical models done in the previous chapter show that this force is present in the tension piles in the static situation. Hence it is found that the amount of tensile stress in the steel rods is sufficient to induce stress corrosion.

## 9.2 Corrosion fatigue

There are stress variations present due to cyclic loading on the tunnel element and its tension piles. Earlier in the report, it was determined that the main constituents of cyclic loading on the tunnel element are; traffic loading, tidal loading and temperature loading due to thermal expansion. The magnitude of the cyclic loading compared to the static loading on the tunnel element is analyzed. This in order to evaluate whether the cyclic loading is able to cause a large stress variation in the steel. If this would be the case, the risk of both corrosion fatigue and stress corrosion increases. Corrosion fatigue embrittles the material, increasing the risk of material cracks. The stress variations support the propagation of cracks in the material.

The first cyclic load to be analyzed is the traffic load. To make an approximation of the amplitude of the traffic load, Eurocode 1, EN 1991-2 is used. This norm contains the design road traffic loads for bridges. A range of 5 to 9 kN/m<sup>2</sup> for very heavy traffic load is proposed in the norm. This cyclic pressure is pointed downwards due to the weight of the traffic and thus increases compressive forces on the tension piles. It is expected that the maximum amplitude of this traffic load is reached during rush hours, two times a day. The assumption is made that the traffic loads are equally distributed among the tension piles assuming that the road deck and tunnel floor have sufficient load redistribution capacity. In case there is a fully stopped traffic jam the present in the tunnel element, the traffic load is assumed to be maximum and also evenly distributed because of the similar geometries of the vehicles. The area of the road deck, the amount of tension piles and the area of the concrete body and steel rod of the tension pile are used to convert the cyclic traffic load into a stress increase in the steel rods. The maximum traffic load causes a fully negative stress variation of 0.18 N/mm<sup>2</sup> in the concrete and a stress variation in the steel material of negative 35.34 N/mm<sup>2</sup>. For these values the design traffic load of 5 kN/m<sup>2</sup> is used. This load is roughly equal to the legally allowable maximum truck load of 50 tons in the Netherlands (Rijksoverheid, 2024) on every lane in the tunnel element and thus is regarded as the most representative. The frequency of this traffic load is assumed to be twice a day during rush hours. The cyclic traffic load can be described using the following formula:

$$\sigma_{var,traffic} = 17.67 \cos\left(730t - \frac{\pi}{4}\right) - 17.67$$

This is a periodic function where a  $t$  represents time and ranges from  $[0, 2\pi]$  where  $2\pi$  represents one year.

The second cyclic load is the tidal load. In Chapter 6.3, Figure 16 the tidal movements in the water level are included in the graph of deep water layers. In the winter & spring, the tidal movements are the strongest. For both the northern and southern part of the EHT the maximum amplitude of the tidal movement is approximately equal to 0.3 meters from the mean water level. This results in a maximum tidal load of 3 kN/m<sup>2</sup> on the tunnel floor. This tidal water level is both positive and negative, so the tidal load is both tensile and compressive. The assumption is made that the tidal loads are also equally distributed among the tension piles. The maximum tidal load causes a stress variation of 24.03 N/mm<sup>2</sup> in the steel material. When looking closely at the frequency in the graph on Figure 16, it is found that there are two governing frequencies which make up the tidal movement in the waterway covering the EHT. The shorter tidal frequency is found to be 12 hours with an amplitude of 0.1 m. This amplitude results in a stress variation of 8.01 N/mm<sup>2</sup>. The longer frequency is found to be 2 weeks with an amplitude of 0.3 m. The short and long cyclic tidal loads can be described using the following formulas:

$$\begin{aligned}\sigma_{var,tidal\_short} &= 8.01 \sin\left(730t - \frac{3\pi}{8}\right) \\ \sigma_{var,tidal\_long} &= 24.03 \sin\left(26t - \frac{\pi}{4}\right)\end{aligned}$$

This is a periodic function where a  $t$  represents time and ranges from  $[0, 2\pi]$  where  $2\pi$  represents one year.

The third cyclic load is the temperature load. This load is caused due to the resistance against thermal expansion/contraction of the material upon the increase or decrease of the temperature respectively. The thermal expansion in the tension piles itself is assumed to be negligible due to the small temperature differences underneath the structure. The main constituent of the temperature load is the temperature difference on the tunnel floor causing bending. The load from the resistance against thermal expansion is transferred from the floor to the tension piles. It is assumed that the main cycle of temperatures is the seasonal temperature difference. To identify the effect of temperature on the tension pile foundation, INSAR-satellite data is used on the EHT to identify possible movements due to seasonal effects. This data is made available for this research. The INSAR-data is collected from 2017 until the start of 2024. To make a just comparison, the temperature data of a station nearby the EHT is collected for the same time span. This data is gathered from the KNMI. The results are shown in Figure 41.

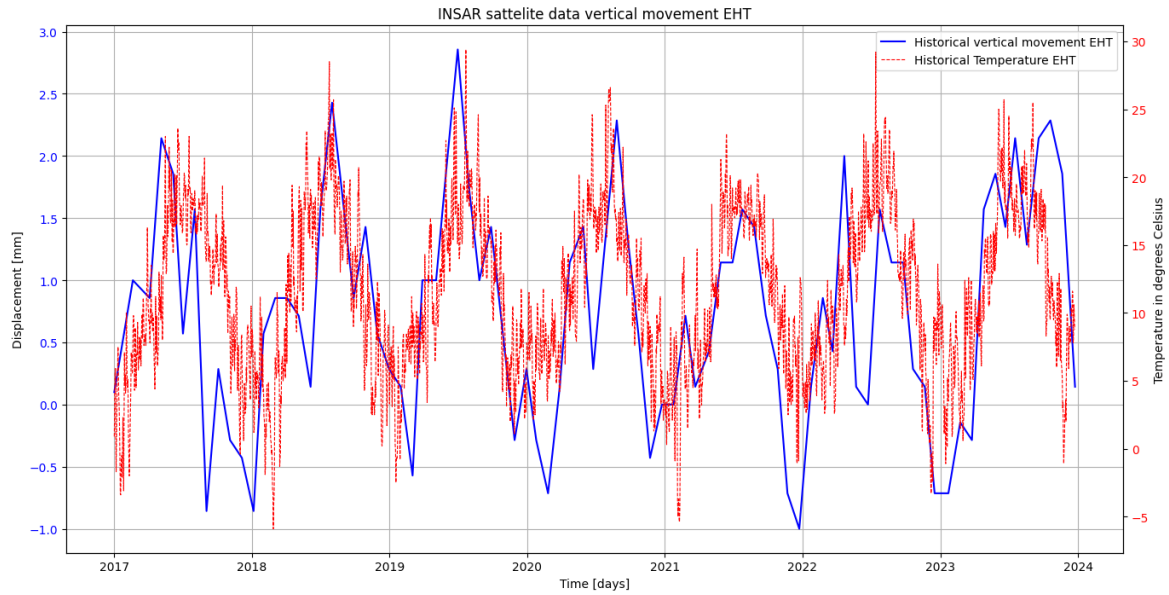


**FIGURE 41: INSAR DATA OF TUNNEL ELEMENT PLOTTED WITH WEEKLY TEMPERATURE DATA (KNMI, 2025)**

From the graph seasonal effect is identified. There is a strong correlation between the temperature and the vertical movement of the EHT. Therefore it is expected that thermal expansion is a relevant cyclic load. The maximum upward vertical movement each cycle is around 2.5 mm, the maximum downward vertical movement each cycle is around 1 mm. By converting this vertical movement to an elongation or contraction of the tension piles, the resulting temperature load can be calculated. It is not yet sure whether the vertical movement of the tunnel floor as measured by INSAR translates into an elongation of 2.5 mm of the tension piles. It must be accounted for that the elongation is probably lower, since the tunnel element is expected to show more bending in locations where there are no piles present. An extreme guess is to attribute the 2.5 mm upward movement to thermal expansion which results in elongation of the tension piles and likewise the downward movement of 1 mm results in contraction of the tension piles. Assuming a linear elastic model for the tension pile, an elongation of 2.5 mm of the steel rods would result in a stress increase of 30.88 N/mm<sup>2</sup> in the steel. A contraction of 1 mm results in a compressive stress of 12.35 N/mm<sup>2</sup>. The frequency for the temperature load is determined from the seasonal effect in 1 year. The short and long cyclic tidal loads can be described using the following formulas:

$$\sigma_{var, temperature} = 21.615 \sin\left(t - \frac{\pi}{4}\right) + 9.265$$

This is a periodic function where a  $t$  represents time and ranges from  $[0, 2\pi]$  where  $2\pi$  represents one year.

Since the periods of the functions all represent one year, the 4 different periodic functions which describe a cyclic load on the tunnel element can be combined through superposition. By doing this, the profile for stress variations is obtained for the tunnel element. This functions are combined and simplified as much as possible. This results in the following formula:

$$\sigma_{var,combined} = 21.615 \sin\left(t - \frac{\pi}{4}\right) + 8.01 \sin\left(\frac{730t - 3\pi}{8}\right) + 24.03 \sin(6.5(t - \pi)) \\ + 17.67 \cos(182.5(t - \pi)) - 8.405$$

This is a periodic function where a  $t$  represents time and ranges from  $[0, 2\pi]$  where  $2\pi$  represents one year.

The following figures show plots of the separate & combined cyclic loads for different timespans. The start period for each of the cyclic loads is the first of January 2024. Firstly the four cyclic loads are separately shown in different plots. Secondly the functions are combined into the combined cyclic load. The first plot spans 1 week, the second plot spans 2 years. This is to get an idea of the influences of the separate cyclic loads on the combined cyclic loads, their return period and amplitude. More timespans are analyzed and included in Appendix A3. The timespans analyzed are; 1 week, 2 months, 1 year, 10 years

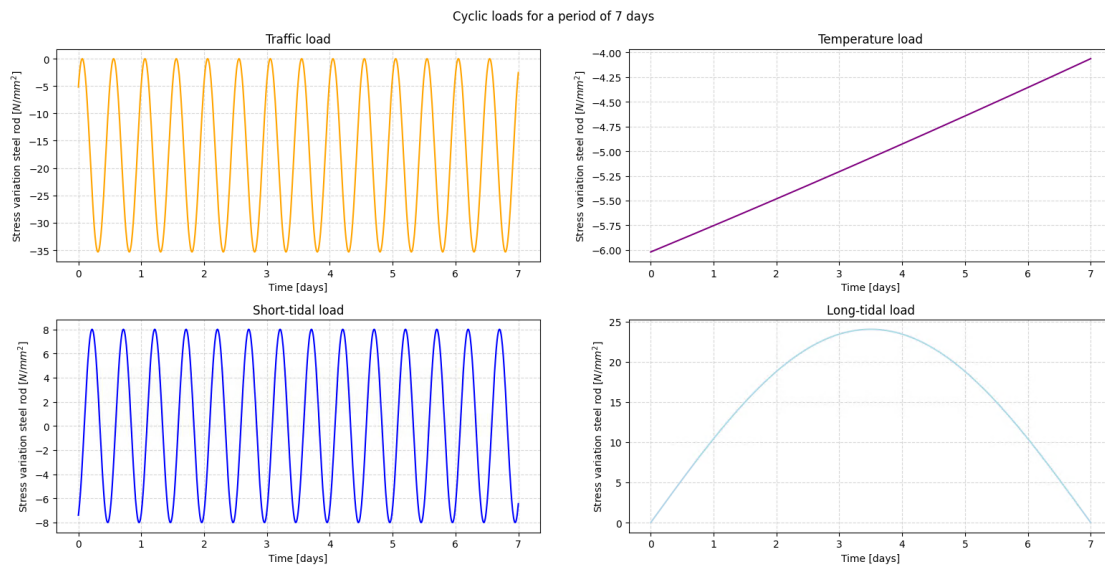


**FIGURE 42: PROFILE OF VARIOUS CYCLIC LOADS ON TUNNEL ELEMENT 1 WEEK**

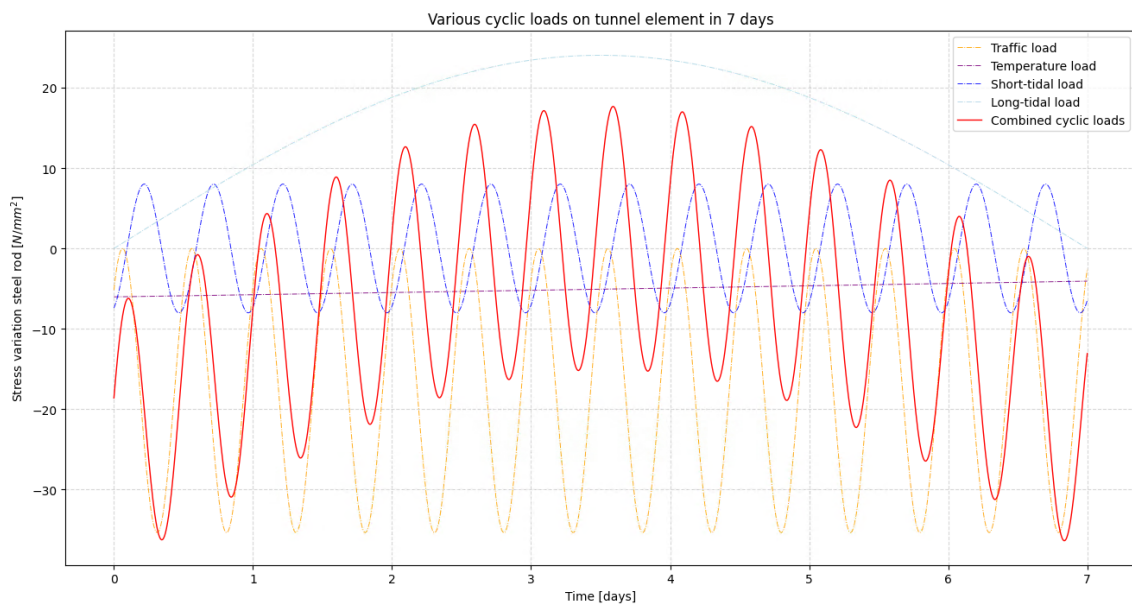


**FIGURE 43: COMBINED PROFILE OF CYCLIC LOADS ON TUNNEL ELEMENT 1 WEEK**

In this relatively short period of one week, it can be seen that the traffic and short-tidal load are contributing to the cyclic nature of the combined function. The long-tidal function is able to go through half its own period, which is one week. The temperature function is hardly contributing to the combined function because of the short period. Also the temperature load is seen to be negative. This is due to the start point of the period being the first of January 2024, where it is still winter which means low temperature.

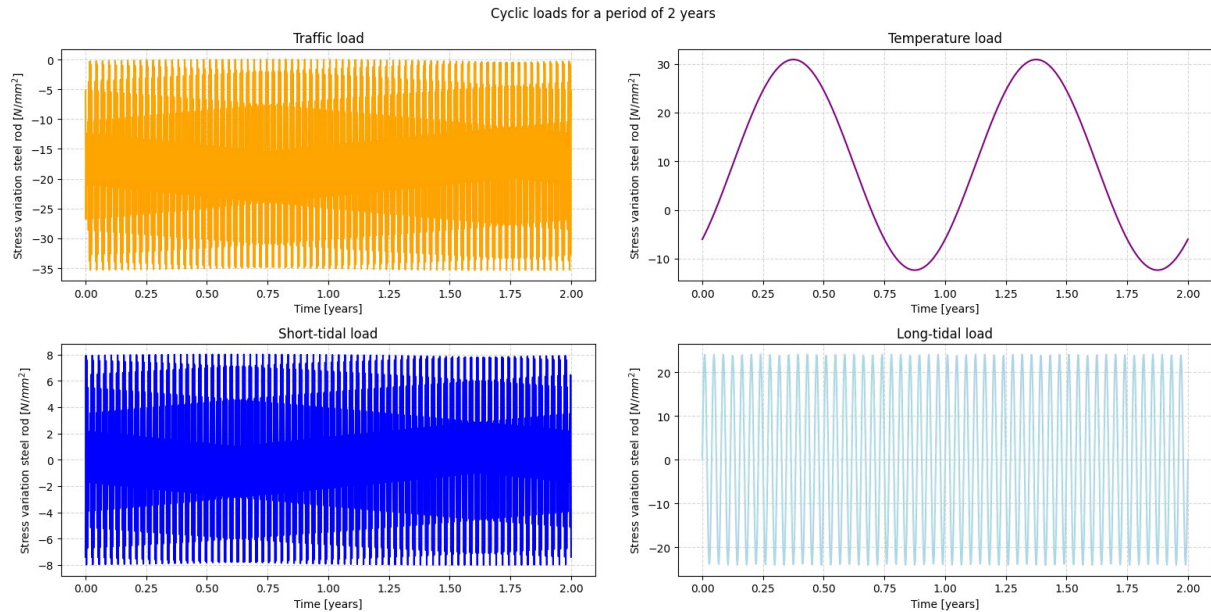


**FIGURE 44: VARIOUS CYCLIC LOADS ON TUNNEL ELEMENT 1 YEAR**

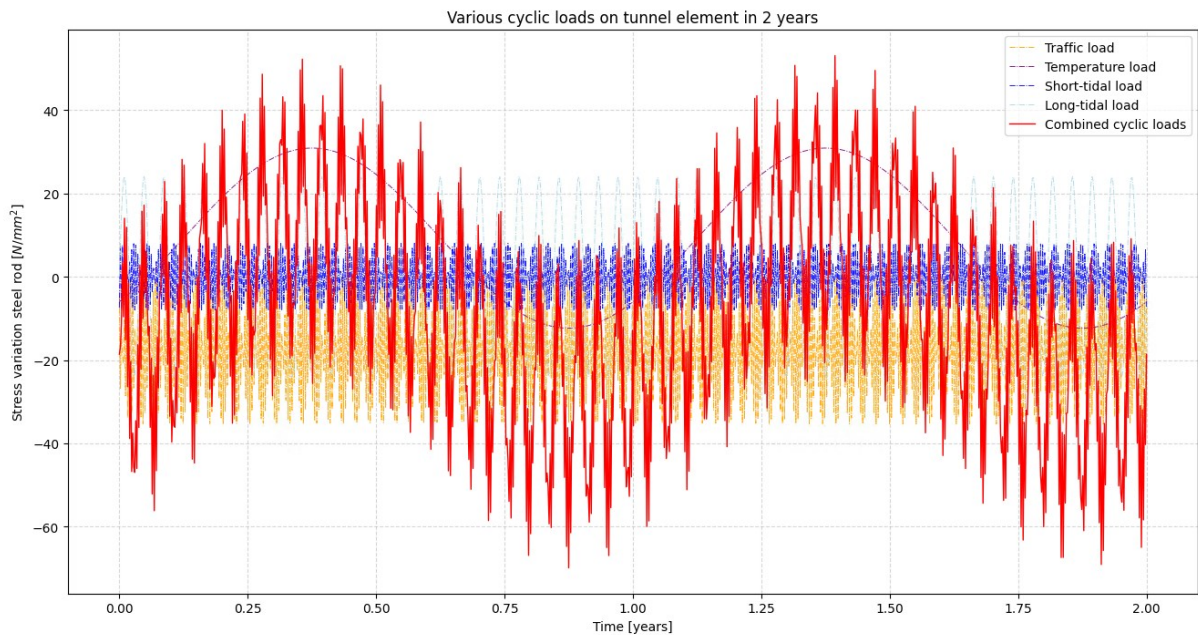


**FIGURE 45: COMBINED CYCLIC LOADS ON TUNNEL ELEMENT 1 YEAR**

In this longer period it can be seen that the traffic and short-tidal loads cycle so much that the phases become unrecognizable in the graph. However now the periods of temperature and long-tidal loads can be seen clearly. The maximum stress variation achieved in this time-series of two years is  $+53.08 \text{ N/mm}^2$  tensile and  $-69.88 \text{ N/mm}^2$  compressive stress respectively. The maximum tensile stress variation is seen in the summer, when the temperatures are high. The high temperature in combination with the tidal loads reaching their maximum tensile variation stress cause positive interference which results in the maximum possible tensile force from the cyclic loads. The maximum compressive stress variation is reached in winter, when temperature is low, in combination with both tides being at their minimum and the traffic load at its maximum, which is always a negative value.



The capacity of the steel in the tension pile amounts to 752.78 kN with safety and 828.38 kN without safety. The stress variations amount to 5.3% and 4.9% respectively of the tensile strength and 7.5% and 6.8% respectively of the compressive strength. This is quite a substantial proportion of the strength originating from the cyclic loads. Dynamic loads are able to behave unpredictably because of the positive interference of different waveforms. Therefore it is important to quantify them for a structure.

The possibility of corrosion fatigue due to these cyclic loads was discussed with a senior tunnel advisor at Rijkswaterstaat, G.M. Wolsink (2024). Here it became clear that due to the prestressing of the tension piles the phenomenon of stress corrosion being accelerated by the variation of tensile stress in the steel can be ruled out. The proof is suggested by G.M. Wolsink (2024). There were no specific calculations done already regarding the contribution of fatigue effects due to stress variations on the failure of the tension piles. It was evident from the start that fatigue did not play a significant role in the failure of the steel rods installed in the tension pile with the prestress included. The phenomenon can be explained numerically as follows.

According to the specifications of the EHT, the prestressing force applied was equal to 65% of the ultimate tensile strength of the steel rods. For the 32 mm diameter rods applied, this resulted in an initial compressive strength in the surrounding concrete of 3.9 N/mm<sup>2</sup>, using a concrete pile diameter of 450 mm. By taking relaxation of the prestressing force into account, it is expected that the stresses would eventually reduce to 3.3 N/mm<sup>2</sup>, which is approximately 85% of the original stress. This assumption is backed by the tension pile design employed for the EHT. The piles have 55 tons of prestress and are designed to have a capacity of 45 tons, the capacity consists of roughly 82% of the prestress.

In the case that the compressive stresses in the concrete due to the prestressing dissipate, for example due to a large increase of water loads equal to the design capacity of the tension pile, the previously calculated stress of 3.3 N/mm<sup>2</sup> in the concrete would reduce to 0. Since the length of the pile in the EHT is equal to 17 m, and with the assumed elasticity modulus of uncracked concrete of 30 GPa, this stress reduction would result in an elongation of 1.87 mm. The following formula is used to calculate this.

$$\Delta L = \frac{\Delta \sigma \cdot L}{E}$$

Using the elongation of the concrete, using the same formula but for the steel rod, the stress variation in the steel can be calculated due to the large increase of the water load. An elasticity modulus of 210 GPa is used for steel. This results in a stress increase of 23.1 N/mm<sup>2</sup> in the steel. This increase is approximately equal to 2.2% of the ultimate tensile strength of the steel rods. This is a very slight increase of the total stress and thus it is not expected that possible stress variations are significant enough to cause corrosion fatigue in the tension piles of the EHT. Furthermore, the increase of water load required to cause the compressive stress in the concrete to dissipate, is an increase of 82% of the water level. This is a very unlikely scenario as overflow would happen in the tunnel much earlier. The combined cyclic loads on the tunnel element consist out of 6.4% to 9.3% of the ultimate steel strength. In order to make the compressive stresses in the concrete dissipate, at least 82% would be needed and thus it is not likely that the stress variations would end up in the steel rod possibly causing corrosion fatigue.

In the European Technical Assessment committee (ETA), information is available on the steel rods as applied for the EHT. In the Table below it is shown that the steel would be able to resist  $2 \cdot 10^6$  load cycles of 200 N/mm<sup>2</sup>. This value is way larger than the calculated maximum stress variation of 53.08 N/mm<sup>2</sup>. Also  $2 \cdot 10^6$  load cycles would take the short-wave tidal load, which is the highest frequency cyclic load EHT, 2739.72 years to complete. Therefore it is expected that the steel rods of the tension piles will not show fatigue upon dynamic loading to this maximum of 200 N/mm<sup>2</sup>.

**TABLE 17: INFORMATION ON FATIGUE RESISTANCE= STEEL**

Additional characteristics				
Total elongation at maximum force <sup>2)</sup> , calculated as $A_g + \frac{R_{m,a}}{E} \cdot 100$	$A_{gt}$	%	5	5 <sup>1)</sup>
Force range $F_r$ , at upper load $F_{up} = 0.70 \cdot F_{m,a}$ and $N = 2 \cdot 10^6$ load cycles	Plain bar		200 N/mm <sup>2</sup> · $S_n$	
	Threadbar	18–40 WR	180 N/mm <sup>2</sup> · $S_n$	
		47 WR	120 N/mm <sup>2</sup> · $S_n$	
Isothermal stress relaxation	Losses from an initial force of $0.70 \cdot F_{m,a}$ after 1 000 h $\leq 3 \%$			

<sup>1)</sup> Quantile for a statistical probability of  $W = 1 - \alpha = 0.95$  (one sided)

<sup>2)</sup>  $E \approx 205\,000$  N/mm<sup>2</sup> and  $A_g$  as plastic extension at maximum force

### 9.3 Modelling failure mechanism

The research done so far on the EHT and stress corrosion shows that the tension pile foundation for the EHT cross all checks required for stress corrosion inducing and development. There is high quality steel (QP105) present in the tension piles with substantial tensile stresses, both from prestressing and tensile loading from the tunnel. The influence of stress variation can be ruled out in this case. The most uncertain factor is whether the environment around the tension piles are able to induce and promote stress corrosion. Further research is recommended on this certain part in order to get a better view on the composition of the different soil layers. Here it should be researched whether chlorides are present in the soil around the tension piles, as well as corrosive agents, either very alkaline or very acidic. Also the quality of coating around the steel rods should be researched. In the case of an imperfect coating, the steel is much more susceptible to a hostile corrosive environment and this increases the probability of stress corrosion occurring in the steel.

The remainder of this report will mostly focus on the consequences of the stress corrosion failure happening in the steel rods of the critical tunnel elements of the EHT. Since stress corrosion is found to be a relevant failure mechanism for the tension piles of the EHT, the numerical PLAXIS 3D model of the critical tunnel elements 3N & 3Z are used to simulate the consequences of the tension piles failing due to stress corrosion. The tension piles are modelled as embedded beams. The influence of stress corrosion failure is included in the model by 'deactivating' a pile in the calculation to model the brittle failure of the steel rod due to stress corrosion.

To scale up the calculations, a Python script is written to automate the PLAXIS 3D models. The Python script runs from an editor which is able to communicate with PLAXIS 3D through the remote scripting server made available by their services. The use of this Python script makes it possible to perform a Monte Carlo analysis of the failure of the tunnel element through the progressive failure of the tension piles.

The algorithm that has been constructed to simulate the consequences of stress corrosion happening gradually for the tunnel element is shown on the next page. The tunnel element models as shown in Section 8.1 for element 3N and Section 8.2 for 3Z are used for this algorithm.

The exact algorithm used to simulate the failure mechanism decomposed in steps is shown Table 18 below.

**TABLE 18: ALGORITHM FOR SIMULATING PILES FAILING DUE TO STRESS CORROSION IN NUMERICAL MODEL**

<b>Input</b>	Number of failed tension piles to be modelled (n_failed_piles) Number of iterations of Monte Carlo analysis (n_iter)
<b>Step 1</b>	Start of Monte Carlo iteration; generate an array of random numbers to signify order of tension piles failing
<b>Step 2</b>	Create a new construction phase based on the previously calculated phase, and deactivate an embedded beam in the new phase until n_failed_piles is reached
<b>Step 3</b>	Let PLAXIS 3D calculate the defined phases
<b>Step 4</b>	Move to PLAXIS 3D Output and extract the parameters desired (maximum displacement, maximum force)
<b>Step 5</b>	Gather the desired parameters per phase and convert it to a Python array
<b>Step 6</b>	Show plots of the progression of desired parameter as more tension piles keep failing and save the array to a database; End of Monte Carlo iteration
<b>Step 7</b>	Repeat from Step 1 until n_iter is reached
<b>Output</b>	Array of desired parameters per phase for every Monte Carlo iteration Number of failed piles at numerical model failure

Since the occurrence of stress corrosion in the tension piles is not yet determined to be location dependent, the embedded beam being deactivated in the new stage in the model is chosen to be random. This means every Monte Carlo iteration holds a different pattern of tension piles failing, which also means a different pattern in displacement and forces. Performing sufficient iterations will give an outline of the structure reactions through spreads in for example difference in displacement or maximum pile forces between the iterations. A small spread means the location and order of tension piles failing have little effect on the outcome. A large spread means the that the total failure is dependent on which failure pattern of the tension piles will occur. This would be a less beneficial outcome as this would make the possible failure mechanism more unpredictable.

The output of the algorithm can be used to determine at how many piles the tunnel is expected to fail, what the displacements/forces are at this failure, and what the progression is throughout the process of tension piles failing consequently. One such Monte Carlo iteration takes a total of around 2 hours, so the model is quite time consuming, especially with increasing amount of iterations.

### 9.3.1 Sensitivity analysis

In order to get an idea of the response of the model upon variation in parameters, a sensitivity analysis is performed. To do this, the most impactful parameters are defined; the elasticity modulus of the tunnel floor, the elasticity modulus of the tension piles, the soil strength & stiffness parameters, the impact of increasing the interface strength of the interfaces between the neighboring tunnel elements.

The first iteration of the algorithm described on the previous page is used to do a sensitivity analysis of the PLAXIS 3D model of tunnel element 3N. A broad range is taken for parameter variation, to get a concise outline of the influence of the most impactful parameters.

#### Concrete floor stiffness

The stiffness of the concrete tunnel floor in the original formulation of the model is equal to 30 GPa. In this analysis, the value is increased and decreased twofold. To get an outline of the extremes a minimal value, representing limp concrete, is assumed to be 10 GPa and a maximum value, representing a completely rigid floor, is chosen at 30 TPa. The results are shown below.

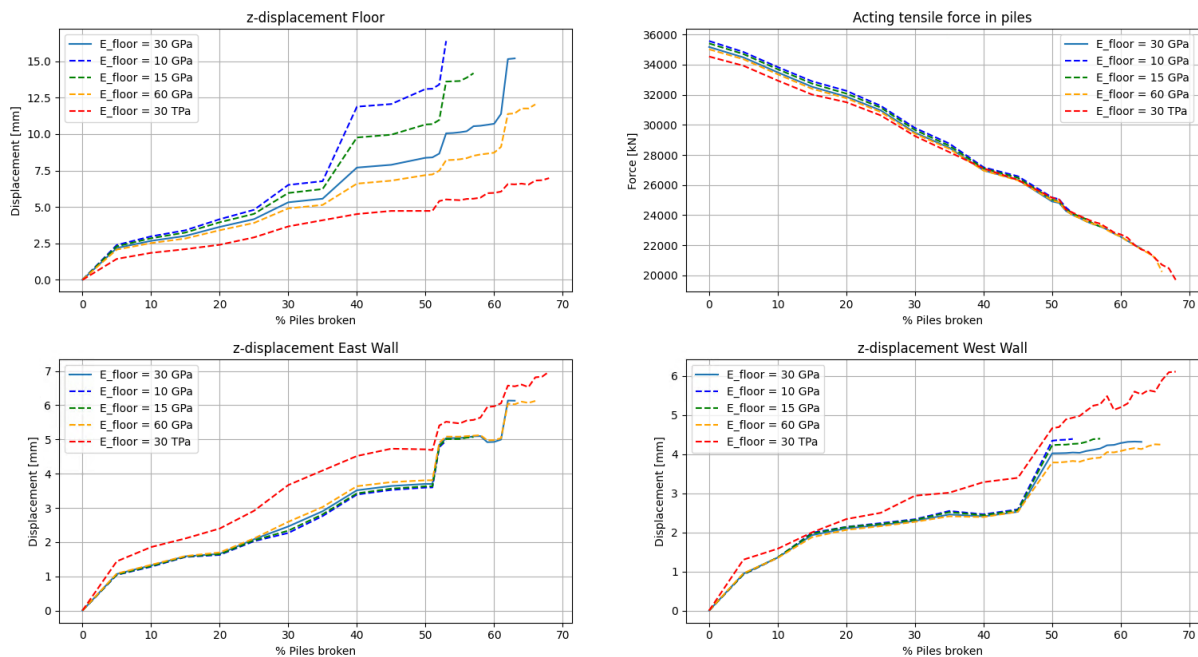


FIGURE 46: SENSITIVITY ANALYSIS OF TUNNEL FLOOR STIFFNESS

The largest influence of the floor stiffness variation is seen in the displacement of the floor. A lower floor stiffness results in a higher maximum displacement and the reverse is true for higher stiffnesses. For the realistic concrete value range from 15 GPa to 60 GPa, which resembles cracked concrete to high density concrete, the floor displacement ranged from a maximum deviation of 3.75 mm for 15 GPa and -3 mm for 60 GPa comparing to the original model formulation.

Also the displacement of the east and west wall is showing more consistent progression of displacement as the floor stiffness increases. As the stiffness increases, the floor is less able to deform locally. Because of this the displacement of the floor happens more uniformly, resulting in more consistent wall displacement.

It is also seen that upon increasing the stiffness, the numerical stability of the model increases. At the minimum stiffness value numerical failure occurred at 53% of piles failed and at the maximum stiffness value it occurred at 69% of piles failed.



### Tension pile stiffness

Similar to the concrete floor stiffness, the tension pile stiffnesses are varied. The value of pile stiffness in the original formulation of the model is equal to 30 GPa. The range of stiffness values is similar to those of the concrete floor stiffness. The results are shown below.

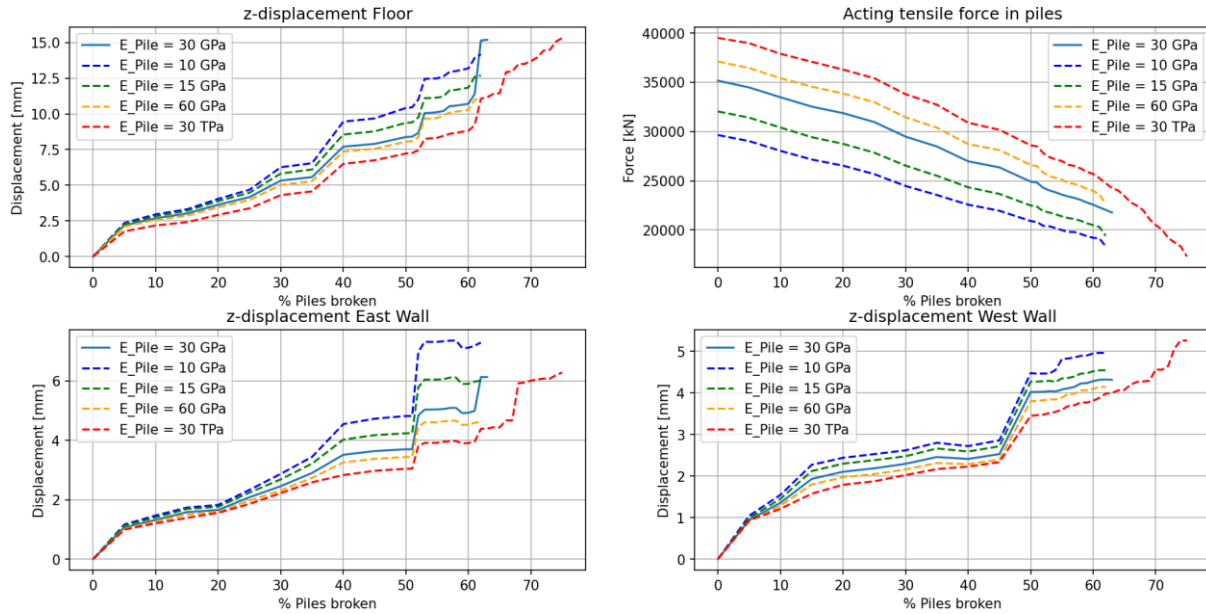


FIGURE 47: SENSITIVITY ANALYSIS OF TENSION PILE STIFFNESS

The stiffness of the tension piles have a notable influence on the model outcomes. As the piles become more stiff, they deform less under the same force.

For the realistic concrete value range from 15 GPa to 60 GPa, which resembles cracked concrete to high density concrete, the floor displacement ranged from a maximum deviation of 1.5 mm for 15 GPa and -0.5 mm for 60 GPa comparing to the original model formulation.

A lower stiffness results in a decrease of the acting force in the tension pile foundation. This is due to the larger displacements taking up the force.

The numerical stability was not influenced as much as with varying the tunnel floor stiffness. However for piles with an extremely high stiffness value of 30 TPa, the model failure occurred at 76% of piles failed, compared to the failure at 62% piles failed for the other stiffness ranges.

### Soil strength and stiffness

The influence of the soil strength and stiffness parameters are varied to assess their influence on the model outcomes. This is done by both increasing and decreasing the hardening soil parameters by 25% and 50% of the layers in which the tension piles are present. The stiffness parameters to be varied are  $E_{50}$ ,  $E_{\text{oed}}$  and  $E_{\text{ur}}$ . For cohesive soils, the strength parameters are both cohesion ( $c$ ) and friction angle ( $\phi$ ). For sandy soils, the only strength parameter varied is the friction angle ( $\phi$ ).

This section continues on the next page.

The results of soil parameter variation are shown below. The value  $R$  represents the increase/decrease of soil parameters with its respective value.

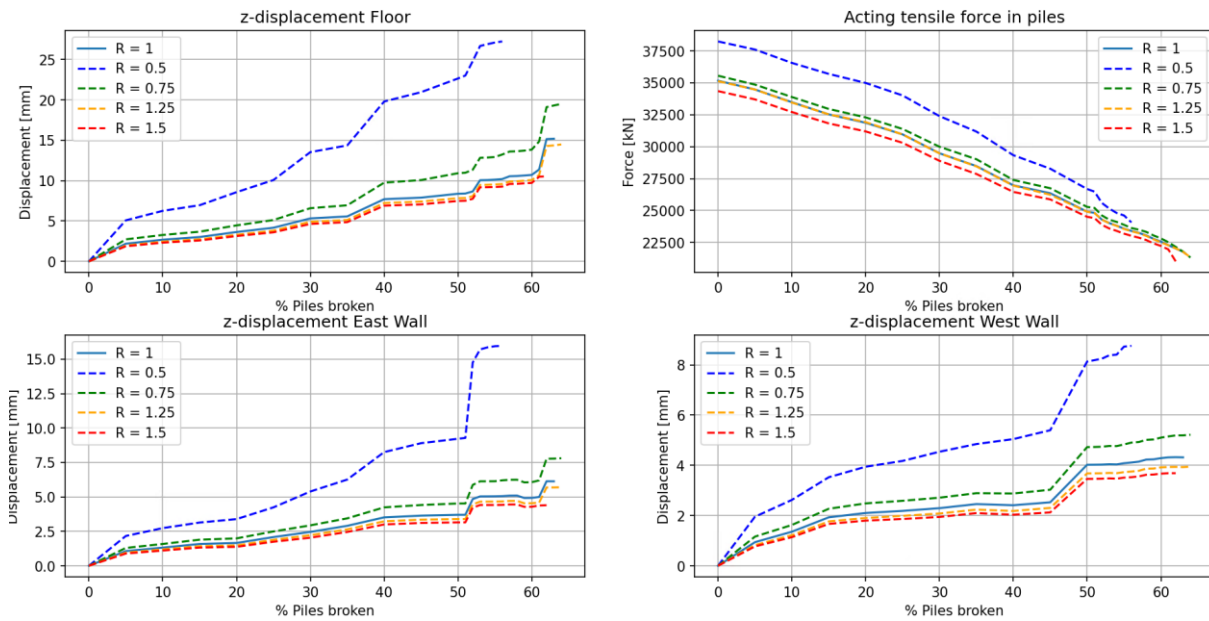


FIGURE 48: SENSITIVITY ANALYSIS OF SOIL PARAMETERS

It is seen that especially the decrease of soil parameters results in larger displacements. As the parameters are increased, the displacements decrease, the magnitude however is smaller than the displacement increase upon soil parameter decrease. For the realistic range of uncertainty of 75% to 125% of strength and stiffness parameters, the displacement reaches a maximum deviation of +4 mm and -0.5 mm respectively. If the soil would be less stiff than assumed, the displacements could turn out larger than simulated in the numerical model.

#### *Influence of wall friction neighboring elements*

To analyze whether the friction between the neighboring tunnel elements have an influence on the model outcomes, the  $R_{\text{inter}}$  value of the rubber interfaces between the tunnel elements is increased. In the original formulation the tunnel elements were assumed to be uncoupled which is modelled as  $R_{\text{inter}} = 0$ . The range of  $R_{\text{inter}}$  values was chosen to be 25%, 50%, 75% and 100%. The results are shown below.

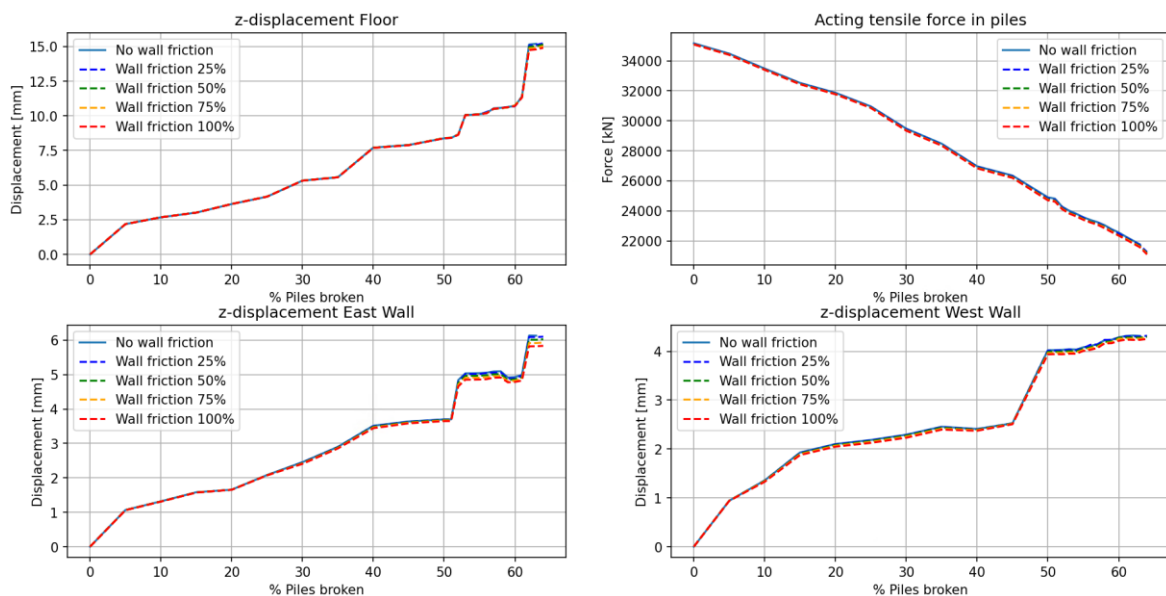


FIGURE 49: SENSITIVITY ANALYSIS OF WALL FRICTION NUMBER

The friction between the neighboring tunnel elements seem to have a very minimal influence on the model outcomes. It can be seen that as the wall friction increases, the displacement of the floor and walls decreases slightly. However, this is approximately 0.2 mm deviation which is relatively small to the displacement values.

### 9.3.2 Tunnel element 3N

Performing a total of 50 iterations of the Monte Carlo analysis described for tunnel element 3N, the progression of the maximum displacement of the elements' floor and walls and the mobilized capacity of the tension pile foundation are shown in the graphs in Figure 50. The mobilized capacity is the force found by taking the sum of tensile forces in the tension piles. In these graphs, the x-axis shows the percentage of tension piles deactivated in the model, which are assumed as failed due to the occurrence of stress corrosion in the steel rods.

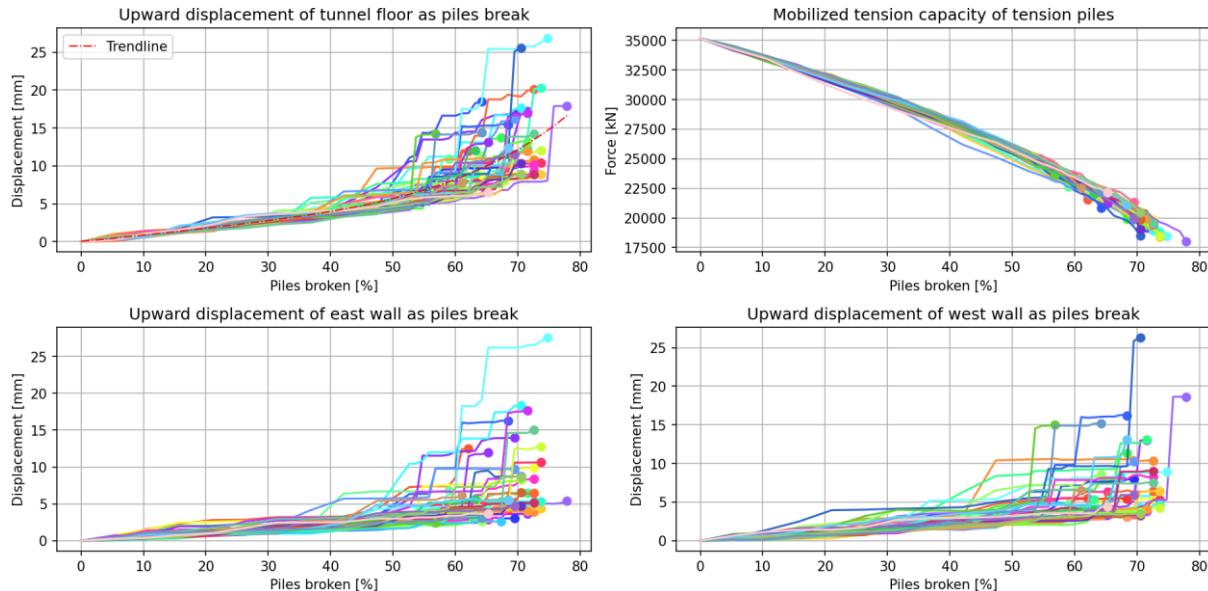


FIGURE 50: 50 MONTE CARLO ITERATIONS OF PILES FAILING SEQUENTIALLY IN ELEMENT 3N

From the graphs it is seen that the displacement profile of the walls and the floor are quite different. The displacements of the tunnel floor generally show higher upward displacement than the tunnel walls. Because of this, the tunnel floor is regarded as the critical element and is analyzed in more detail in order to determine warning levels of this failure mechanism.

The maximum and minimum displacement reached at model failure is equal to 26 mm and 7 mm respectively. This is quite a broad range. The high variance is explained by the influence of the sequence in which the tension piles break. For example, if piles in close proximity would fail sequentially in the model, this would result in larger displacement. It is assumed that upon further tension piles failing after the model failure has happened, the displacements will increase very rapidly since there is no tensile capacity left to withstand the buoyant pressure.

The mobilized capacity of the tension pile foundation did not vary a lot between the different iterations. This shows that the tension pile foundation is able to redistribute the buoyant force if tension piles would fail.

The iterations where the tension pile row installed underneath the walls have failed can be identified from their respective displacement graphs. Upon failure of the whole tension pile row, the displacement value jumps up.

Based on the upward displacement of the tunnel floor and the percentage of piles failed from the different Monte Carlo iterations, a signal level and intervention level is determined. The purpose of these levels is to assist with monitoring purposes of the uplift failure mechanism due to corrosion in the EHT.

The histogram of the amount of failed piles at model failure is shown in Figure 52.

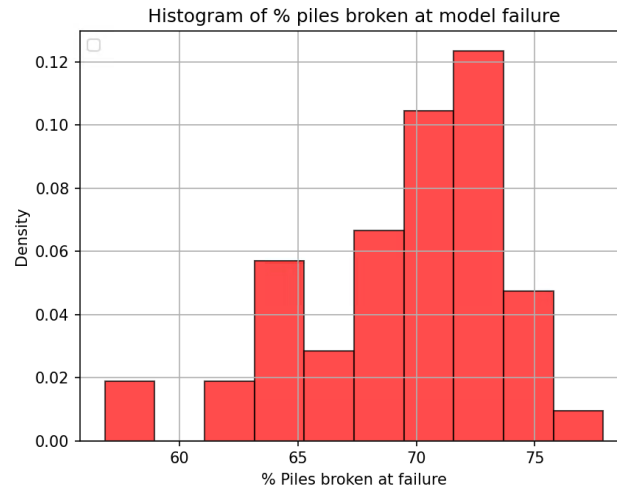


**FIGURE 51: HISTOGRAM OF MODEL FAILURE OCCURRING AT % OF PILES FAILED 3N**

The values range from failure at 57% of piles failed to a maximum of 78% of piles failed. This range is quite broad. This shows that the sequence in which the tension piles fail has a large influence on the stability and outcome of the numerical model.

When looking at the shape of the histogram, a left-skewed Gumbel distribution is expected. The statistical function is as follows.

$$f(x, \mu, \beta) = \frac{1}{\beta} e^{\left(\frac{x-\mu}{\beta}\right)} e^{-e^{\left(\frac{x-\mu}{\beta}\right)}}$$

In this formula  $x$  represents the percentage of piles failed,  $\mu$  represents the mean of the iterations and  $\beta$  the scale, which controls the spread of the left-skewed Gumbel distribution. The PDF-plot fitted to the histogram is shown in Figure 53.

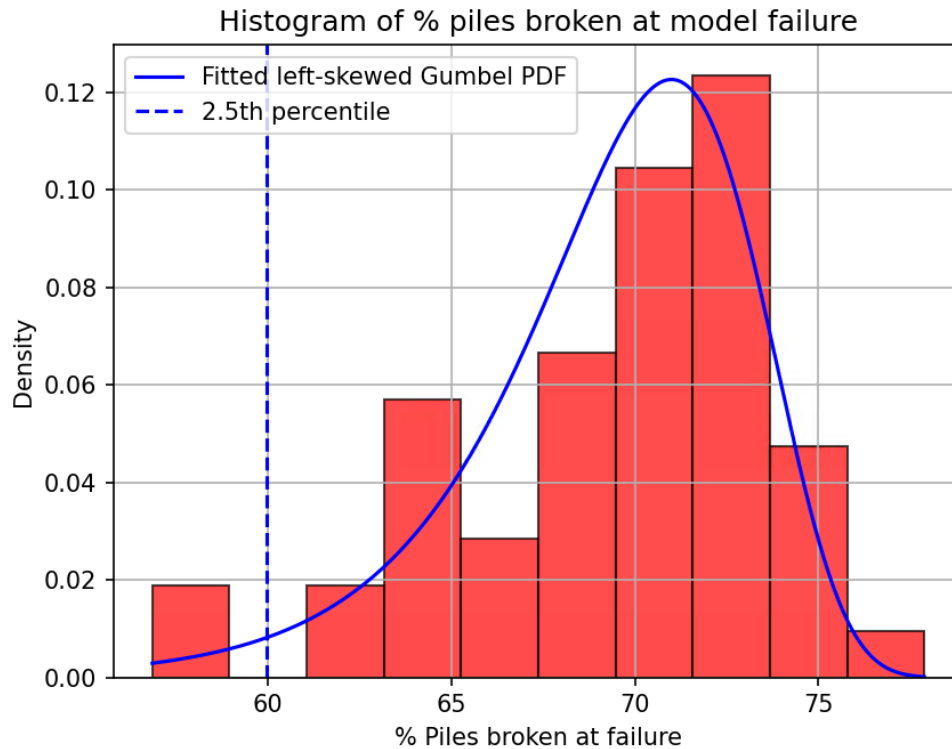


**FIGURE 52: FITTED LEFT-SKEWED GUMBEL DISTRIBUTION TO HISTOGRAM 3N**

The fitted distribution in Figure 53 is regarded as satisfactory, as the PDF describes the tops of the bins of the histogram well. This PDF is found with  $\mu = 71$  and  $\beta = 3.54$ . As more iterations would be carried out, the histogram shape would average out more and the goodness of fit would increase.

The 2.5<sup>th</sup> percentile is calculated to determine the 95% confidence interval for the amount of piles failed at model failure. The percentile value is a conservative estimate for the model failure happening at a certain percentage of piles failed. The 2.5<sup>th</sup> percentile is equal to 60% piles failed. The intervention level should be at least below the 2.5<sup>th</sup> percentile value of the fitted statistical distribution for model failure. Below this level, the risk of uplift failure happening is relatively small. It is important to have a small buffer, in order to put intervention measures in place as the amount of failed piles progresses. Based on the statistical distribution and analyzing the progression of the Monte Carlo analysis graph bundle visually, the intervention level is chosen at 55% of piles failed. After this level, the progression in displacements start to increase rapidly before reaching model failure. The maximum floor displacement at 55% of piles failed has a mean equal to 7.5 mm determined from the Monte Carlo iterations.

Similar to the intervention level, the signal level is determined. This value is based on a much smaller percentile than the one used for the determination of the intervention level. The 99.99999% confidence interval or the 0.000005<sup>th</sup> percentile of the fitted distribution is equal to 34% of piles failed.

When analyzing the displacement progression of the graph bundle as piles fail visually, it is seen that the different iterations behave similarly until a displacement of 4 mm at 35% of piles failed. This would amount to 33 piles failed of the total of 95. In the graph this zone is regarded as the safe zone, and is colored in green. In this phase piles of the tension pile foundation have failed but have not resulted in a major displacement in the tunnel floor.

Beyond 4 mm displacement at 35% of piles failed the iterations start to behave more chaotic. Due to more tension piles failing the buoyant force cannot be redistributed as well resulting in increasing displacements. This phase is regarded as the signal zone, and is colored in orange. If this phase would be reached the tunnel element would have to be monitored closely and mitigation measures could be put in place in order to prevent the failure mechanism to progress to the next phase.

Based on the statistical distribution and the visual analysis of the displacement profile the signal value is chosen to be 35% of piles failed. The displacement and this amount of tension piles failed is equal to 4 mm.

Based on the upward displacement of the tunnel floor and the percentage of piles failed from the different Monte Carlo iterations in combination with confidence intervals of the assumed statistical function, a signal level and intervention level is determined. The purpose of these warning levels is to assist with monitoring purposes of the uplift failure mechanism due to corrosion in the EHT.

The graph shows the tunnel floor displacements, as well as different color-coded zones which indicate the current level of failure risk of the failure mechanism occurring in the tunnel.

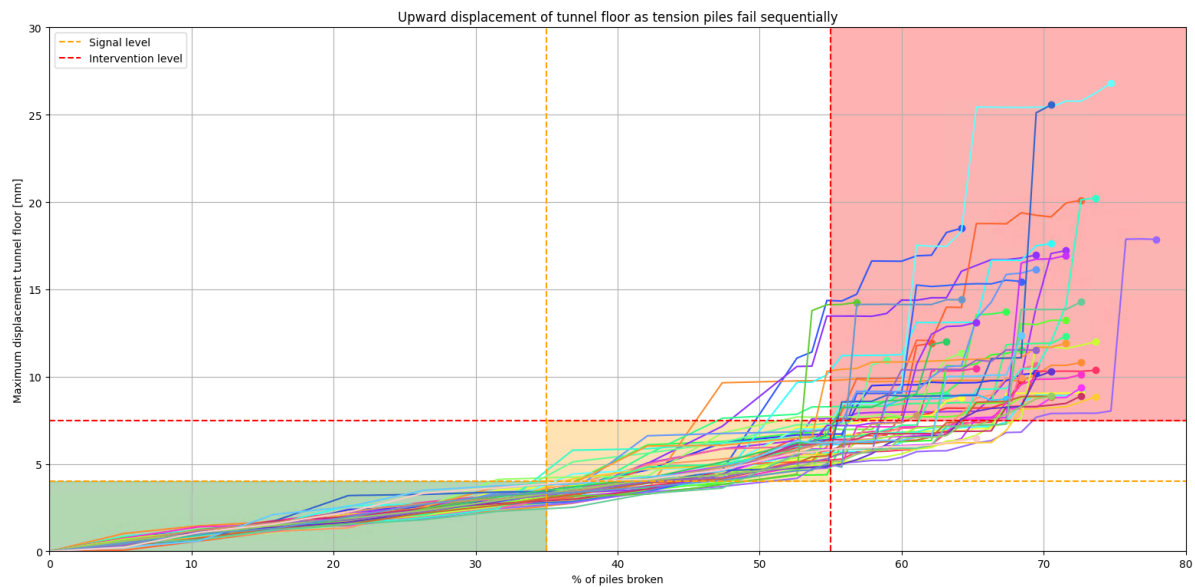


**FIGURE 53: WARNING ZONES OF UPLIFT FAILURE DUE TO STRESS CORROSION ELEMENT 3N**

The progression of the displacement profile is divided in three different zones. The first green ‘safe’ zone signifies that the failure mechanism is progressing, but displacements develop uniformly and slowly among the iterations as more piles fail. After passing the intervention level the orange ‘increased risk’ zone is reached. In this zone the displacements progress more chaotically among the iterations and increase more rapidly. Upon exceeding the intervention level, the ‘failure’ zone is reached, where displacements increase uncontrollably. Actually reaching the ‘failure’ zone of the tunnel should be avoided at all costs to prevent damages and obstruction of the facilitation of traffic.

### 9.3.3 Tunnel element 3Z

The analysis done for element 3Z is similar to the analysis of element 3N in the previous Section 9.3.2. Therefore some parts of the explanation are only mentioned in that section.

A total of 50 iterations of the Monte Carlo analysis for tunnel element 3Z are performed. The results are collected in the graph in Figure 54. In these graphs, the x-axis shows the percentage of tension piles deactivated in the model, which are assumed as failed due to the occurrence of stress corrosion in the steel rods.

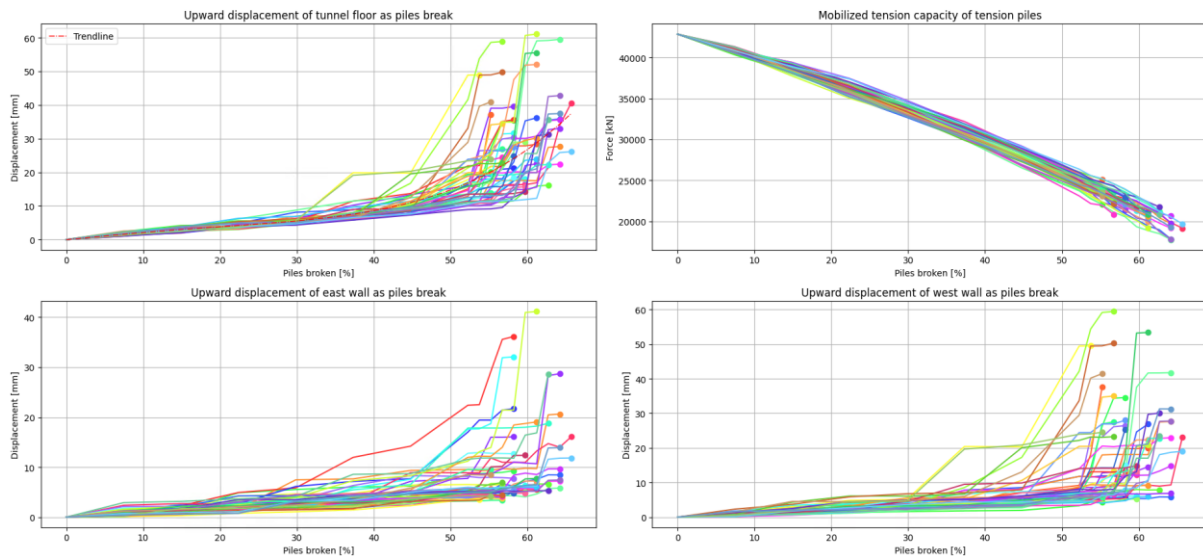


**FIGURE 54: 50 MONTE CARLO ITERATIONS OF PILES FAILING SEQUENTIALLY IN ELEMENT 3Z**

From the graphs it is seen that the displacement profile of the walls and the floor are quite different. The displacements of the tunnel floor generally show higher upward displacement than the tunnel walls. Because of this, the tunnel floor is regarded as the critical element and is analyzed in more detail in order to determine warning levels of this failure mechanism.

The maximum and minimum displacement reached in the tunnel floor at model failure is equal to 60 mm and 15 mm respectively. This is quite a broad range. The high variance is explained by the influence of the sequence in which the tension piles break. For example, if piles in close proximity would fail sequentially in the model, this would result in larger displacement. It is assumed that upon further tension piles failing after the model failure has happened, the displacements will increase very rapidly since there is no tensile capacity left to withstand the buoyant pressure.

The mobilized capacity of the tension pile foundation did not vary a lot between the different iterations. This shows that the tension pile foundation is able to redistribute the buoyant force if tension piles would fail.

The iterations where the tension pile row installed underneath the walls have failed can be identified from their respective displacement graphs. Upon failure of the whole tension pile row, the displacement value jumps up.

Comparing to the results of element 3Z to element 3N, the displacements seem to develop faster as more piles fail. After 30% the displacements begin to develop slightly faster, and when 50% of piles failed the displacements start to increase rapidly which indicates foundation failure. For element 3N, this occurred at 55% of piles failed, and the displacements developed slower throughout the 'failure zone'. Once foundation failure occurs, the displacements of element 3Z increase more rapidly than element 3N.

The histogram of the amount of failed piles at model simulation failure for each Monte-Carlo iteration is shown in Figure 56.

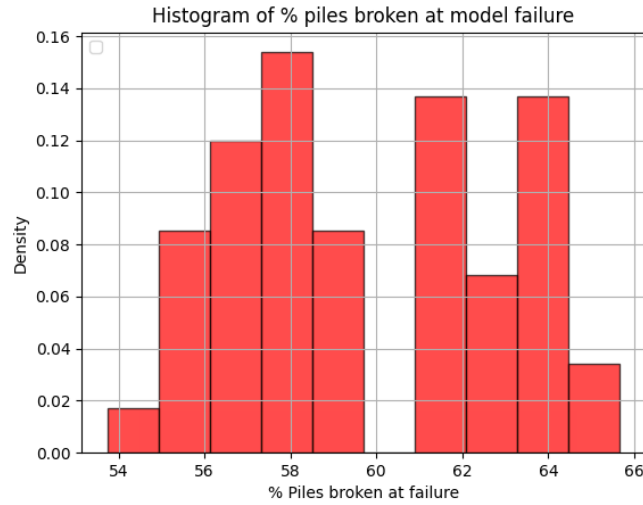


FIGURE 55: HISTOGRAM OF PERCENTAGE FAILED PILES AT MODEL FAILURE

The values range from failure at 54% of piles failed to a maximum of 66% of piles failed. This range is quite broad. This shows that the sequence in which the tension piles fail has a large influence on the stability and outcome of the numerical model simulation.

When looking at the shape of the histogram, a normal distribution is expected. The statistical function is as follows.

$$f(x, \mu, \sigma^2) = \frac{1}{\sigma\sqrt{2\pi}} e^{-\frac{(x-\mu)^2}{2\sigma^2}}$$

In this formula  $x$  represents the percentage of piles failed,  $\mu$  represents the mean of the iterations and  $\sigma^2$  the scale, which controls the spread of the normal distribution. The PDF-plot fitted to the histogram is shown in Figure 57.

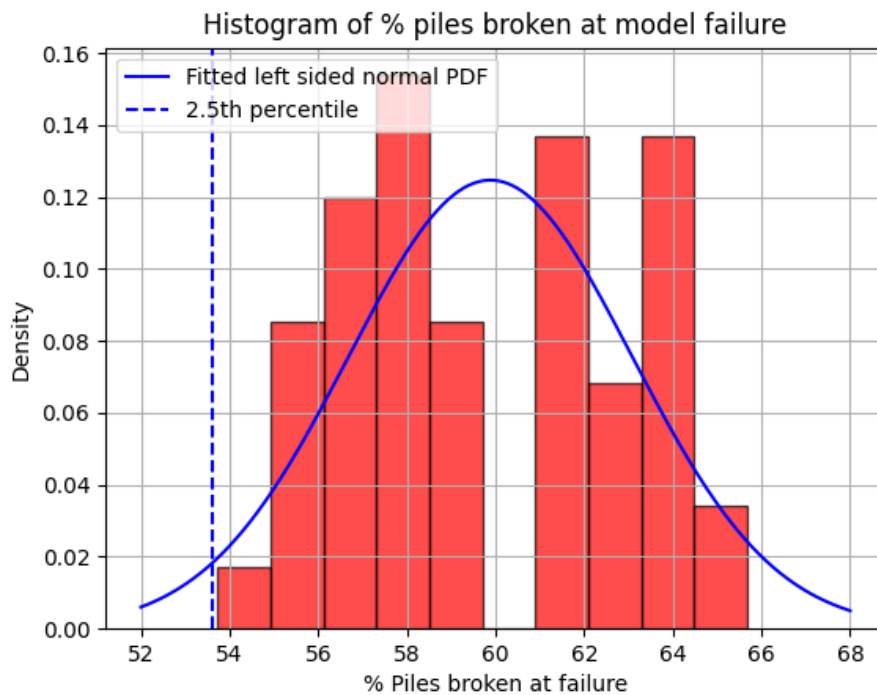


FIGURE 56: FITTED LEFT-SKEWED GUMBEL DISTRIBUTION TO HISTOGRAM 3Z



The fitted distribution in Figure 57 is regarded as satisfactory, as the PDF describes the tops of the bins of the histogram well. This PDF is found with  $\mu = 59.88$  and  $\beta = 3.2$ . As more iterations would be carried out, the histogram shape would average out more and the goodness of fit would increase.

The 2.5<sup>th</sup> percentile is calculated to determine the 95% confidence interval for the amount of piles failed at model failure. The percentile value is a conservative estimate for the model failure happening at a certain percentage of piles failed. The 2.5<sup>th</sup> percentile is equal to 53.5% piles failed. The intervention level should be at least below the 2.5<sup>th</sup> percentile value of the fitted statistical distribution for model failure. Below this level, the risk of uplift failure happening is relatively small. It is important to have a small buffer, in order to put intervention measures in place as the amount of failed piles progresses. Based on the statistical distribution and analyzing the progression of the Monte Carlo analysis graph bundle visually, the intervention level is chosen at 45% of piles failed. After this level, the progression in displacements start to increase rapidly before reaching model failure. The maximum floor displacement at 45% of piles failed has a mean equal to 10 mm taking into account the iterations.

Similar to the intervention level, the signal level is determined. This value however should be based on a much smaller percentile than the intervention level. The 99.99999% confidence interval or the 0.000005<sup>th</sup> percentile of the fitted distribution is equal to 45% of piles failed. This value is equal to the assumed intervention level. Therefore the signal level determination is based on the progression of the Monte-Carlo iteration graph bundle.

When analyzing the displacement progression of the graph bundle as piles fail, it is seen that the different iterations behave similarly until a displacement of 5 mm at 25% of piles failed. This would amount to 20 piles failed of the total of 67. In the graph this zone is regarded as the safe zone, and is colored in green. In this phase piles of the tension pile foundation have failed but have not resulted in a major displacement in the tunnel floor.

Beyond 5 mm displacement at 25% of piles failed the iterations start to behave more chaotic. Due to more tension piles failing the buoyant force cannot be redistributed as well resulting in increasing displacements. This phase is regarded as the signal zone, and is colored in orange. If this phase would be reached the tunnel element would have to be monitored closely and mitigation measures could be put in place in order to prevent the failure mechanism to progress to the next phase.

Therefore the signal value is assumed to be 25% of tension piles failed. The displacement at this amount of tension piles failed is equal to 5 mm.

Based on the upward displacement of the tunnel floor and the percentage of piles failed from the different Monte Carlo iterations in combination with confidence intervals of the assumed statistical function, a signal level and intervention level is determined. The purpose of these warning levels is to assist with monitoring purposes of the uplift failure mechanism due to corrosion in the EHT.

The graph below shows the tunnel floor displacements, as well as different color-coded zones which indicate the current level of failure risk of the failure mechanism occurring in the tunnel.

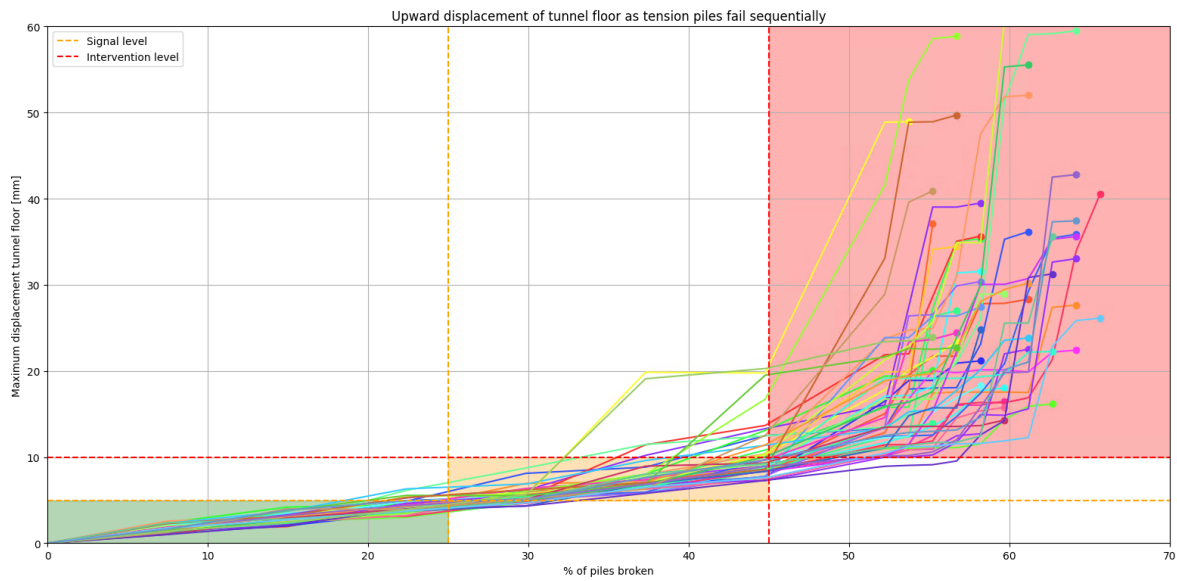


**FIGURE 57: WARNING ZONES UPLIFT FAILURE DUE TO STRESS CORROSION ELEMENT 3Z**

The progression of the displacement profile is divided in three different zones. The first green ‘safe’ zone signifies that the failure mechanism is progressing, but displacements develop uniformly and slowly among the iterations as more piles fail. After passing the intervention level the orange ‘increased risk’ zone is reached. In this zone the displacements progress more chaotically among the iterations and increase more rapidly. Upon exceeding the intervention level, the ‘failure’ zone is reached, where displacements increase uncontrollably. Actually reaching the ‘failure’ zone of the tunnel should be avoided at all costs to prevent damages and obstruction of the facilitation of traffic.

#### 9.4 Monitoring the warning levels

To maintain the signal and intervention values for both tunnel entrance element 3N & 3Z in monitoring practices, the displacement should be measured frequently at different locations in the tunnel element. According to the results of modelling the failure mechanism in Plaxis3D, the displacement in the tunnel floor is the maximum measurable displacement. When it is possible, it is advised that various points located on the tunnel floor are measured. These points should then be combined and interpolated in order to get an estimation of the actual displacement of the tunnel floor according to the measurements. This model of the floor can then be compared with the different iterations of the Plaxis3D model in order to find the expected failure mechanism.

A less accurate, but currently available measuring method for measuring tunnel element displacements are the INSAR satellite measurements. This method is not very accurate, but it is very easy to perform. The INSAR-data of both tunnel element 3N & 3Z of the EHT have been measured since June 2009 up until June 2024. In this data it is not known what part of the tunnel entrance elements have caused the reflection of the signal which is being interpreted by the satellite. It is assumed that the INSAR-data represents the actual movement of the tunnel elements 3N & 3Z.

The INSAR-data of both tunnel elements 3N & 3Z are shown in the graph below.

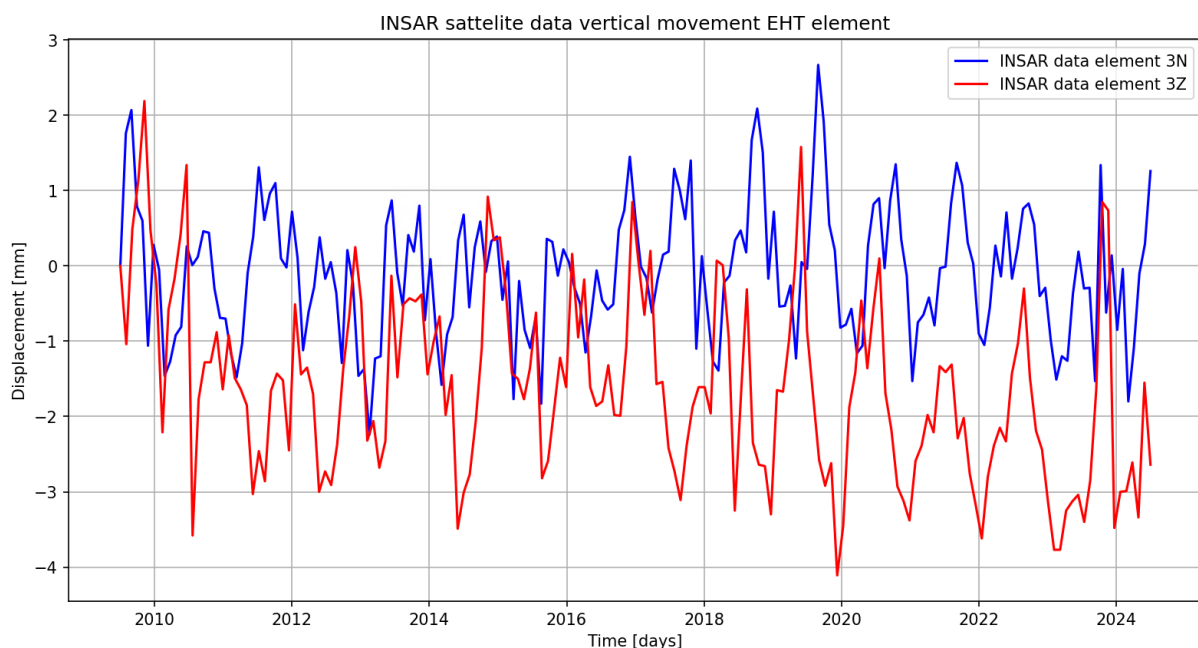


**FIGURE 58: INSAR DATA 3N & 3Z 2009-2024 (RWS CIV, 2024)**

Since the EHT was constructed in 1968, the current available timespan of the INSAR-data is not representative for the full displacement profile of the tunnel elements. Still this available information can be used to define possible trends and make predictions based upon them.

In the previous chapter the warning levels for both elements were determined based upon an algorithm which modelled the uplift failure mechanism due to corrosion. The warning levels consist of a signal level and an intervention level.

To judge the current situation of the critical elements and to assess the future, the warning levels are included in the graph on the next page for element 3N & 3Z respectively. Also the available INSAR-data is used to create a first order polynomial, which is used to identify trends in the data. If there would be an upward displacement trend throughout the years, it might be caused by tension piles breaking gradually.

For element 3N, the signal value was determined to be 4 mm and the intervention value 7.5 mm. The values combined with the trend are added to the graph of the INSAR-data.

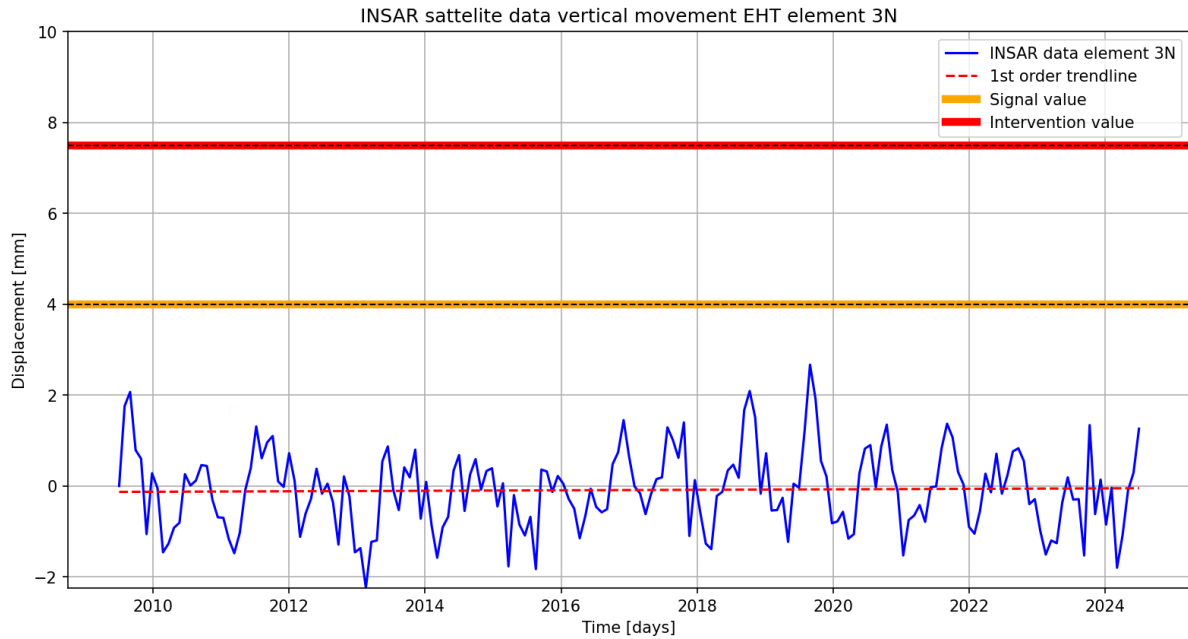


**FIGURE 59: INSAR-DATA 3N WITH WARNING LEVELS**

It can be seen that the defined trend of the INSAR-data of element 3N is near zero. This means that throughout the years the tunnel is staying roughly in the same vertical position.

This negative displacement trend gives a larger margin from the current displacement value to the signal & intervention values. This may seem like a positive effect, piles could still fail due to stress corrosion and the tensile capacity could decrease resulting in a greater upward movement than the assumed settlement.

The currently measured INSAR-data not reach the signal value and does not have a trend. Based on this, it is assumed that the uplift failure mechanism analyzed in this research is not identifiable from the data, and thus not present for both elements 3N. However the mechanism could still develop in the future. In order to identify this timely, active monitoring of the tunnel elements should continue.

For element 3Z, the signal value was determined to be 5 mm and the intervention value 10 mm. The values combined with the trend are added to the graph of the INSAR-data.

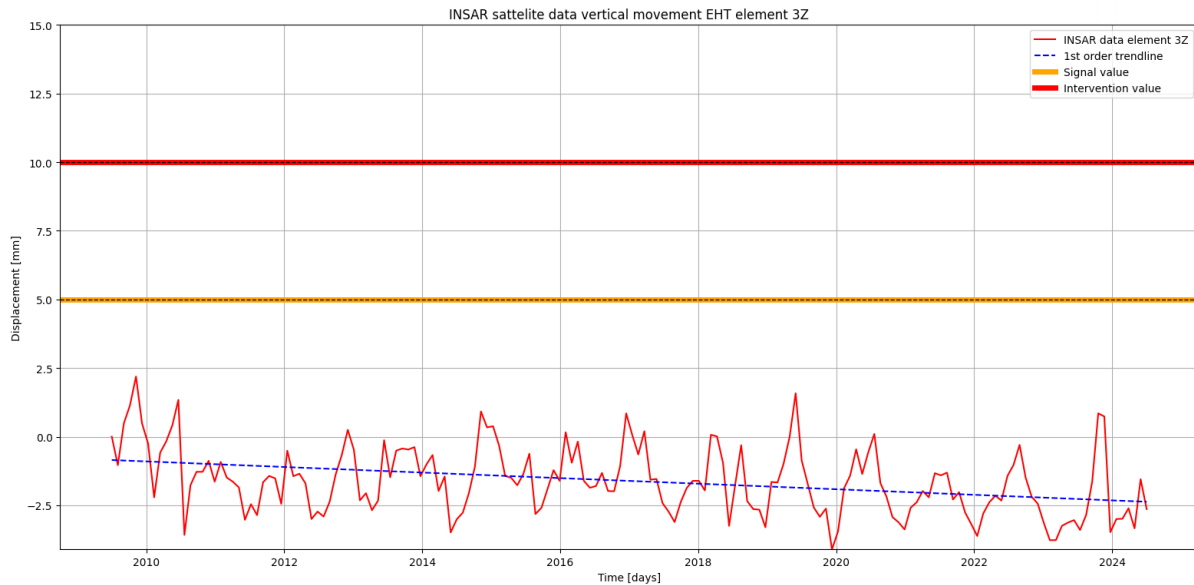


**FIGURE 60: INSAR-DATA 3Z WITH WARNING LEVELS**

It can be seen that the trend of the INSAR-data of element 3Z is negative with a coefficient of  $-0.1$  mm/yr. This means that throughout the years the tunnel is slowly settling. A possible explanation is the presence of soft soils in the southern entrance. These soft soils are known to show a lot more creep settlement than sandy soils.

This negative displacement trend gives a larger margin from the current displacement value to the signal & intervention values. This may seem like a positive effect, but piles could still fail due to stress corrosion and the tensile capacity could decrease resulting in an upward trend of the vertical movement. This positive trend however might be masked by the negative trend which is seen in Figure 60. To prevent wrong interpretation of the displacement profile, it is advised to remove possible identified negative trends which cannot be attributed to the uplift failure mechanism. For example the assumed creep settlement of  $-0.1$  mm/yr.

As seen on the graph, the currently measured INSAR-data not reach the defined warning levels. Element 3Z has a downward trend, moving away from the warning levels as time goes on. Based on this, it is assumed that the uplift failure mechanism analyzed in this research is not identifiable from the data, and thus not present for both elements 3N & 3Z. However this could still develop in the future. In order to identify this timely, active monitoring of the tunnel elements should continue.

## 10. Conclusions

This research aimed to analyze and model a potential failure mechanism for tension pile foundations applied in immersed tunnels, specifically investigating the uplift failure mechanism due to stress corrosion. The incident which followed from the tension pile foundation failure of the Prinses Margriet tunnel (PMT) served as the incentive for this research. The first Heinenoordtunnel (EHT) was selected as a case study for analysis due to its similar foundation system to that of the PMT.

The two main research questions are posed as follows:

‘What is the relevant potential failure mechanism for the tension pile foundation of the EHT and to what extent can its reliability be assessed?’

‘How can a numerical model assist in the monitoring of the tension pile foundation of the EHT, in order to assess possible detection levels of the progress of a failure mechanism?’

Prior research identified stress corrosion as the cause of the uplift failure mechanism for the PMT, which was further validated in this study by defining the three necessary conditions for stress corrosion to occur: high-quality reinforcement steel, a corrosive soil environment, and significant tensile stresses. For the tension pile foundation of the EHT, these three conditions all apply. Therefore it was deemed that stress corrosion is a relevant cause of failure for the tension piles. On top of that the influence of stress variation was studied to assess the risk of corrosion fatigue. The maximum magnitude of the stress variations was found to be up to 5.3% of the total capacity of the steel. The mechanism of corrosion fatigue was deemed insignificant after expert consultations.

A historical review of tension pile design in the Netherlands revealed that the geotechnical capacity determination was more conservative at the time of construction of the EHT comparing to current standards. Comparing the tension pile foundation capacity design value to results from current models used in geotechnical practices showed an increase of 53% in tensile capacity. The increase is explained by the development of more advanced calculation models and less conservative safety factors applied. The current standard of geotechnical calculation models also used in geotechnical practices was employed for validation of the numerical model developed in PLAXIS 3D.

The critical tunnel elements for the uplift failure mechanism of the EHT was found to be the third deepest elements 3N & 3Z. These elements were chosen as modelling objective in order to be able to describe the uplift failure mechanism due to stress corrosion.

The geometry of the tunnel elements were modelled in the FEM software PLAXIS 3D. The numerical model was validated by comparing the tensile capacity at a maximum displacement of 10 mm with the most actual calculation model relevant in the Netherlands. Here it was found that the outcome of the numerical model matched the results with a slight overestimation of 1.7% of the safe capacity and an underestimation of 21% of the limit capacity for the northern element 3N. For the southern element 3Z the validation resulted in a 17% overestimation of the safe capacity and an underestimation of 10% of the limit capacity. Since the capacity according to the numerical model for both elements fall within the range of safe and limit capacities of DFoundation it is validated.

The numerical model was then used to determine the ultimate tensile capacity by increasing the buoyant pressure on the tunnel floor until failure in order to determine the safety factors of the elements. Here it was found that the safety factor of the critical element 3N was equal to 2.68. At failure the maximum displacement is equal to 31.17 mm. For critical element 3Z the safety factor amounted to 3.1 with a displacement of 19.37 mm.

The failure mechanism of uplift due to stress corrosion was modelled by assessing the behavior of the numerical model upon tension piles failing sequentially. Upon performing 50 Monte-Carlo simulations for both critical elements with tension pile failure sequences as a random element, the displacement profile of the failure mechanism of uplift due to stress corrosion is obtained.

This displacement profile as piles fail gradually is used to identify warning levels for monitoring of the tunnel entrance elements. For tunnel element 3N the signal value for maximum displacement in the tunnel floor is proposed to be 4 mm, where it is expected that 35% of the tension piles have failed. The value for floor displacement is found to be 7 mm at 55% of the tension piles failed. For tunnel element 3Z the signal value for maximum displacement in the tunnel floor is proposed to be 5 mm, where it is expected that 25% of the tension piles have failed. The value for floor displacement is found to be 10 mm at 45% of the tension piles failed. After this point upon pile failure, the displacements increase rapidly until total failure of the tunnel element occurs. Exceeding the intervention value should be avoided in order to guarantee the safe facilitation of traffic through the tunnel. The models predicted a more rapid displacement increase and sooner model failure for tunnel entrance element 3Z after the intervention level. This is due to the application of less amount of tension piles for the southern entrance.

The available historical INSAR-data was used to check the actual displacement profile of the critical elements 3N & 3Z. Here it was found that there is no positive trend identifiable in the data for both elements which could signal the development of stress corrosion in the tension piles. Tunnel element 3Z is even settling with -0.1 mm/year. This shows that both critical tunnel elements are not approaching the signal level and are not undergoing any uplift movements as of now.

This conclusion is in agreement with the field research that was carried out by Heijmans in 2017, where it none of the piles tested showed failure. The reason of the stress corrosion occurring at the PMT and not at the EHT could possibly be explained by the difference in protective coatings used on the steel. Asphalt used for the EHT may be able to provide better protection against corrosion than the grease used for the PMT. There could also be a less corrosive environment present in the subsoil of the EHT. These expectations however have not been confirmed.

## 11. Recommendations

This chapter provides recommendations based upon this thesis for future research and monitoring of tunnels. Firstly the recommendations for this research are suggested, and secondly the recommendations for monitoring the uplift failure mechanism due to corrosion.

In determining the risk of stress corrosion occurring in the tension piles of the First Heinenoordtunnel, it is assumed that the environment of the subsoil is able to induce corrosion based on the failure that occurred in the Prinses Margriet tunnel. There is no actual research carried out in order to determine whether the composition of the subsoil around the tension piles is a corrosive environment. In order to gain insights regarding the composition of the subsoil and the possibility of inducing stress corrosion in steel elements, additional site investigation is recommended.

In the sensitivity analysis, the influence of the rubber joints installed between the tunnel elements was simulated. Here only the friction force between the rubber and concrete was modelled. The effect of possible clamping force of the neighboring tunnel elements generated by thermal expansion of the tunnel elements has not been studied. In the models, the clamping force is assumed as zero which is the worst-case scenario for the uplift failure mechanism.

In the formulation of the finite element models, the sequential failure of the tension piles due to stress corrosion was only simulated on the tension pile foundation of the critical tunnel elements. The neighboring tunnel elements have been modelled for correct boundary conditions, but they have not been modelled with tension piles. The effect of tension pile failure due to stress corrosion of the neighboring tunnel elements on the critical element has not been studied. This could be studied by also modelling the neighboring tunnel elements with tension piles and adjusting the algorithm to let these tension piles fail at the same time.

In the simulations of the critical elements on the northern and southern side, the main difference between one and another was the amount and length of tension piles used in the foundation. For the northern entrance, 95 tension piles of 17 m were used. For the southern entrance, 67 tension piles of 21 m were used. In the simulation of the uplift failure mechanism due to stress corrosion, it was found that the developments of displacements develop more rapidly for the southern entrance. Also model failure occurred sooner. This shows that the usage of more tension piles with less length results in a higher redistribution capacity for the tension pile foundation, resulting in more resistance against the uplift failure mechanism due to stress corrosion.

The finite element models of the critical elements are validated and therefore have much more possibilities than solely the modelling of the uplift failure mechanism due to stress corrosion in this research. For example, intervention measures such as ballasting could be modelled in order to assess their influence on the tunnel element. Another example is assessing the influence of differences in ground water level on the tunnel element.

The INSAR-data available only dates back to 2017. In order to identify trends over a longer period of time, it is advised to go back further in time to analyze the actual displacement profile of the tunnel elements. There might be a trend identified which could be attributed to stress corrosion.

### *Recommendations for monitoring*

The results of the simulations of the critical tunnel elements are used to monitor the actual failure mechanism in the tunnel. In the latest chapter of this research, the currently available INSAR-data of the EHT was analyzed in order to identify possible upward movements and compare them with the modelling results. Here it was found that there is no upward trend identifiable from the INSAR-data and therefore concluded that the uplift failure mechanism due to stress corrosion is not developing currently. This however is no guarantee that it could still develop in the future. Here the recommendations for monitoring the uplift failure mechanism due to stress corrosion for the EHT are given based on this research and available INSAR-data.

Using the numerical models, it was found that the signal and intervention value for the monitoring of the uplift failure mechanism due to stress corrosion for the critical element of the northern tunnel entrance of the First Heinenoordtunnel amounts to 4 mm and 7.5 mm of the tunnel floor respectively. For the critical element of southern tunnel entrance these values amount to 5 mm and 10 mm of the tunnel floor respectively. These warning levels could be used for monitoring the failure mechanism based on displacements. Here an exceedance



of the signal value would mean the transition from the 'safe' zone to the 'increased risk' zone. If this would occur it is advised to start monitoring the tunnel continuously.

If the intervention value would be exceeded, the 'increased risk' zone transits to the 'danger' zone. Rapid displacements could occur in this zone leading up to permanent damage and loss of function of the tunnel. Therefore this zone should be avoided at all costs.

The warning levels are based on the maximum displacement in the floor of which the location is dependent on the pile failure sequence in the model. Ideally, it is recommended to monitor the full displacement profile of the tunnel floor. With current available technology and the facilitation of continuous traffic on the tunnel floor, this is unfeasible. It is advised to measure the displacement on the side- and middle walls using INSAR-data and assume the largest value of these three as maximum in order to identify the current approximated maximum displacement.

It is advised to keep monitoring the available INSAR-data approximately every 10 days while in the 'safe' zone. The variation of the displacement throughout every 10 days should be compared to determine the variation in displacement between two periods. The displacement measured in INSAR-data has many different sources. As explained in this research; traffic, tidal and temperature influences cause vertical displacements. Also horizontal displacements of the tunnel might cause a vertical displacement through the interaction of the separated tunnel elements. If the variation would exceeds the at least signal value as determined in this research, the transition from the 'safe' zone to the 'increased risk' zone is assumed. Immediate continuous monitoring on top of the INSAR-data is advised of the tunnel element where the maximum displacement is measured. This transition value is regarded as a conservative value, as the displacement which reaches the signal value is not only dependent on the upward displacement of the failure mechanism due to stress corrosion, but also other effects as described.

The continuous monitoring could be done with more frequent monitoring of INSAR-data. However it is advised to deploy extra measures to increase the accuracy of the continuous displacement measurements and their exact location in the tunnel element. When the signal value is exceeded for a certain tunnel element, it is advised to deploy a multitude of Robotic Total Stations (RTS) to continuously measure the vertical displacement at different measuring points (prism). It is advised to create the amount of prisms required to measure the vertical displacement every 2 meters in both directions of the plane of the floor and walls. The amount of RTS necessary should be determined per tunnel element, as line of sight is required on the prisms for the RTS to function correctly. The RTS will return the displacement profile of both floor and walls with high accuracy. Through the displacement profile the location of maximum vertical displacement can be determined and possible intervention measures can be taken accordingly.

In case the RTS cannot be placed at the desired locations to measure the vertical displacements in the tunnel walls and floor, another possibility is to measure the vertical displacement in the tunnel joints using joint meters. On top of this, inclinometers could be installed in the middle of the tunnel elements to calculate the displacement profile using the vertical joint displacements. However it is expected that this results in less accurate measurements and a less concise displacement profile of the tunnel element with increased risk compared to using RTS.

Another method is the application of distributed fiber optic sensors which can measure the vertical displacements continuously in a transversal or longitudinal direction of the tunnel, making real-time vertical displacement monitoring possible along the direction of the cable. The feasibility of these fiber optic sensors in traffic tunnel elements should be studied prior to deployment.

Upon the transition from the 'increased risk' zone to the 'danger' zone, immediate intervention measurements are recommended. Two effective, feasible intervention measurements that are advised are lowering the ground water level reducing the buoyant force or applying ballast to increase the weight of the tunnel element. From these two, lowering the water level using deep wells is a more workable and reversible solution. The application of ballast will result in a lot of cubic meters of for example sand to be applied inside of the tunnel element, obstructing the facilitation of traffic. The possibility of applying deep wells to lower the water level without causing large settlements/groundwater flow in the effective reach of the wells should be analyzed prior to applying the wells. In case the lowering of groundwater level is not possible, the application of ballast is advised. The effectiveness of the intervention measure can be identified using the continuous monitoring.

## 12. Bibliography

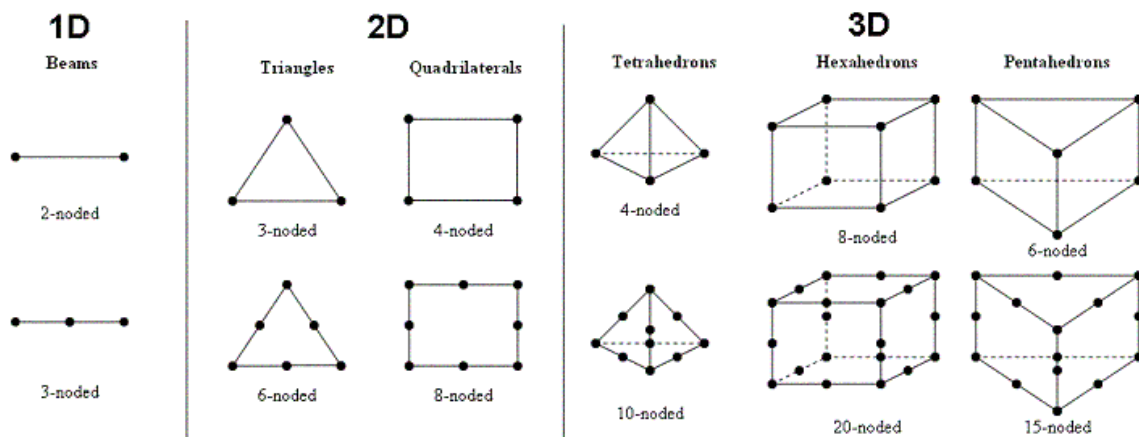
- Al-Bayati, A., Al-Neami, M., & Rahil, F. (2023). *Enhancing Pullout Load Performance of Under-Reamed Piles in Homogeneous Layered Clay: A Numerical Comparative Study*. Engineering and Technology Journal.
- ASM international. (1997). *Metals handbook*. American society for metals.
- Bezuijen, A., & Litjens, P. (1999). *Eerste Orde Evaluatie K100 BT-A Boorfrontstabiliteit*. Delft: Grondmechanica Delft.
- Bonfix. (2023, 1 1). *Spanningscorrosie*. Opgehaald van Bonfix: <https://www.bonfix.nl/nl/spanningscorrosie>
- Borsje, H., & Schuring, E. (2023). *Onderzoek voorspanstaven Prinses Margrietunnel*. Delft: TNO.
- Bosch, W.-R. (2005). *Electrochemical impedance spectroscopy for the detection of stress corrosion cracks in aqueous corrosion systems at an ambient high temperature*. Elsevier.
- Bylapudi, G., Mondal, K., Spearing, A., & Bhagwat, A. (2015). *Stress corrosion cracking - hypothetically a major threat to underground mine roof support systems and rock anchors*. Society for Mining, Metallurgy & Exploration.
- CUR98-9. (2001). *Ontwerpregels voor trekpalen*. Delft: COB.
- Djeddi, L., Khelif, R., Benmedakhene, S., & Favergeon, J. (2013). *Reliability of Acoustic Emission as a Technique to Detect Corrosion and Stress Corrosion Cracking on Prestressing Steel Strands*. Elsevier.
- Engin, E., & Brinkgreve, R. (2010). *Validation of empirical formulas to derive model parameters for sand*. Delft: TU Delft.
- Engin, H., & Brinkgreve, R. (2009). *Investigation of Pile Behaviour Using Embedded Piles*. Delft: TU Delft.
- Eurocode7. (2006). *Eurocode 7*. Brussels: European Commission.
- Faizi, K., Armaghani, D. J., Sohaei, H., Rashid, A. S., & Nazir, R. (2014). *Deformation model of sand around short piles under pullout test*. Malaysia: Elsevier.
- Fattah, M. Y. (2016). *Three-Dimensional Finite Element Simulation of the Buried Pipe Problem in Geogrid Reinforced Soil*. -: Researchgate.
- Fugro. (2024). *Measured head heights at Heinenoordtunnel*. Utrecht: Virgeo monitoring.
- Grondmechanica Delft. (1994). *Veldonderzoek langzaam-verkeerstunnel te Heinenoord*. Delft: Grondmechanica Delft.
- Hemeda, S. (2022). *Geotechnical modelling and subsurface analysis of complex underground structures using PLAXIS 3D*. Egypt: Springer.
- Hernandez-Valle, F., Clough, A., & Edwards, R. (2014). *Stress corrosion cracking detection using non-contact ultrasonic techniques*. Elsevier.
- Ideal-tek. (2012). *Carbon steel type C*. Opgehaald van Ideal-tek: [https://www.ideal-tek.com/public/files/11-TDS\\_Carbon\\_steel\\_type\\_C.pdf](https://www.ideal-tek.com/public/files/11-TDS_Carbon_steel_type_C.pdf)
- Jones, R. (2017). *Irradiation-Assisted Stress-Corrosion Cracking*. ASM International.
- Khalifeh, A. (2019). *Stress Corrosion Cracking Behaviour of Materials*. InTechOpen.
- Martin, & Bastidas. (2022). *Stress corrosion cracking failure analysis of AISI 1018 carbon steel reinforcing bars in carbonated and chloride contaminated environment*. Akron: Elsevier.
- Miller, L., Mintz, T., He, X., Pabalan, R., & Pan, Y. (2013). *Effect of Stress Level on the Stress Corrosion Cracking Initiation of Type 304L Stainless Steel exposed to Simulated Sea Salt*. San Antonio: Southwest Research Institute.
- Mink, C. (1975). *Kathodische bescherming*. KIWA.

- NEN. (2023, 1 1). *De waarde van normen*. Opgehaald van NEN: <https://www.nen.nl/>
- NEN 6740. (1991). *NEN 6740 - Basiseisen geotechniek*. Nederland: NEN.
- NEN 9997-1. (2023). *NEN 9997-1*. Nederland: NEN.
- OIB. (2018). ETA-05/0123. *European Technical Assessment* (p. ANNEX 41). Europe: IOB.
- Ramadan, S., Gaillet, L., Tessier, C., & Idrissi, H. (2008). *Detection of stress corrosion cracking of high-strength steel used in prestressed concrete structures by acoustic emission technique*. Elsevier.
- Rijksoverheid. (2012). *Bouwbesluit 2012*. Nederland: Rijksoverheid.
- Rijkswaterstaat. (2024, 1 1). *A7: herstel Prinses Margriettunnel*. Opgehaald van Rijkswaterstaat: <https://www.rijkswaterstaat.nl/wegen/projectenoverzicht/a7-herstel-prinses-margriettunnel>
- Rijkswaterstaat. (2024, Maart 28). *Werkzaamheden Prinses Margriettunnel duren jaar langer dan gedacht*. Opgehaald van <https://www.rijkswaterstaat.nl/wegen/projectenoverzicht/a7-herstel-prinses-margriettunnel>: Werkzaamheden Prinses Margriettunnel duren jaar langer dan gedacht
- RWS directie sluizen & stuwen. (1962). *Bestek SS415a*. Utrecht: RWS directie sluizen & stuwen.
- Ryltenius, A. (2011). *FEM Modelling of piled raft foundations in two and three dimensions*. Lund: Lund University.
- Sheil, B., & McCabe, B. (2012). *Predictions of friction pile group response using embedded piles in PLAXIS*. Nicosia: Near East University.
- Simulia. (2007). *Analysis of Driven Pile Setup with Abaqus/Standard*. Simulia.
- Stam, F., & van der Poel, J. (1994). *Berekening van de opneembare trekbelasting bij een palengroep*. Delft: Grondmechanica Delft.
- Stevelink, W. (1969). De Heinenoordtunnel. *OTAR*, 141-147.
- Stochasticandlangrangian. (2011, Juli 17). *What does shape function mean in finite element formulation*. Opgehaald van Stochasticandlangrangian: <https://stochasticandlangrangian.blogspot.com/2011/07/what-does-shape-function-mean-in-finite.html>
- Tomlinson, M., & Woodward, J. (2008). *Pile design and construction practice*. Oxon: Taylor & Francis.
- van Baars, S., & van Niekerk, W. (1999). *Numerical modelling of tension piles*. Rotterdam: Balkema.
- van Noortwijk, D., Everts, H., & Janse, E. (1994). *Onderzoek trekpalen 2e Beneluxtunnel*. Delft: Grondmechanica Delft.
- Wegenwiki. (2023, September 23). *Heinenoordtunnel*. Opgehaald van Wegenwiki: <https://www.wegenwiki.nl/Heinenoordtunnel#:~:text=De%20Heinenoordtunnel%20is%20een%20tunnel,%20met%20langzaam%2Dverkeerstrook>.
- White, F. (2016). *Fluid Mechanics, 8th edition*. Asia: McGraw-Hill Education.
- Zienkiewicz, Taylor, & Zhu. (2013). *The Finite Element Method: Its Basis and Fundamentals*. ScienceDirect.

## 13. Appendix

### A1: Finite element method

PLAXIS uses the finite element method to make calculations. The finite element method is a numerical technique that is widely used in geotechnical and structural engineering. The method involves discretizing a complex geometry into a finite number of elements. As for the type of elements, many options are available based on the amount of dimensions chosen. The type of element should be chosen based on the nature of the problem. The figure below shows some possible element shapes for 1D, 2D and 3D.



Each element has a certain number of nodes. These nodes are the locations where the different elements from the discretized geometry are connected. The nodes are also the locations where the unknown value of interest, such as deflection or stress is calculated.

Each element also has their own set of shape functions. These shape functions are mathematical formulas that interpolate the known nodal values to unknown nodal values. The shape functions describe how the value of the unknown nodal value varies within a discretized element. These can be chosen according to the problem that is to be solved.

The nodal values and shape functions together make a local set of equations for each element. The next step is to assemble the local matrices of each element into a global set of equations, which is encapsulating the complex geometry as defined. The local matrices should be connected where nodes are shared across the elements.

The next step is to impose boundary conditions on the global set of equations. The boundary conditions contain nodal values which are known beforehand.

Finally, the global set of equations including boundary conditions is solved directly or iteratively. An example direct method is Gaussian elimination and an iterative method is static equilibrium (CIEM2110, 2023).

Once the global set of equations is solved, the unknown values at all the nodes should be known, and the system can be analyzed based on these now known values. PLAXIS 3D shows the geometry of the model with discrete elements and color coding to resemble values of the calculated nodal values.

## A2: Plaxis3D

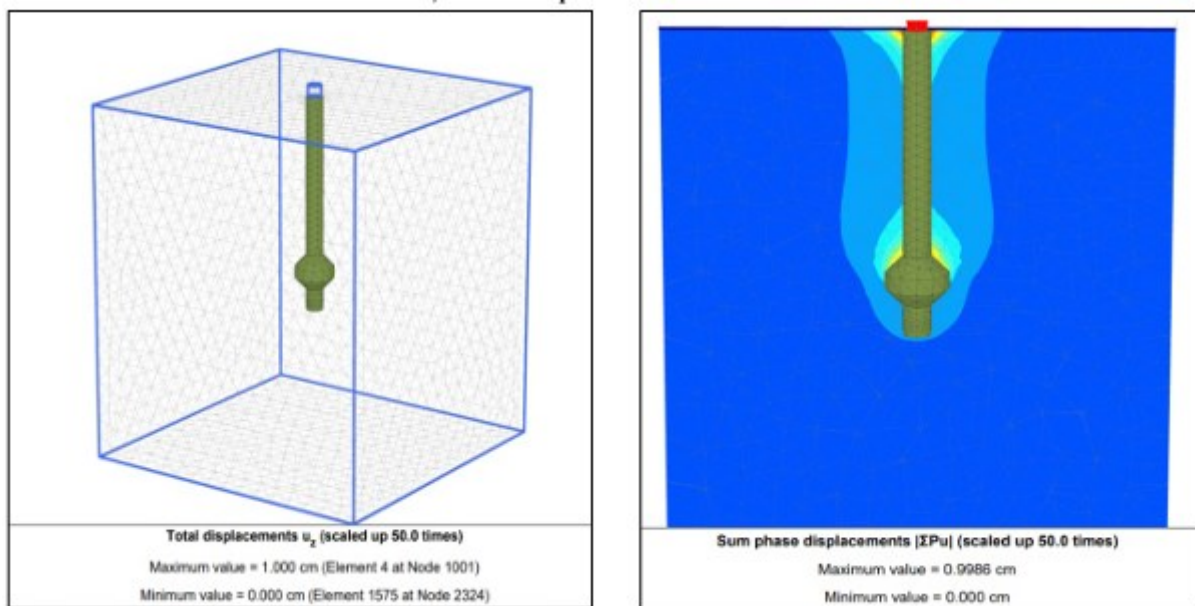
*This part was mostly written for myself to learn and understand Plaxis3D*

In geotechnical practices, PLAXIS is a well-known software program used to model soils and structures for the analysis of geotechnical problems. The calculations are carried out using the Finite Element Method with constitutive relations derived from advanced soil models which have been made accessible in the software. PLAXIS has a 2D and a 3D version. The difference between one another is the amount of dimensions the modelling is done with. For tension pile modelling specifically, the radial stresses around the tension pile play an important role. To reduce over simplification of these stresses, the 3D version is used as the extra dimension adds more complexity to the model. This chapter will delve into the usage of PLAXIS 3D for the given problem of the tension pile foundation of the EHT.

The input in the PLAXIS 3D model consists of the geometry of the structure, the geotechnical profile and external forces acting on the tunnel such as water pressure or friction. The advanced soil models are chosen along with the determination of the geotechnical profile.

The PLAXIS 3D package also contains an Application Programming Interface (API). This API makes communication between an automation software for example built in Python and PLAXIS 3D possible. This makes parametrical design through an application possible. It also is an interesting opportunity for automating calculations.

An example outcome of PLAXIS 3D is shown in the figure below. In this research the influence of application of bulbs on a tension pile in clay on the displacement profile is analyzed. The geometry of the problem is shown on the left side of the figure, the displacement profile is shown on the right side of the figure. A blue color coding resembles low total displacement, and red color coding resembles high total displacement. This figure shows that the displacement profile around the tension pile is calculated quite accurately in the PLAXIS 3D software.



### General modelling

The general modelling procedure in PLAXIS is to model the soil volume and stratigraphy, define geometry with elements and corresponding materials, define the loads and boundary conditions relevant for the geometry, create a Finite Element mesh on the geometry, define the initial condition and perform the Finite Element Method calculation. This chapter will highlight these different steps in more detail. The general information is based on the PLAXIS 3D Reference Manual made available by Bentley Systems.

## Ground modelling – Soil Mode

In ground modelling, the soil stratigraphy is defined using boreholes and is limited to a defined soil contour. The soil contour defines the boundary of the model and can be adjusted accordingly in the program. Inside the soil contour soil clusters can be defined which act as a volume element containing soil. These clusters are used to define geometric distinction within the soil stratigraphy.

The boreholes define the vertical depth of the model. The borehole is divided into layers, with each layer having a different soil type assigned. These soil types each have their own soil properties which are defined as materials. Based on the type of advanced soil model chosen, the program asks different soil parameters. The advanced soil models are chosen along with the material properties. These advanced soil models describe the constitutive relation between stress and strain in the soil. The possible types of advanced soil models are described further on in this chapter.

The software also gives the possibility to define multiple boreholes on the horizontal x-z plane. The defined layers of the boreholes are interpolated towards each other, creating non-uniformly distributed soil layers in the horizontal direction. This makes for more detailed modelling of actual soil stratigraphy's.

The assumed pore pressure distribution along the borehole is also defined in the soil mode.

## Modelling loads and structures – Structure mode

### *Geometric entities*

To model loads and structures, the geometry of the model is defined using geometric entities. Features such as loads and structures are assigned to geometric entities. PLAXIS 3D offers four basic geometric entities; points, lines, surfaces and volumes. These entities are used to formulate complex geometries of geotechnical problems. Other entities such as loads and structures can be assigned to a geometric entity. The geometric entities are also used to formulate boundary conditions.

### *Loads*

Loads in PLAXIS are features that are assigned to the previously defined geometric entities. Loads can be either modelled as static or dynamic. Due to the scope of this research, only static loading is covered. Static loads are either expressed as forces or prescribed displacements. Line and surface loads can be defined as uniform or linear.

### *Structural entities*

To model the structures in PLAXIS, the structural entities should be used. The structural entities can be assigned to previously defined geometric entities. This chapter goes over the main applicable structural entities. By using defined material properties, the structural entities are able to be assigned a certain material.

### *Anchors*

There are two types of anchors available in PLAXIS. These are the fixed-end anchors and the node-to-node anchors. Both anchors are modelled as springs.

The fixed-end anchor is a one node element that signifies a fixed connection in one specified direction. The node-to-node anchor is two node element that connects two point elements together.

### *Beams*

Beams are used to model slender structures with significant bending stiffness and axial stiffness. The beam can be assigned to a line element.

These elements are composed of 3-node line elements with six degrees of freedom per node, namely the translational and rotational degrees of freedom. For the calculation of deflection due to shearing and bending, Mindlin's theory is implemented in PLAXIS 3D. It is also able to account for change in length when axial force is applied on the beam.

### *Embedded beams*

Embedded beams are composed of beam elements that can be placed in an arbitrary direction in the sub-soil and interacts with the sub-soil through special interface elements. These special interface elements are used to model

pile-soil interactions. Through these special interface elements, forces on the embedded beam such as skin resistance can be modelled.

PLAXIS denotes three different behaviors of embedded beams. Namely Pile, Rock bolt and Grout body. These behaviors should be chosen accordingly for the geotechnical problem at hand. Embedded beams modelled as piles are not able to include installation effects, these installation effects must be incorporated elsewhere in the model.

### Plates

Plates are structural entities mostly used to model thin two-dimensional structures in the ground such as walls, floors or tunnel lining. The plates are composed of 6-node triangular plate elements with six degrees of freedom. The modelling of a plate element is similar to a beam element. The difference that the plate is meshed in 2D, and the beam is meshed in 1D.

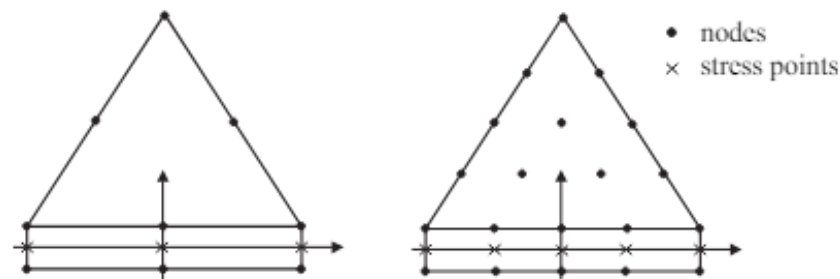
### Geogrids

Geogrids are elements that are composed of 6-node triangular surface elements with three transitional degrees of freedom. Geogrids only have a tensile strength and can be used to model tensile reinforcement of soil. Geogrids function similarly to cables which can be modelled in the subsoil.

### Interfaces

Interface elements are joint elements that are used to model the interaction between two elements. Through interfaces, the nodes of the elements to be connected are coupled. For example, the interface between plates and soil volumes can be used to model skin friction.

Interfaces are composed of 12-node interface elements. These nodes are modelled as pairs of nodes, making them compatible with for example a 6-noded triangular side of a soil or plate element. This is visually depicted in the figure below, where the triangle represents a soil or a plate and the rectangle represents the interface.



The roughness of the interaction depicted by an interface is modelled by choosing a suitable value for the strength reduction factor ( $R_{inter}$ ). This factor relates the interface strength to the soil strength and generally holds a value of  $2/3$ . The properties of an interface are based on the chosen model with respective parameters of the surrounding soil. However, the properties could also be defined by creating a new material specific for the interface element.

Loads			
Point	Line	Surface	Volumes
Load Prescribed displacement	Load Prescribed displacement	Load Prescribed displacement	Volume strain
Assignable structures and conditions			
Fixed-end anchor	Beam Node to node anchor Embedded beam Well Line drain	Geogrid Plate Interface (Positive/ Negative) Contraction Surface drain Surface groundwater flow boundary condition	

The table on the previous page gives an overview of applicability of the geometric entities, loads and structural elements.

### **Material models & properties**

In PLAXIS, to model soil, interface and structure behaviour, certain material models are available for usage. These material models include the constitutive relations of stress and strain in soils and interfaces and vary in complexity and functionality. Different material models require different parameters. Each material model has a special use case and should be chosen accordingly to the geotechnical problem at hand.

Soils tend to react in a highly non-linear fashion upon loading. This non-linear stress strain behaviour can be modelled at different levels of complexity through the use of advanced soil models. Each soil models require a different set of model parameters. Generally more complex models require more model parameters. The advanced soil models implemented in PLAXIS and relevant for Dutch soils are covered.

#### *Linear elastic model*

This model is the least complex model and is based on Hooke's law of isotropic linear elasticity. Generally this model is regarded as too simplified for use cases in soil due to its high nonlinearity.

#### *Mohr-Coulomb model (MC)*

A more complex, yet simplified model is the Mohr-Coulomb model. This is a linear elastic perfectly plastic model and is mostly used as a first approximation of soil behavior as calculation times are quick and results are easily interpreted. The Mohr-Coulomb uses yield surfaces to convey a failure envelope. Once the yield surface is reached, dependent normal and shear stress, failure is assumed in the model.

#### *Hardening-soil model (HS)*

The Hardening-Soil model is an advanced model based on an elastoplastic type hyperbolic model. This model introduces soil hardening as a reaction of soil upon loading. This hardening can happen under both shear and compression. This hardening comes from irreversible compaction upon loading which is also known as plastic deformation.

#### *Hardening-soil small strain model (HSsmall)*

This model is similar to the Hardening-Soil model, as the name suggest. The difference is that this model introduces more complexity by incorporation strain dependant stiffness values. This strain dependant stiffness is used to simulate the different reactions of soils upon different strain levels.

#### *Soft-soil creep model (SSC)*

The Soft-soil creep model is a model that is used to model time dependant behaviour of soils. It uses a logarithmic compression behaviour to express stress-dependant stiffness. The model is mostly used for soft soils such as compressible clays or peat and is suitable when the settlement through time plays a large role of importance in the geotechnical problem.

For details on the different advanced models and other applicable models provided by PLAXIS, the reference is made to the reference manual (PLAXIS, 2023). Once a model type suitable for the geotechnical problem of this research is chosen, it will be explained in more detail.



## Meshing & calculation phases

Once the soil and structure is modelled in the PLAXIS software using geometric, soil and structural entities, the program can start the calculations. This calculation consists of a generation of a mesh along the geometry and the definition of construction stages. The generation of the mesh is the subdivision of the defined geometry into finite elements.

The generation of the mesh is an important step in PLAXIS as the level of refinement of the mesh is a trade-off between computation time and accuracy of the results. As complex structures modelled in PLAXIS 3D have been known to occupy a lot of computation time.

Local mesh refinement at locations in the model where large stresses or displacements are expected and a coarse mesh where this is not the case. This creates a balance between computation time and accuracy of results.

The meshing of the model is done automatically by the PLAXIS software. Soil elements consist of a 3D 10-node tetrahedron elements. Where necessary, the user is able to define local mesh refinement if more accurate results are desired at certain locations in the geometry. For example the defined mesh of a single soil cluster can be refined using the software.

In addition to creating the finite element mesh, the project should also be divided in calculation phases similar to construction phases of the actual geotechnical project. In each phase certain elements or boundary conditions of the model can be activated or deactivated in order to simulate real world conditions as accurate as possible.

For each calculation phase, a calculation type can be specified. For the initial phase of the soil in the model, the available methods in PLAXIS are the K0-procedure, Field stress and Gravity loading. These methods are different ways to obtain the initial effective stress and water pressure state of the model. If K0 is determined, the K0-procedure works well. Otherwise the gravity loading works well for standard geotechnical problems.

After the initial conditions of the model has been defined using the initial state, the remaining calculation phases of the defined model can be calculated. For these calculations, four main types of analyses exist in PLAXIS for static application. These are Plastic calculation, Consolidation calculation, Fully coupled flow-deformation analysis and Safety calculation.

The plastic calculation is for elastic-plastic deformations and is used when failure and stability of the model is analyzed. It does not take into account time-dependent effects and thus is mainly used for calculating final settlement of a structure.

The time-dependent effects of for example consolidation in soils with low permeability can be approached with the consolidation calculation. This is calculation method is mainly used to analyze settlement throughout time.

The fully coupled flow-deformation analysis is conducted when it is necessary to analyze the development of deformations and pore pressures in saturated soils as a result of time dependent changes.

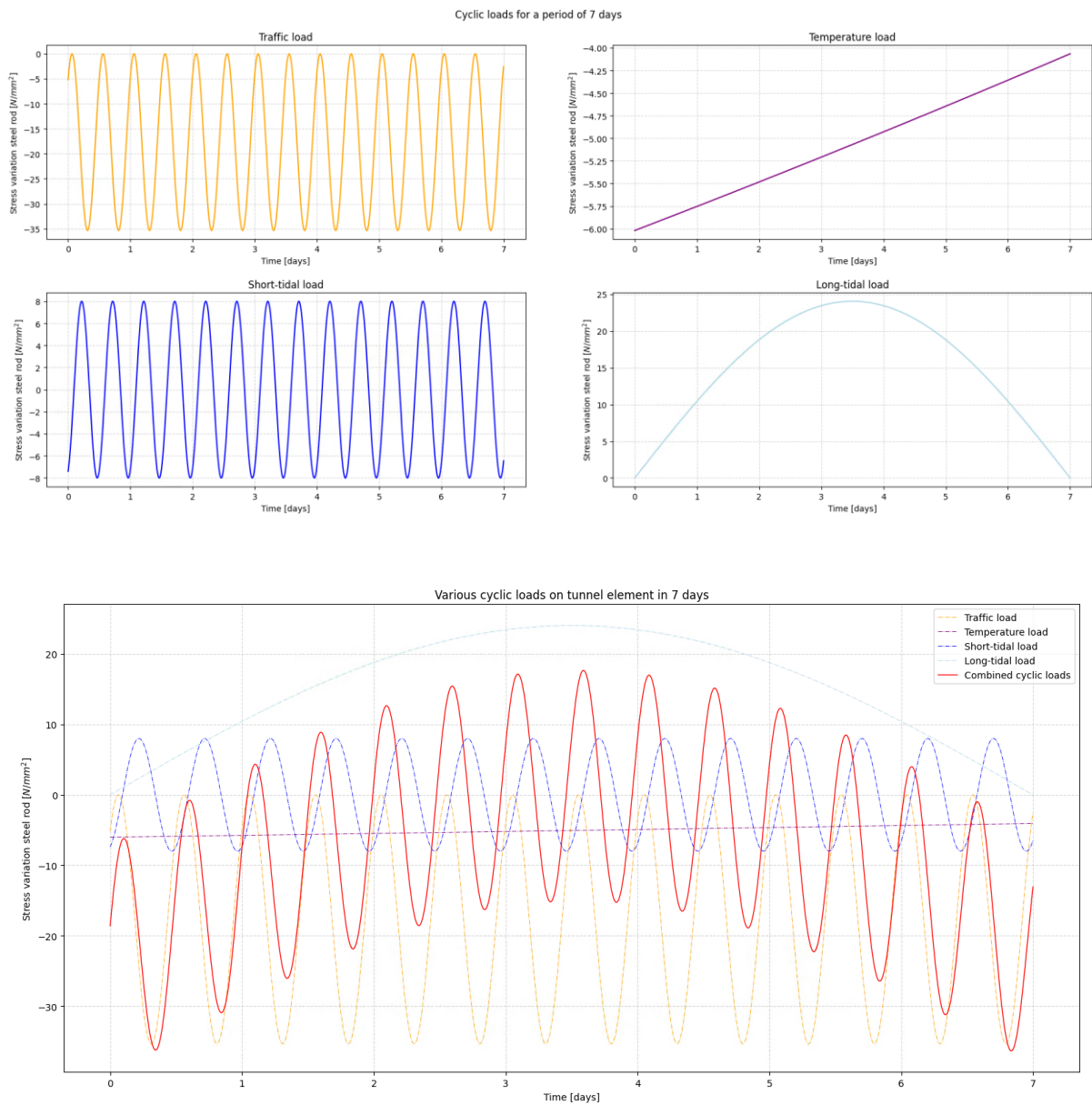
The safety analysis is similar to the plastic calculation. In the safety analysis a method called phi-c reduction is applied. This method incorporates a reduction of the initial soil and interface strength parameters until failure of the model is reached. The safety factor of the model can then be derived by dividing the available strength by the strength at failure.

Once the calculation is finished, the results of the model are defined in the output program of PLAXIS. This output program mainly includes the stress and deformation distribution on the defined geometry of the structure and soil. This information can be seen at every defined node in the geometry.

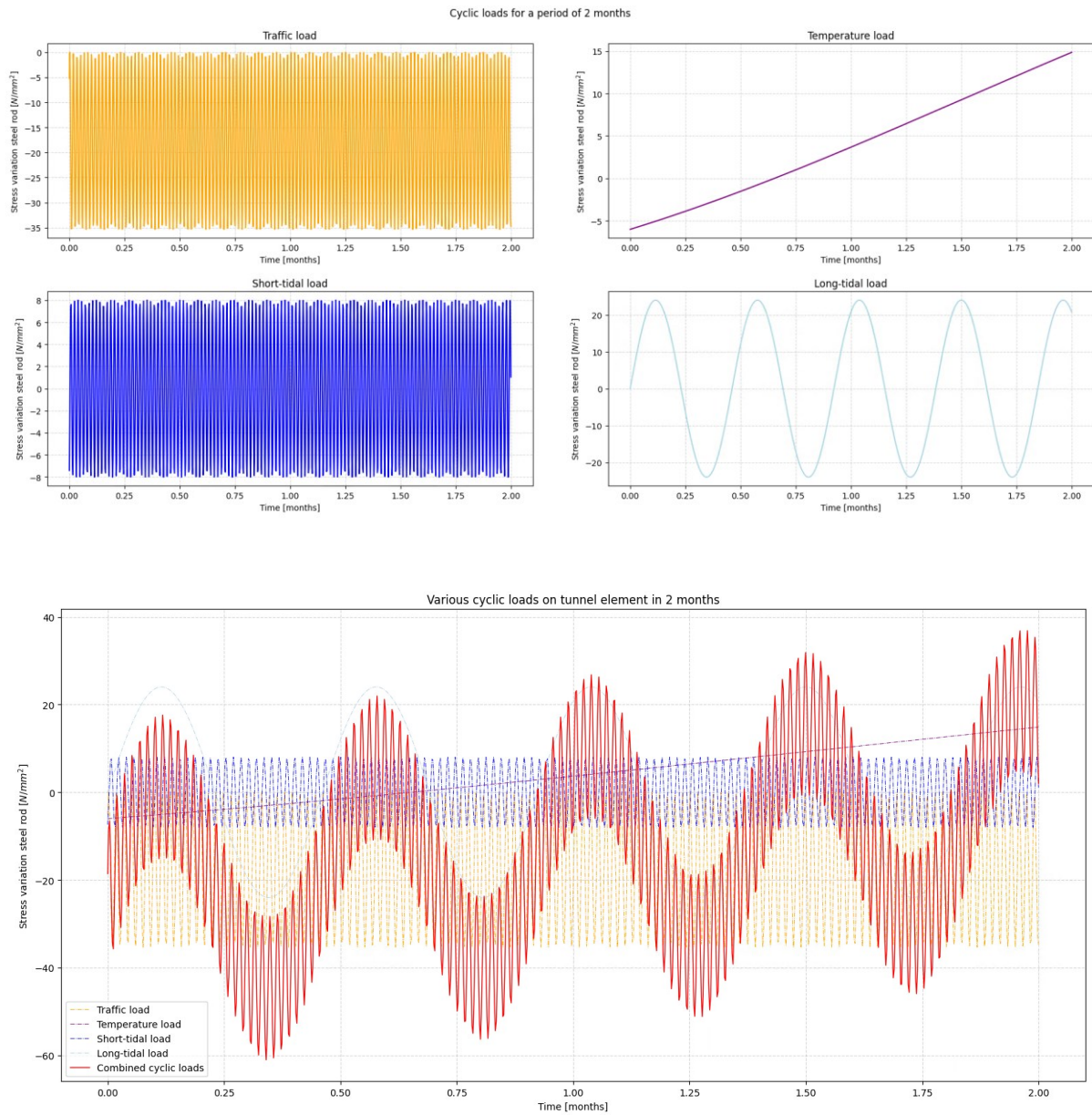
### A3: Dynamic loads on tension piles

Calculated dynamic loads on the tension piles for different timeframes.

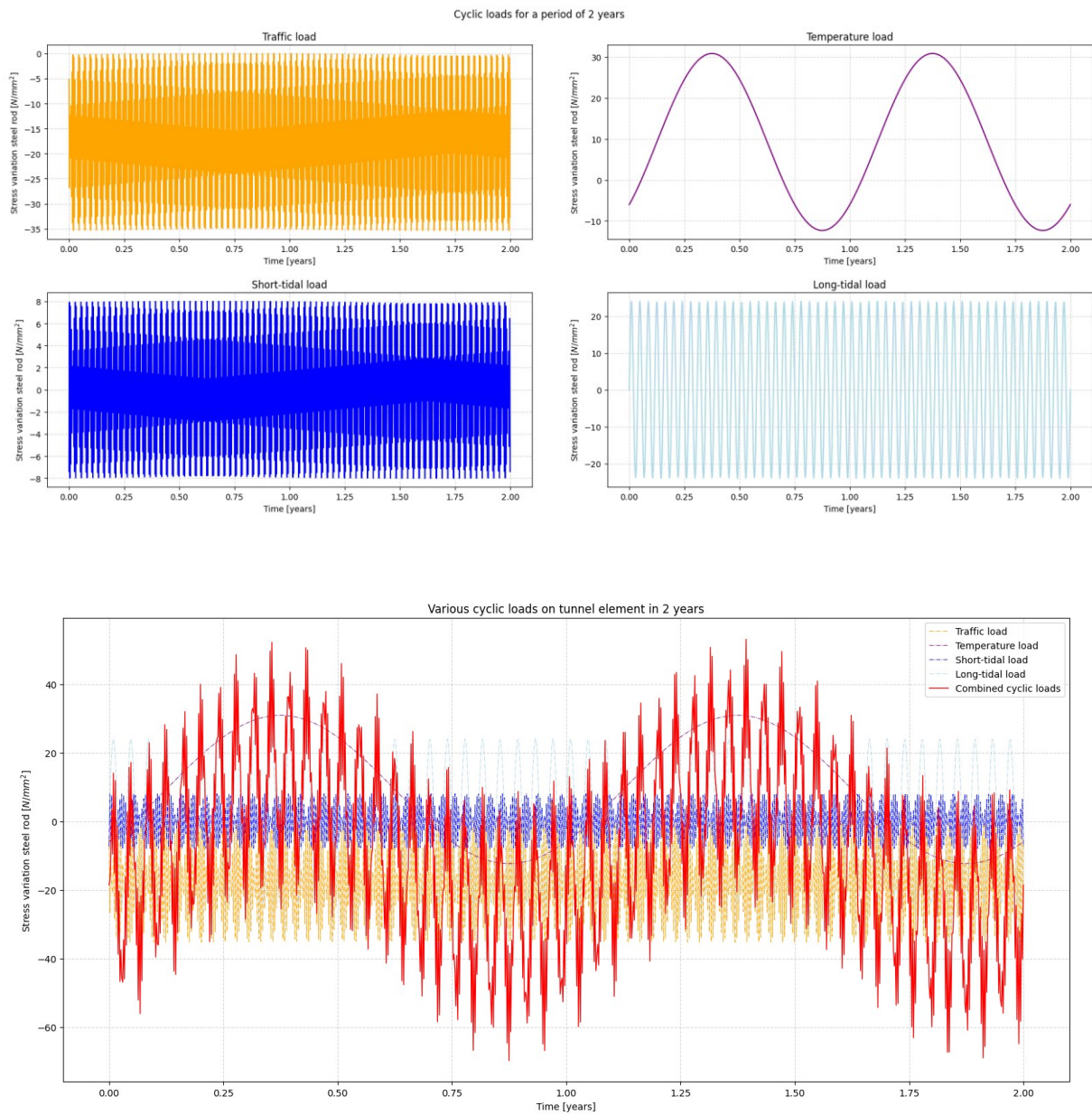
*1 week:*



2 months:

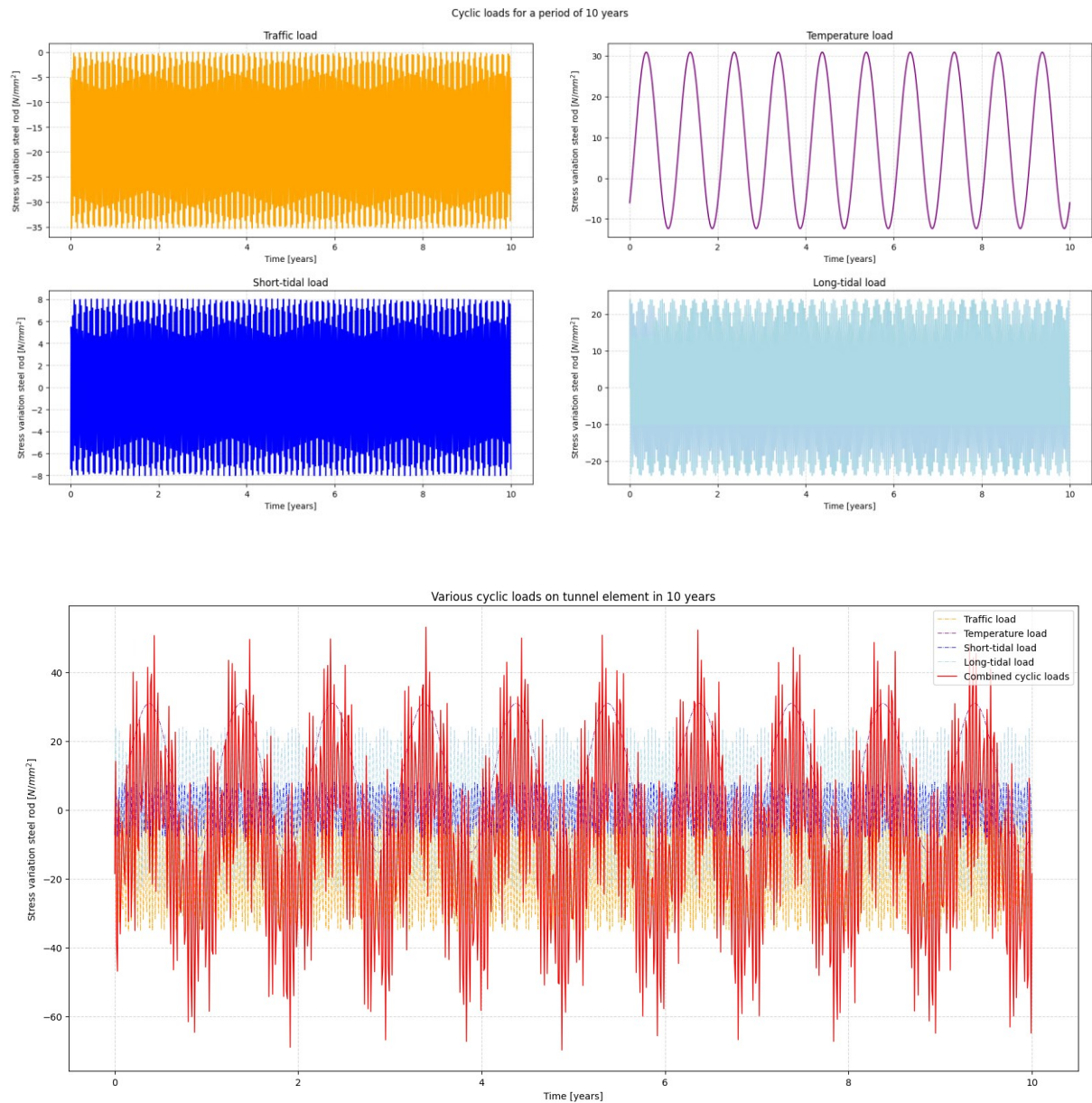


2 years:





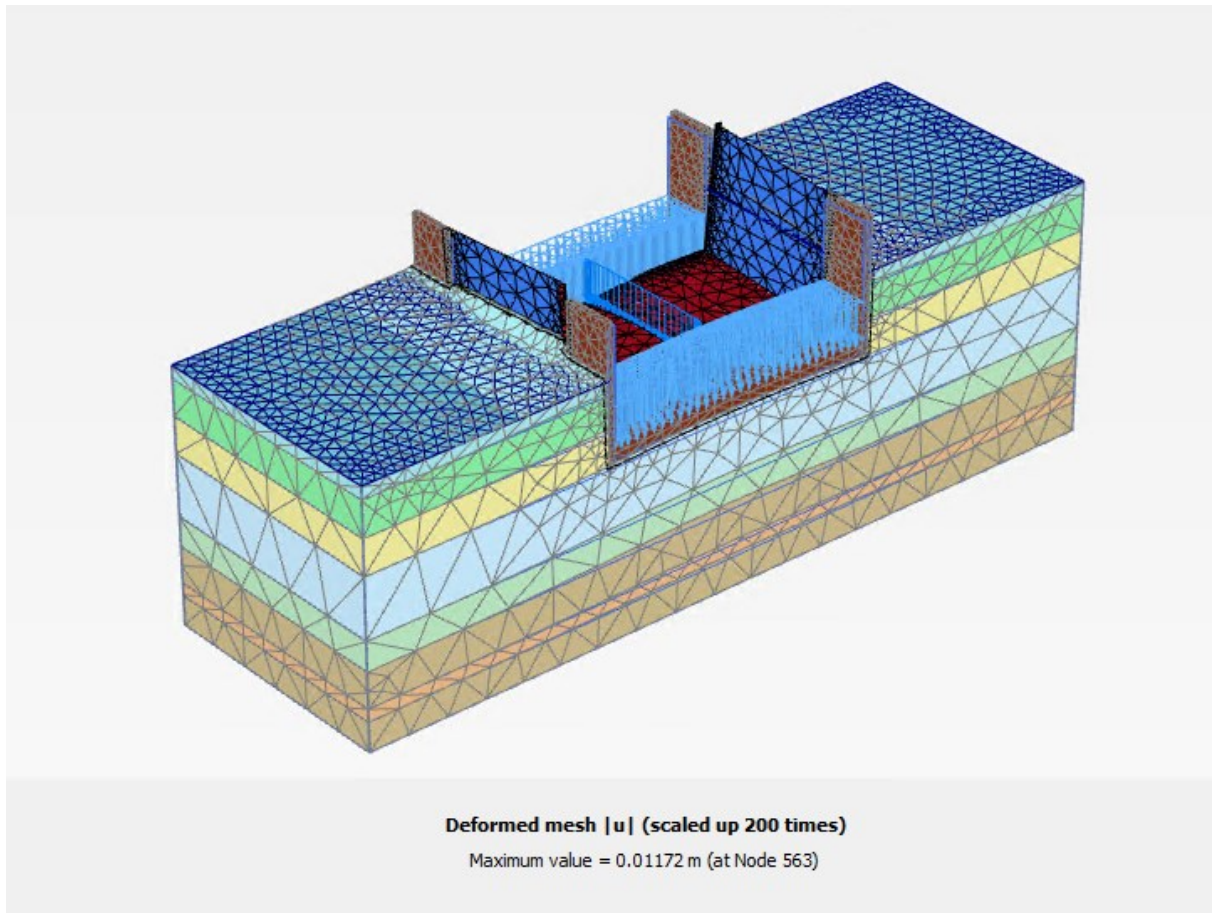
10 years:



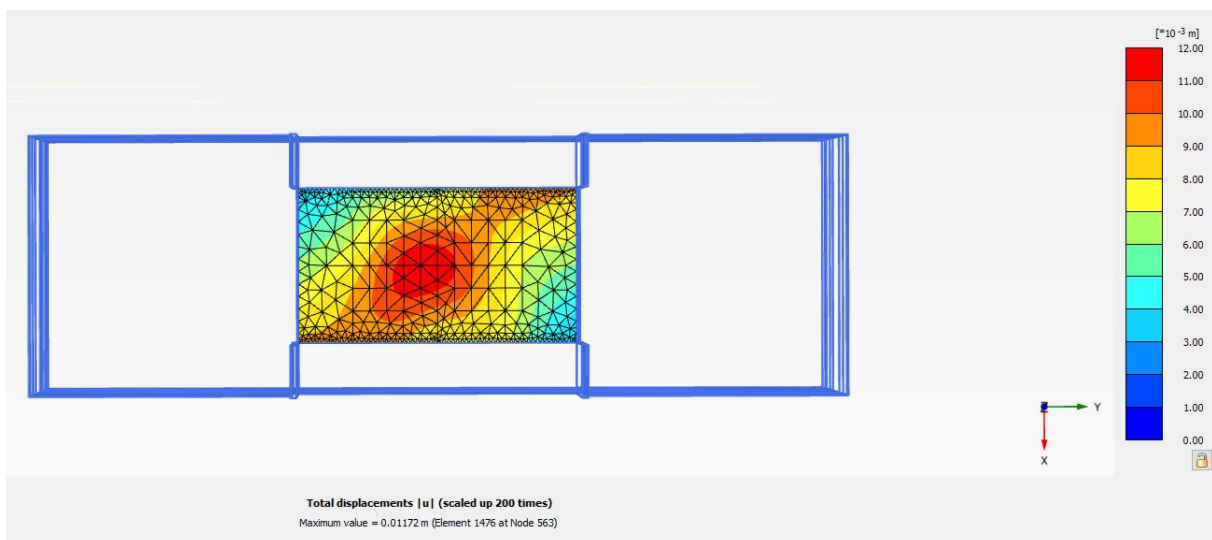
## A4: Plaxis3D model failure

Snippets of the geometry of the Plaxis3D model at model failure of iteration 31 of element 3N. This iteration of the Monte Carlo analysis is picked at random to show what a model failure looks like. The iteration is picked randomly.

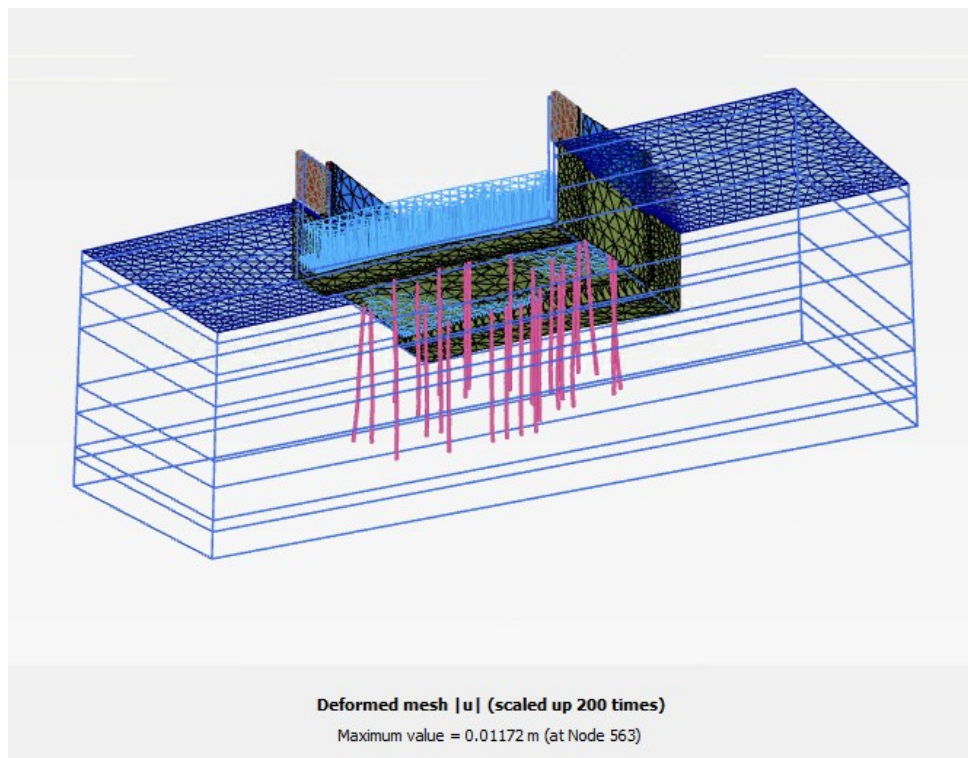
*Deformed mesh:*



*Tunnel floor displacements:*



*Remaining tension piles:*



*Wall displacement:*

